Adaptive Coded Modulation Performance and Channel Estimation Tools for Flat Fading Channels

Henrik Holm

A DISSERTATION SUBMITTED IN PARTIAL FULFILLMENT
OF THE REQUIREMENTS FOR THE DEGREE OF

DOKTOR INGENIØR

Department of Telecommunications
Norwegian University of Science and Technology

2002

Norwegian University of Science and Technology
Department of Telecommunications
N-7491 Trondheim
Norway

Doktor ingeniøravhandling 2002:18
Rapportnr. 420203

ISBN 82-471-5410-2
ISSN 0809-103X

Abstract

The need for spectrally efficient transmission on mobile and wireless channels is prevalent. A promising scheme for such transmission is adaptive coded modulation. In this thesis, techniques for assessing the performance of such systems are presented. One of the vulnerable points of such systems is the need for a reliable feedback channel. Channel prediction is proposed as a technique to combat the harmful effects of feedback delay.

The Nakagami distribution is often employed in a model for the fading envelope of a wireless channel; this leads to a gamma-distributed signal-to-noise ratio. Nakagami (1960) provides expressions for the probability density function (PDF) of the product, sum, and ratio of two correlated gamma-distributed random variables (RVs). However, such an expression for the difference between two such RVs has not been provided by Nakagami. A new expression for this PDF is provided in this dissertation, and it is shown that it is closely related to a distribution first described by McKay (1932). Applications of the new PDF include outage probability calculation in an environment with self-interference and assessment of the quality of certain channel estimation techniques.

Preface

This dissertation is submitted in partial fulfillment of the requirements for the degree of *doktor ingeniør* at the Department of Telecommunications, Norwegian University of Science and Technology (NTNU). My advisors have been Professor Geir E. Øien at Department of Telecommunications, NTNU and Professor II Kjell J. Hole at Department of Informatics at the University of Bergen (UiB).

The studies have been carried out in the period from January 1998 to February 2002. The work includes the equivalent of a year of full-time course studies and 14 months of being a teaching assistant in various undergraduate and graduate classes. Most of the time I spent at NTNU in Trondheim, but I have also spent shorter and longer periods in close collaboration with Prof. Hole at UiB—the longest taking place during the summer and autumn of 1999. From July 2000 to June 2001 I was invited to stay at the Department of Electrical and Computer Engineering at the University of Minnesota, Minneapolis, USA, where I was a part of Assistant Professor Mohamed-Slim Alouini's research group.

The work was funded by a scholarship from the Research Council of Norway, via the project Wideband Radio Access (WIRAC), under grant number 11939/43. For the one-year visit at the University of Minnesota, I received a grant from WIRAC. The teaching assistantship was funded by the Department of Telecommunications, NTNU.

Acknowledgments

I would like to thank my supervisors, Professor Geir E. Øien and Professor II Kjell J. Hole. Without their encouragement I would probably not have started on the PhD studies. The first part of the thesis, dealing with adaptive coded modulation, was at large done in cooperation with them. Assistant Professor Mohamed-Slim Alouini has also been a great help for me. His enthusiasm and knowledge, both in wireless communications and

in mathematics and statistics are invaluable. During the stay at the University of Minnesota his ideas, tips, pointers and suggestions enabled me to carry out the work that ended up as the second part of the thesis, dealing with statistical methods relevant to wireless communications.

I am also in debt to other researchers at NTNU, most notably Professor Peter Lindqvist and Professor Henning Omre at the Department of Mathematical Sciences. They have guided me in mathematical questions that were probably trivial to them, however far from obvious to me.

PhD studies should not only be dry research; a living and vital work environment is also essential. My colleagues in the Signal Processing Group at the Department of Telecommunications have provided that environment for me. I will miss the elevated discussions during lunch, the wine meetings, and the Julebord. In particular, I will thank my office mate Hallstein Lervik who has showed me how the smallest gear in a clockwork can be vital for correct operation.

During the year in Minnesota I made many friends. I hope the people that showed up at my good-bye party didn't do that only because they were happy I was leaving; I might come back to bother them again.

During the last stages of the preparation of the dissertation I had invaluable help from some non-experts; Jan B. Tønnessen and Basobi Patel helped me untangle some of the longer and more incomprehensible sentences.

Lastly, I would like to thank family and my parents, Otto and Ada Lill Holm for their support and encouragement.

Trondheim, February 2002
Henrik Holm

Contents

Figures

Tables

Notation and Symbols

Vectors are usually written in bold, upright, lowercase, whereas matrices are in bold uppercase. Compare "x", "$\mathbf{x}$", "X", and "$\mathbf{X}$". Vectors are column vectors, unless otherwise explicitly defined.

In the occasions where it is important to separate a random variable (RV) from the corresponding realization, uppercase letters are used for RVs and lowercase for the realization. This applies chiefly to the second part of the dissertation. However, it is not always feasible to do this—such a practice may for instance conflict with the convention of writing vectors as lowercase and matrices as uppercase. Also, the usage of uppercase Greek letters can be more confusing than clarifying. In conflicting cases, arising mainly in the first part of the dissertation, the lowercase vector/uppercase matrix notation is pursued.

Some symbols are used only short-term during a proof, a lemma, a small identity or formula, etc. Such symbols are not defined in this list of symbols.

There is no general accepted consensus regarding the terminology of "whole numbers"—in this thesis, the terminology suggested on the WWW site `http://mathworld.wolfram.com/WholeNumber.html` is followed.

x^*	Complex conjugate
$\mathbf{x}^\mathsf{T}$	Transpose
$\mathbf{x}^\mathsf{H}$	Hermitian (conjugate transpose)
$\mathbf{X}^{-1}$	Matrix inversion
$\lvert x \rvert$	Absolute value
$\lVert \mathbf{x} \rVert$	Norm of a vector, $\sqrt{\mathbf{x}^\mathsf{H}\mathbf{x}}$
$[\mathbf{x}]_k$	Element number k in the vector $\mathbf{x}$
$[\mathbf{X}]_{mk}$	Element in row m and column k of the matrix $\mathbf{X}$

$(\cdot)!$	Factorial
α	1. Channel gain 2. Shape parameter to the gamma distribution
$\alpha(k)$	Channel gain at time k
α_h, $\alpha_h(k)$	Branch gain (at time k)
$\hat{\alpha}$	Predicted channel gain
$\hat{\alpha}_h$	Predicted branch gain
β	1. Ratio between minimum squared Euclidean distance of a code and of a signal constellation, namely d_E^2/d_0^2 2. Scale parameter to the gamma distribution
β_1, β_2	1. Scale parameters to the bivariate gamma distribution 2. Scale parameters of two independent gamma-distributed RVs
γ	1. Channel signal-to-noise ratio (CSNR) 2. Signal-to-interference-and-noise ratio (SINR)
γ_h	CSNR on antenna branch h
γ^*	The fixed CSNR of an AWGN channel
γ_n	The lowest CSNR attaining the target BER when code n is used
γ_n^l	The lowest CSNR for which the exponential approximation to the BER–CSNR relationship is relevant when code n is used
$\bar{\gamma}$, $\bar{\gamma}_h$	Expected value of the CSNR (on antenna branch h)
$\hat{\gamma}$	Estimated/predicted CSNR
$\bar{\hat{\gamma}}$	Expected value of the estimated CSNR
γ_{th}	SINR threshold, below which an outage occurs
$\Gamma(\cdot)$	Gamma function
$\Gamma(\cdot,\cdot)$	Complementary incomplete gamma function
Δ, δ	Symbol used to denote the RV (and the corresponding realization) arising from subtracting two gamma-distributed RVs

Δ_{dB}, δ_{dB}	The RV (and corresponding realization) arising when subtracting two gamma-distributed RVs measured in dB
$\theta(k)$	Phase component of the fading at time instant k
λ	Wavelength
μ_Z	Mean of the RV Z
ρ	Correlation coefficient
Σ, σ	Symbol used to denote the RV (and the corresponding realization) arising from adding two gamma-distributed RVs
σ_n^2	Noise variance
σ_Z^2	Variance of the RV Z
$\sigma_{e(j)}^2$	Error variance with a feedback delay of jT_s
τ	Feedback delay (in real time)
Φ, ϕ	The fraction of two gamma-distributed RVs (and the corresponding realization)
Ω	Variance of the fading on one antenna branch
$\widehat{\Omega}$	Variance of the predicted fading on one antenna branch
a	One of the parameters in the McKay distribution
a_n	Parameter in exponential approximation to the BER–CSNR relationship for code no. n
a_p	Pilot symbol amplitude
$\mathbf{A}$	Matrix holding the transmitted pilot symbols
$\mathcal{A}$	Region in a quadrant of a QAM/CROSS constellation
b	One of the parameters in the McKay distribution
b_n	Parameter in exponential approximation to the BER–CSNR relationship for code no. n
B	Transmission bandwidth
$\mathcal{B}_1$, $\mathcal{B}_2$	Regions in a quadrant of a CROSS constellation

BER	Bit error rate (BER)
BER_0	Target BER
$\overline{\text{BER}}$	Average BER
$\overline{\text{BER}}_n$	Average BER when code n is used
$\text{BER}_n(\gamma \mid \hat{\gamma})$	BER for a CSNR of γ when the predicted CSNR is $\hat{\gamma}$.
c	1. Speed of light, $c = 3 \cdot 10^8\,\text{m/s}$ 2. One of the parameters in the McKay distribution
$\text{Cov}(\cdot,\cdot)$	Covariance
d_E	Minimum Euclidean distance between code words
d_0	Minimum Euclidean distance between symbols in signal constellation
G	Number of channel symbols per code symbol
$E[\cdot]$	Expectation
E_{avg}	Average energy of the symbols in a QAM constellation
E_i	Energy of symbol no. i in a QAM constellation
E_{cr}	Average energy of the symbols in a CROSS constellation
$E_{8\text{-}cross}$	Average energy of the symbols in the 8-CROSS constellation
E_{sq}	Average energy of the symbols in a square QAM constellation
$f_A(a)$	Univariate probability density function (PDF)
$f_{A,B}(a,b)$	Bivariate PDF
$F_A(a)$	Cumulative distribution function (CDF)
f_c	Carrier frequency
f_D	Doppler frequency
$f_{j,h}(k)$	Predictor filter coefficient
$\mathbf{f}_{j,h}$	Vector of predictor filter coefficients
$\mathbf{f}_{j,\text{MAP}}$	MAP optimal predictor filter coefficients

${}_2F_1(\cdot,\cdot;\cdot;\cdot)$	Gauss' hypergeometric function
$\mathcal{G}(\alpha,\beta)$	Gamma distribution
$\mathcal{G}(\alpha,\beta_1,\beta_2,\rho)$	Bivariate gamma distribution
h	Subchannel (antenna branch) index
H	Number of antenna branches
$H(\cdot)$	Heaviside (unit step) function
$\mathbf{I}$	Identity matrix
$I_\nu(\cdot)$	Modified Bessel function of the first kind and of order ν
$I_x(\cdot,\cdot)$	Normalized incomplete Beta function
$\mathcal{I}1(n)$	Component in the expression for $\overline{\mathrm{BER}}_n$
$\mathcal{I}21(n)$	Component in the expression for $\overline{\mathrm{BER}}_n$
$\mathcal{I}22(n)$	Component in the expression for $\overline{\mathrm{BER}}_n$
j	1. Feedback delay (measured in number of transmission periods) 2. Imaginary unit
$J_\nu(\cdot)$	Bessel function of the first kind and of order ν
$\mathcal{J}1(n,\hat{\gamma})$	Component in the expression for $\overline{\mathrm{BER}}_n$
$\mathcal{J}21(n,\hat{\gamma})$	Component in the expression for $\overline{\mathrm{BER}}_n$
$\mathcal{J}22(n,\hat{\gamma})$	Component in the expression for $\overline{\mathrm{BER}}_n$
k	1. Time index 2. Number of bits that can be conveyed by a QAM constellation
k_n	Number of transmitted bits when signal constellation no. n is used.
K	The number of pilot symbols the prediction is based upon; predictor filter length
$K_\nu(\cdot)$	Modified Bessel function of the second kind and of order ν
L	Distance (counted in number of channel uses) between two consecutive pilot symbols

m	1. Nakagami parameter 2. Time index
M, M_n	Number of symbols in a signal constellation (in constellation no. n)
n	1. Code number/CSNR bin number 2. Noise 3. Time index
$n(k)$	Noise at time instant k
n_h, $n_h(k)$	Noise in antenna branch h (at time instant k)
$\mathbf{n}_h$	Noise disturbing the channel (branch h) at pilot symbol instants
N	Number of codes utilized in the adaptive transmission scheme
N_0	Noise spectral density
p	Number of information bits used to generate a $2G$-D code symbol
P	1. Average transmit power 2. A number associated with the number of symbols along a quadrature component (in Appendix A)
P_n	Probability that code n is used
P_{out}	Outage probability
$Q(\cdot)$	Area under the tail of the standardized Gaussian distribution
$Q(\cdot,\cdot)$	Normalized incomplete gamma function
$Q_H(\cdot,\cdot)$	Nuttall function, AKA the generalized Marcum Q-function, AKA the non-central chi-square distribution
r	Ratio between the predicted and the actual CSNR—equivalently, between the predicted and actual variance of the fading

$\mathbf{r}_j$	Vector containing the normalized correlation between the fading at pilot symbol instants and the fading to be predicted
$\mathbf{r}_{z,y}$	Cross correlation vector
$R(\cdot)$	Normalized autocorrelation function
$\mathbf{R}$	Normalized correlation matrix
$\mathbf{R}_y$	Autocorrelation matrix for the process y
$\mathbf{R}_n$	Noise correlation matrix
R_n	Information rate (the number of information bits per channel symbol) of code no. n.
$\mathrm{Re}(z)$	The real part of the complex argument $z = x + jy$
$\bar{S}$	Average fading power
S_D, $\bar{S}_D$	Power of desired signal in an environment with interference, average power
S_I, $\bar{S}_I$	Power of interfering signal, average power
T_s	Time between transmission of two consecutive 2-D channel symbols
v	Terminal speed
$\mathrm{Var}(\cdot)$	Variance
w_{d_E}	The average number of information bit errors associated with codewords of distance d_E from the correct one
x	1. Transmitted channel symbol 2. realization of a gamma-distributed RV
X	Gamma-distributed RV
$x(k)$	Transmitted channel symbol at time k
X_1, x_1, X_2, x_2	Gamma-distributed RVs and corresponding realizations
y, $y(k)$	Received symbol (at time k)
y_h, $y_h(k)$	Symbol received on antenna branch h (at time k)
$\mathbf{y}_h$	Set of channel observations on branch h

z, $z(k)$	Complex fading (at time k)
z_h, $z_h(k)$	Complex fading on antenna branch h (at time k)
$\mathbf{z}_h$	Vector of the fading at the pilot symbol instants, on branch h
$\tilde{z}_h(k)$	ML estimate of the fading based on one received observation on branch h
$\tilde{\mathbf{z}}$	Vector of ML fading estimates
$\tilde{\mathbf{z}}_{h,n}$	Vector of ML estimates on branch h, up to time index n
$\hat{z}$	Prediction or estimate of the fading
$\hat{z}_h(k)$	Prediction of the fading on branch h at time k
$\hat{z}_{\mathrm{MAP}}$	MAP optimal prediction of the fading
$\mathcal{Z}_\nu(\cdot)$	Generalized modified Bessel function
$\mathbb{Z}$	The set of integers $\{\dots, -2, -1, 0, 1, 2, \dots\}$
$\mathbb{Z}^\star$	The set of non-negative integers $\{0, 1, 2, \dots\}$
$\mathbb{Z}^+$	The set of positive integers $\{1, 2, \dots\}$

Abbreviations

2-D	2-dimensional
ACM	Adaptive coded modulation
AR	Auto-regressive
ASE	Average spectral efficiency
AWGN	Additive white Gaussian noise
BER	Bit error rate
CDF	Cumulative distribution function
codec	Encoder and decoder
CROSS	Cross-shaped variant of a QAM constellation
CSI	Channel state information
CSNR	Channel signal-to-noise ratio
DA	data-aided
dB	Decibel
IEEE	Institute of Electrical and Electronics Engineers
LOS	Line-of-sight
MAP	Maximum a posteriori
ML	Maximum likelihood
MRC	Maximal ratio combining
MSED	Minimum squared Euclidean distance
NMF	Nakagami multipath fading
OFDM	Orthogonal frequency division multiplexing
PDF	Probability density function
PSAM	Pilot symbol assisted modulation
QAM	Quadrature amplitude modulation
RV	Random variable
SINR	Signal-to-interference-and-noise ratio
TCM	Trellis coded modulation
WSS	Wide-sense stationary

Chapter 1

Introduction to Adaptive Coded Modulation (ACM)

Today's society demands fast and reliable wireless radio communication, and the radio spectrum grows more and more crowded as a consequence of this. More spectrally efficient transmission schemes are therefore called for; being able to transmit more bits per Hz bandwidth can relieve the pressure on the bandwidth resources. One way of accomplishing this is by transmitting several bits of information per channel symbol, using quadrature amplitude modulation (QAM) and similar techniques (Hanzo, Webb, and Keller, 2000). The radio signal often propagates in a very hostile environment. Unfortunately, this makes spectrally efficient modulation difficult. For instance, the signal will frequently suffer from dispersion due to multipath transmission; transmission via different reflectors causes a large variety of propagation path delays. For wideband applications, the dispersion will cause inter-symbol-interference. The hostility of the wireless channel increases with the degree of mobility. When the receiver or the transmitter is moving, the interference pattern due to the multipath transmission will change. The effect of this is commonly known as fast multipath fading. In addition to specular reflection (caused by obstacles of size much greater than the radio wave length), also scattering (appearing when the radio waves interact with objects with dimension on the order of a wavelength or less) and diffraction (appearing when a radio wave "bends around" an obstacle) perturb the signal (Jamali and Le-Ngoc, 1994; Prasad, 1998; Stüber, 2001). Other contributors to the non-stationary nature of the radio channel are the slower log-normal shadowing and the change in path loss due to variation in the relative distance between transmitter and receiver. These mechanisms will not only affect wideband applications; narrowband radio

transmission will also be disturbed by a changing channel signal-to-noise ratio (CSNR). The multipath fading is for the narrowband case referred to as flat fading, also denoted as frequency nonselective fading. When the fading is flat, the bandwidth of the transmitted signal is smaller than the coherence bandwidth. In the time domain, this implies that the duration of a modulated symbol is much greater than the time spread of the propagation path delays. On the contrary, frequency-selective (or non-flat) fading arises when the bandwidth of the transmitted signal is greater than the coherence bandwidth. The flat fading of narrowband transmission is often modeled well by stochastic distributions, such as Rayleigh, Rice, or Nakagami (Nakagami, 1960; Prasad, 1998; Stüber, 2001). The Rice model represents the fading as a sum of a line-of-sight (LOS) component and an indirect scattered component—Rayleigh fading is the special case where no LOS component is present. Although a fading model exists that leads to the Nakagami fading formula (Yacoub, Bautista, and de Rezende Guedes, 1999), the model is referred to most often because of its experimental consistency (Sheikh, Handforth, and Abdi, 1993) and computational tractability. The Nakagami model also has Rayleigh as a special case, and the Nakagami and Rice distributions are closely related through certain values of their parameters (Nakagami, 1960). An advantage of the Nakagami over the Rice model is the relatively simple expression for the probability density function (PDF) and bivariate PDF of the received CSNR, since the power of a Nakagami-distributed signal is gamma-distributed. Indeed, while the gamma PDF contains no complicated special functions, the PDF of the signal power in the Rician case contains a modified Bessel function. On the other hand, the bivariate distribution of two correlated gamma-distributed random variables (RVs) has a relatively simple closed-form expression, while (to the best of the author's knowledge) no simple formula is yet known for the joint PDF of the power of two Rician RVs.

The changing CSNR exhibited by a fading channel can cause severe error bursts. A method for combating the channel quality fluctuation is adaptive transmission, utilizing a feedback channel to provide channel state information (CSI) at the transmitter. This is not a new idea. In 1971, Murakami and Nakagami suggested such a technique to combat the fading experienced in deep-space satellite-to-earth communication, by using the earth-to-satellite link as a feedback channel. One way of battling the decrease of the channel quality is to use channel inversion. Then the transmitter uses CSI in order to vary the transmitted power so as to keep the CSNR at the receiver constant. Alas, the high power requirements imposed by a deep fade will contribute to unpredictable co-channel interference. In addition, the transmitter will need to be able to transmit at very high power

levels. In fact, it is shown by Goldsmith and Varaiya (1997) that the capacity of a channel inversion scheme is zero. A different manner of adapting to the varying channel conditions is to vary the transmission rate. However, this technique suffers from a varying bandwidth, making it unsuitable when fixed bandwidth is required. A promising method is to vary the constellation size (Steele and Webb, 1991; Webb, Hanzo, and Steele, 1991) and the coding scheme (Goldsmith and Chua, 1998) according to the quality of the channel. Combinations of these methods with the other adaptive techniques have also been proposed (Goldsmith and Chua, 1997). For further references to adaptive modulation and coding techniques, look to the tutorial paper by Hole and Øien (2001).

Goldsmith and Varaiya (1997) have derived the channel capacity of a flat-fading single-user channel in terms of the PDF of the fading amplitude when perfect CSI is available both at the transmitter and the receiver at any time. The CSI in question is here the CSNR. The special case of Nakagami multipath fading (NMF) channel is discussed by Alouini and Goldsmith (1997). They obtain closed-form expressions for the capacity of such channels. Goldsmith and Varaiya also showed that the capacity of a channel with arbitrary fading distribution can be attained using a certain rate/power-adaptive transmission scheme in which the number of information bits per channel symbol is instantly and continuously updated according to the CSNR. It has also been shown that the capacity of a rate-adaptive system (with constant transmit power) approaches the capacity—with only a small decline in average transmission rate—of an optimal system. The instantaneous transmission rate of this scheme is high when the CSNR is high, decreasing smoothly as the CSNR decreases and going to zero below a threshold value.

A more practical adaptive modulation scheme was proposed by Goldsmith and Chua (1997); Alouini and Goldsmith (2000). This scheme is designed to operate at a bit error rate (BER) below a certain target (BER_0), having a certain set of transmission rates available, and where the transmit power is constant. Improving the performance of such a system has later been pursued by introducing channel coding (Webb *et al.*, 1991; Goldsmith and Chua, 1998). Goldsmith and Chua studied a practical variable-rate scheme based on multi-level QAM and Ungerboeck's trellis codes (Ungerboeck, 1982). This system utilizes a set of 2-dimensional (2-D) trellis codes with different rate.

An important aspect in phase-modulated communication systems is the coherent detection, i.e., that the receiver is able to detect the absolute phase of the incoming signal or that the constellation is rotationally invariant. The latter can be accomplished with differential encoding such that the re-

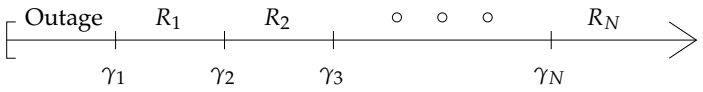

FIGURE 1.1: The CSNR range is split into $N+1$ CSNR bins. When the instantaneous CSNR falls in the lowest interval, an outage occurs; whereas in the upper N intervals, a code with rate R_n is employed.

ceiver only needs to detect the relative phase shifts in the incoming signal. As Webb *et al.* point out, the traditional square-shaped QAM constellations have the disadvantage that false phase locks can occur. However, the square QAM constellations are widely used and this thesis will henceforth concentrate on such constellations.

Hole, Holm, and Øien (2000) developed a technique in order to assess the performance merits of a general adaptive coded modulation (ACM) system on an NMF channel. In such a system, the transmitter will switch between signal constellations (and, in the case of coded transmission, channel codes) of varying size at discrete time instants. At a given time, the transmitter chooses symbols from the biggest constellation meeting the BER requirements for the available CSI, thus ensuring maximum spectral efficiency for the given acceptable BER.

The adaptive coder/modulator has available a set of N transmitter–receiver pairs, denoted as transmitter–receiver pair $n = 1, \ldots, N$. Transmitter n has a rate of R_n information bits per symbol, such that $R_1 < R_2 < \cdots < R_N$. The CSNR range[1] is split into $N+1$ *CSNR bins*, as depicted in Figure 1.1, and transmitter–receiver pair n is to be used when CSNR γ falls in the interval $[\gamma_n, \gamma_{n+1}\rangle$. Here, γ_n is—for each $n = 1, \ldots, N$—chosen as the lowest CSNR necessary for transmitter–receiver pair n to be able to operate at a BER below the designer-specified target bit error rate, BER_0, at transmit power P. Letting $\gamma_0 = 0$ and $\gamma_{N+1} = \infty$ results in $\gamma_{n+1} > \gamma_n$ for all $n \in \{0, \ldots, N\}$. No available transmitter–receiver pair satisfies the BER requirement when the CSNR is lower than bin γ_1; hence, no information is transmitted when γ falls in the interval $[0, \gamma_1\rangle$, and there will consequently be an outage during which information must be buffered at the transmitter end.

Note that a system as the one described above relies on accurate CSI, which has to be estimated at the receiver and then conveyed to the transmitter through a feedback channel. This process is prone to several types of errors:

[1] Most of the calculations are done based on the CSNR γ and not on the square of the fading envelope α^2 or even α. The calculations are then substantially simpler to perform.

- Depending on the estimation method, the CSNR estimate will exhibit some inaccuracy.

The receiver will need time to process and generate the CSNR estimate, the feedback channel is subject to some transmission delay, and lastly the transmitter may need some time before the updated CSNR estimate can be utilized to choose a more appropriate code. The total delay will be referred to at "feedback delay".

- Due to the feedback delay, it is probable that the transmitter will operate employing outdated CSI.

- There is a probability of errors in the feedback channel.

Of these possible error sources, the last one is the most harmful; an error in the feedback channel will cause the transmitter and receiver to operate on different codes, effectively disenabling correct decoding. However, since it is sufficient to feed back the CSNR bin index only—yielding an information of at most $\log_2(N+1)$ bits—it is fairly easy to protect the fed back CSI with a strong error control code. In the systems discussed in this thesis, the feedback channel is assumed to be error-free.

A non-data-aided method (Meyr, Moeneclaey, and Fechtel, 1998) for estimation of the channel quality is based on the received signal strength indicator (Steele and Webb, 1991; Webb and Steele, 1995) where the average magnitude of the baseband signal level is monitored in order to provide an indication of the CSNR. Data-aided (DA) methods (again Meyr *et al.*, 1998), in which training symbols are inserted into the data sequence, are able to provide a more accurate estimate than non-data-aided methods. Unfortunately, DA methods exhibit lower spectral efficiency since the inserted training symbols do not convey information. However, obtaining accurate CSI is imperative for satisfactory performance of an ACM system, and it is therefore chosen to pursue a data-aided method here. Cavers (1991) proposes one such method in which regularly spaced pilot symbols are inserted into the data. Pilot symbol assisted modulation schemes have since been investigated, for instance by Torrance and Hanzo (1995) and Tang, Alouini, and Goldsmith (1999).

Since the feedback delay can be made predictable, it makes sense to attempt to take into consideration the full feedback delay. This involves predicting the CSNR at the time instant in the future when the transmitter is able to change to the most favorable code. Thus, in order to compete the two first error sources, a system using prediction based upon received pilot symbols will be proposed.

When studying processes that are described by the Nakagami distribution, it is advantageous to have good knowledge of its derivatives, and to assess their statistical properties. While investigating the properties of an estimate of a Rayleigh random variable (RV), it turned out that an expression for the PDF of two correlated gamma-distributed RVs would be helpful. Nakagami (1960) supplies formulas for the PDF of the product and ratio of two Nakagami-distributed RVs, and also a formula for the square root of the sum of the squares of two correlated Nakagami-distributed RVs. In addition, the PDF of the sum and difference between two *uncorrelated* gamma-distributed RVs is known, and it can be shown that the sum and difference follows the two forms of a distribution known in the literature as McKay's distribution (McKay, 1932; Bhattacharyya, 1942; Johnson, Kotz, and Balakrishnan, 1994). However, to the best of the author's knowledge, the PDF of the difference between two correlated gamma-distributed RVs has not yet been found. The second part of this thesis proceeds to find an expression for this PDF in closed-form. It will be shown that also the sum and difference of two correlated gamma-distributed RVs are described by the two forms of McKay's distribution. In addition, expressions for the moments of this distribution is provided, and an important special case—related to Rayleigh fading—is scrutinized in order to obtain especially simple expressions. In the special case, closed-form expressions are found for the moments of McKay's distribution and also for the cumulative distribution function (CDF).

The dissertation is largely based on a collection of papers. Every chapter starts with a note on where the material have appeared, or where it is submitted. In particular, the main contributions of Chapter 3 have not yet been submitted for publication. Some modifications to the material in the other chapters have been made, mostly to provide a common notation and to avoid overlap. Nevertheless, there is some overlap between the chapters, mostly in the introductory sections. Also, some symbols have several meanings, as is reflected in the list of notations that is provided. However, it should be clear what each symbol means from its context.

The remainder of the dissertation is organized as follows: In Part I, the technique proposed by Hole *et al.* (2000) is discussed. Chapter 2 applies the technique in order to evaluate the average spectral efficiency of a coding scheme utilizing any set of multi-dimensional trellis codes originally designed for additive white Gaussian noise (AWGN) channels. Chapter 3 discusses a method of predicting the future CSI with the aid of regularly transmitted pilot symbols, and then proceeds to investigate how different estimation parameters and channel parameters affect important system performance merits.

In Part II of the thesis, the formulas related to McKay's distribution are presented as theorems in Chapter 4, as are expressions for the PDF of the sum and difference of two correlated gamma-distributed RVs. The chapter concludes with presenting an application of this new result related to outage probability calculations in a self-interfering environment. Chapter 5 then proceeds to employ some of the results from the previous chapter in assessing the quality of certain estimators.

The last chapter, Chapter 6, draws some conclusions, outlines the main contributions of the thesis, and suggests some areas for further research.

There are, in addition to the regular chapters, four appendices in this thesis. Appendix A provides closed-form expressions for the average energy of a QAM constellation, for a variant of the QAM constellation called a CROSS constellation, and lastly for a special constellation called 8-CROSS. These formulas are employed in Chapter 2. In Chapter 3, some statistical properties of a predicted fading amplitude are needed; these properties are provided in appendix B. Appendix C then provides expressions to aid in finding the BER of an ACM system utilizing prediction. Appendix D is the last appendix of the thesis, in which proofs of the theorems in Chapter 4 are provided.

Part I

Adaptive Coded Modulation

Chapter 2

Spectral Efficiency of ACM under Perfect Channel Knowledge

This chapter is based on a paper presented at the conference *NORSIG* (Holm, Hole, and Øien, 1999) and a paper that have appeared in *IEEE J. Select. Areas Commun.* (Hole, Holm, and Øien, 2000).

2.1 Introduction

The purpose of this chapter is to obtain an expression for the average spectral efficiency (ASE) of a general variable-rate coding scheme for Nakagami multipath fading (NMF) channels. Let G be some positive integer. The coding scheme can utilize any set of $2G$-dimensional ($2G$-D) trellis codes originally designed for additive white Gaussian noise (AWGN) channels.

The chapter is organized as follows: In Section 2.2, we give a brief overview of the system model. We then show, in Section 2.3, that there exists a simple expression characterizing the relationship between the CSNR and the bit-error-rate (BER) for trellis codes on AWGN channels. In Section 2.4, the BER–CSNR relationship is employed to approximate the ASE of the general variable-rate coding scheme. As an example, we use our technique to approximate the ASE of a specific variable-rate encoder and decoder (codec) in Section 2.5. A discussion follows in Section 2.6.

2.2 System Overview

We model the NMF as a multiplication of the transmitted signal by a time-varying factor. The signal is then disturbed by AWGN. Thus, the receiver reads a signal with a time-varying CSNR. The probability density function (PDF) of the instantaneous received CSNR, γ, is found to be (Alouini and Goldsmith, 2000):

$$f_\gamma(\gamma) = \left(\frac{m}{\bar{\gamma}}\right)^m \frac{\gamma^{m-1}}{\Gamma(m)} \exp\left(-m\frac{\gamma}{\bar{\gamma}}\right), \quad \gamma \geq 0 \tag{2.1}$$

where $\bar{\gamma}$ is the expected value of the CSNR and m is the Nakagami fading parameter, a positive number $m \geq 1/2$.

It is known that a variable-rate codec based on trellis codes originally designed for AWGN may be used on a NMF channel (Goldsmith and Chua, 1997, 1998; Goldsmith and Varaiya, 1997; Alouini and Goldsmith, 2000; Hole *et al.*, 2000). We consider a general codec that utilizes a set of N different $2G$-D trellis codes for AWGN. The codes are based on 2-D QAM signal constellations with different number of symbols $M_n = 2^{k_n}$, where k_n is some positive integer and $n = 1, 2, \ldots, N$. For $n < N$, $M_n < M_{n+1}$, thus the codes have different robustness against noise. The $2G$-D code symbols are transmitted as G consecutive 2-D modulation symbols, each drawn from one of the QAM constellations. An illustration of such a constellation of size $M = 256$ is shown in Fig. 2.1, where the minimum Euclidean distance between the modulation symbols is denoted by d_0.

If the N constellations are nested within each other, as indicated in Fig. 2.1, then it is possible to design an encoder/ decoder-structure which is able to encode and decode all N codes (Goldsmith and Chua, 1998). Consequently, the hardware complexity is reduced considerably compared to a system where a separate encoder and decoder are needed for each of the codes.

As an example, we consider a variable-rate encoder and a variable-rate Viterbi decoder based on the International Telecommunications Union ITU-T V.34 modem standard. The codec utilizes $N = 8$ nested QAM signal constellations containing 4, 8, 16, 32, 64, 128, 256, and 512 symbols to encode and decode eight 4-D trellis codes (Hole *et al.*, 2000). The seven smallest constellations are the ones shown in Fig. 2.1.[1]

To determine a good variable-rate codec, the relationship between the CSNR and BER on an AWGN channel must be known for the different

[1]The 512-QAM constellation is omitted from the figure due to space and visibility requirements.

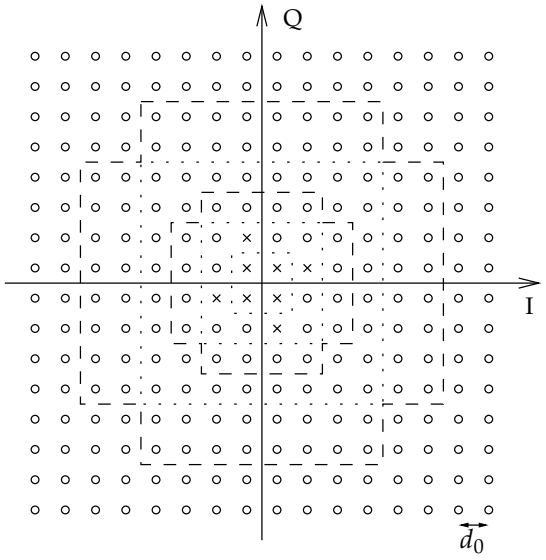

FIGURE 2.1: QAM constellation with 256 symbols. The 4, 8, 16, 32, 64, and 128 symbol constellations are nested within the 256-QAM constellation. The crosses constitute the 8 symbol constellation.

codes. The BER performance of the codes used in the example codec have been simulated, and the BER for different CSNRs are plotted in Fig. 2.2, represented by boxes. It is shown in Section 2.3 that a simple exponential function approximates the BER–CSNR relationship closely, as indicated by the solid lines in Fig. 2.2. The function is invertible, so the smallest CSNR required to achieve a given target BER, denoted by BER_0, can be found.

Assume that N quantization regions (or CSNR bins) are used to represent the instantaneous received CSNR on the NMF channel. For each code n, the smallest CSNR required to guarantee the target BER_0 is denoted by γ_n. The set $\{\gamma_n\}_{n=1}^{N}$ constitutes the lower thresholds for the N CSNR bins.

Let T_s be the time between the transmission of two consecutive 2-D modulation symbols. Every $G \cdot T_s$ seconds, the receiver estimates the value of the instantaneous CSNR to determine which code $n \in \{1, 2, \ldots, N\}$ to use. The receiver then utilizes a feedback channel to inform the transmitter of its decision. We assume here that the feedback channel is both delay-free and error-free. The encoder requests $p = G \cdot k_n - 1$ information bits, and generates $p + 1 = G \cdot k_n$ coded bits. The coded bits determine G transmittable 2-D modulation symbols from the signal constellation with $M_n = 2^{k_n}$ symbols.

The information rate for code n, measured in information bits per channel use, is equal to $R_n = p/(G \cdot T_s \cdot B) = (k_n - 1/G)/(T_s B)$, where B is

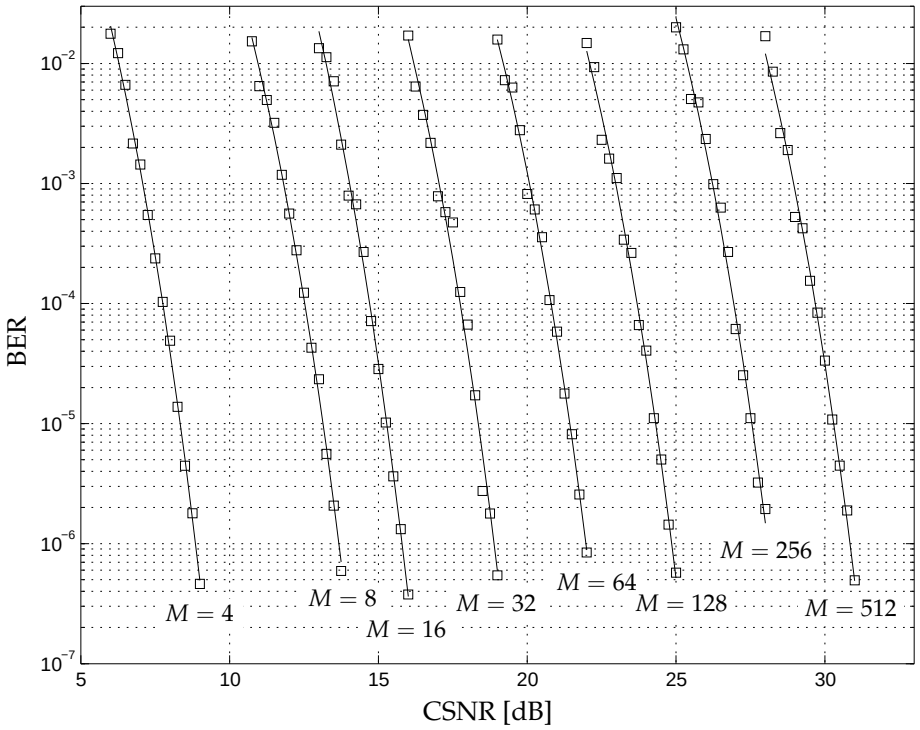

FIGURE 2.2: CSNR/BER relationship for example codec. The boxes represent simulated BER, and the solid lines represent the values obtained from a simple exponential function.

the signalling bandwidth. Assuming ideal Nyquist pulses, the bandwidth used is $B = 1/T_s$, and the spectral efficiency of code n is equal to

$$R_n = k_n - 1/G \tag{2.2}$$

measured in bits/s/Hz (or equivalently, in bits per channel symbol). The codes should have spectral efficiencies which increase with γ, i.e., $k_n < k_{n+1}$ for $n = 1, 2, \ldots, N-1$. This makes it possible to transmit at high spectral efficiency when the instantaneous received CSNR is high and to reduce the spectral efficiency as the CSNR decreases.

2.3 Approximation of BER–CSNR Relationship

In this section, we show that the BER for a 2G-D trellis code on an AWGN channel can be approximated by the expression

$$\text{BER} \approx a \cdot \exp\left(-\frac{b\gamma^*}{M}\right) \tag{2.3}$$

where γ^* is the fixed CSNR, the constants a and b are determined by the weight distribution of the trellis code, and $M = 2^k$ is the size of the signal constellation for some integer k.

An approximation of the BER for a trellis code in AWGN in terms of the area under the standardized Gaussian tail is (Wicker, 1995, Eq. 14-21):

$$\text{BER} \approx \frac{w_{d_E}}{p} Q\left(\sqrt{\frac{d_E^2}{2}\gamma^*}\right) \tag{2.4}$$

where d_E^2 is the minimum squared Euclidean distance (MSED) between any two code words and w_{d_E} is the average number of information bit errors associated with the codewords in squared distance d_E^2 from the correct one. The number of information bits per 2G-D code symbol is given by p. Using the upper bound $Q(y) \leq 1/2 \exp(-y^2/2)$, we find that

$$\text{BER} \approx \frac{w_{d_E}}{2p} \exp\left(-\frac{d_E^2}{4}\gamma^*\right). \tag{2.5}$$

Forney, Jr., Gallager, Lang, Longstaff, and Qureshi (1984) have calculated approximations for the average energy of QAM constellations with $d_0 = 2$. In Appendix A, Eq. (A.15), we determine exact expressions for the average energy of QAM constellations with arbitrary d_0 and size $M = 2^k$:

$$E_{avg} = \begin{cases} \frac{1}{6}d_0^2(M-1) & \text{for even } k \geq 2 \\ \frac{1}{6}d_0^2\left(\frac{40}{32}M - 1\right) & \text{for } k = 3 \\ \frac{1}{6}d_0^2\left(\frac{31}{32}M - 1\right) & \text{for odd } k \geq 5 \end{cases} \tag{2.6}$$

(Sterian (1997) obtained the expression in Eq. (2.6) for the special case $d_0 = 2$ and $k \geq 4$.) For all k, an approximation for E_{avg} is $(1/6)d_0^2 M$, and we therefore have that

$$d_0^2 \approx \frac{6E_{avg}}{M}. \tag{2.7}$$

The MSED is linearly dependent on d_0^2, and it may be written as $d_E^2 = \beta d_0^2$ for some positive real β. Substituting Eq. (2.7) for d_0^2, we find

$$d_E^2 \approx \frac{6\beta E_{avg}}{M}. \tag{2.8}$$

Substituting Eq. (2.8) in Eq. (2.5), we obtain the following approximation for BER,

$$\text{BER} \approx \frac{w_{d_E}}{2p} \exp\left(-\frac{3\beta E_{avg}}{2}\frac{\gamma^*}{M}\right) \tag{2.9}$$

which has the desired form (Eq. 2.3) for $a = w_{d_E}/2p$ and $b = 3\beta E_{avg}/2$.

The approximation in Eq. (2.4) is only valid for large CSNR, and so is the approximation in Eq. (2.9). However, plots of BER found in the literature (Biglieri, Divsalar, McLane, and Simon, 1991) (see also Fig. 2.2) strongly indicate that we can use curve fitting techniques to determine values for a and b so that the expression can be used with good accuracy also for medium and low CSNRs.

The proposed variable-rate coding scheme utilizes N trellis codes originally designed for AWGN channels. As we shall see in the next section, good values of the a and b parameters in Eq. (2.3) are needed for each code n in order to approximate the ASE of the proposed coding scheme. We assume that a simulation of the BER performance and a curve fitting technique are used to obtain good parameter values, denoted by a_n and b_n, for each code.

2.4 Approximation of the ASE

The variable-rate coding scheme for NMF channels uses a set of N different trellis codes with spectral efficiencies $k_n - 1/G$. The ASE is the weighted sum of the information rates $R_n = k_n - 1/G$ for the individual codes. The weight factors are here the probability P_n that code n is used, i.e., the probability that the CSNR falls in the CSNR bin n:

$$\text{ASE} = \sum_{n=1}^{N} R_n \cdot P_n = \sum_{n=1}^{N} (k_n - 1/G) P_n. \tag{2.10}$$

In order to calculate the probabilities P_n in Eq. (2.10), the thresholds γ_n for the CSNR bins must be known. Each code has a BER–CSNR relationship given by Eq. (2.3) with known a_n and b_n parameters. Thus, it is possible to calculate the smallest CSNR value γ_n which guarantees that the

target BER_0 is achieved for code n. Substituting γ_n, M_n, a_n, b_n for γ^*, M, a, b in Eq. (2.3) and solving for γ_n, we obtain

$$\gamma_n = \frac{M_n}{b_n} \ln(a_n/\mathrm{BER}_0), \quad n = 1, 2, \ldots, N \tag{2.11}$$

where $M_n = 2^{k_n}$.

For Nakagami fading, the probability $P_n = \int_{\gamma_n}^{\gamma_{n+1}} f_\gamma(\gamma) d\gamma$ that the CSNR falls in CSNR bin n is given by Alouini and Goldsmith (2000, Eq. 34):

$$P_n = \frac{\Gamma\left(m, \frac{m\gamma_n}{\bar{\gamma}}\right) - \Gamma\left(m, \frac{m\gamma_{n+1}}{\bar{\gamma}}\right)}{\Gamma(m)} \tag{2.12}$$

where m is the Nakagami fading parameter and $\Gamma(\cdot, \cdot)$ is the complementary incomplete gamma function (see Temme, 1996, Eq. 11.2). The upper threshold for CSNR bin N is $\gamma_{N+1} = \infty$.

For the special case when m is a positive integer, $\Gamma(m) = (m-1)!$. Furthermore, there exists a closed-form expression for $\Gamma(\cdot, \cdot)$ (Temme, 1996, Eq. 11.6):

$$\Gamma(m, \mu) = (m-1)!\, e^{-\mu} \sum_{i=0}^{m-1} \frac{\mu^i}{i!} \tag{2.13}$$

where $m = 1, 2, \ldots$ and $\mu \geq 0$.

2.5 Example Codec

We assume that the example codec described in Section 2.2 is operating on a NMF channel. Values of the a_n and b_n parameters for this codec are tabulated in Table 2.1. The thresholds γ_n calculated from Eq. (2.11) are also listed in the table for target $\mathrm{BER}_0 = 10^{-3}$. The ASE of the example codec may now be calculated from Eq. (2.10) and Eq. (2.12). The spectral efficiency for Nakagami fading parameter $m \in \{1, 2, 4\}$ is plotted in Fig. 2.3 as a function of the average received CSNR $\bar{\gamma}$ in dB.

Hole *et al.* (2000) showed, utilizing the closed-form expression obtained by Alouini and Goldsmith (2000, Eq. 20), that the ASE of the example codec lies about 1.8 bits/s/Hz from the maximum ASE.

2.6 Discussion

We see from Fig. 2.3 that the variable-rate codec obtains both a large ASE and a small target BER because it is able to exploit the time-varying nature of the instantaneous received CSNR. To design a fixed-rate coding

TABLE 2.1: Parameters a_n and b_n for example codec and calculated thresholds γ_n for $\mathrm{BER}_0 = 10^{-3}$.

n	M_n	a_n	b_n	γ_n (dB)
1	4	896.0704	10.7367	7.1
2	8	404.4353	6.8043	11.8
3	16	996.5492	8.7345	14.0
4	32	443.1272	8.2282	17.0
5	64	296.6007	7.9270	20.1
6	128	327.4874	8.2036	23.0
7	256	404.2837	7.8824	26.2
8	512	310.5283	8.2425	29.0

scheme that guarantees the same BER, it is necessary to design a code that achieves the target BER for the minimum observed CSNR. This conservative design choice results in a small spectral efficiency. This was first observed by Goldsmith and Chua (1998). They compared the ASE of variable-rate trellis-coded QAM with that of fixed-rate trellis codes designed for Rayleigh-fading channels and showed that rate adaption may save up to 20 dB in average received CSNR, dependent on the BER requirements.

For satisfactory operation of the variable-rate coding scheme, both the variable-rate encoder and the variable-rate decoder must use the same code at any instant. A fast and error-free feedback channel is therefore essential to ensure error-free signalling between the encoder and decoder. The effect of time delay in the feedback channel has been explored earlier by Alouini and Goldsmith (2000).

During periods of small CSNR, the throughput may be low. A buffer is therefore required at the transmitter. The appropriate size of this buffer is a subject for further research.

The investigations in this chapter are done for single-user NMF channels only. A natural extension is to examine variable-rate coding schemes for cellular systems.

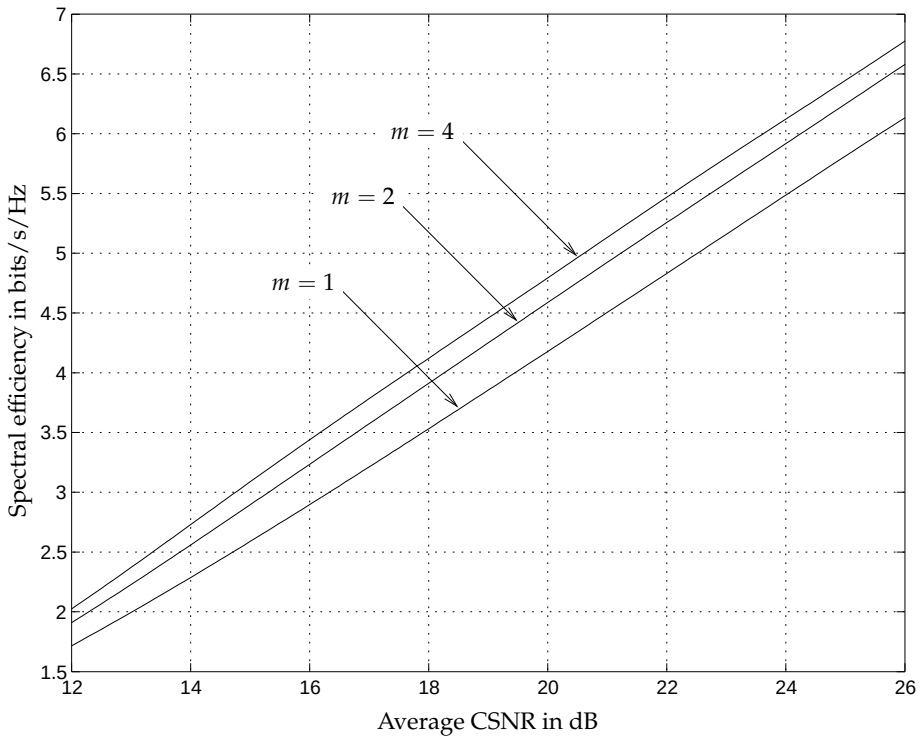

FIGURE 2.3: Approximation of ASE for example codec ($\mathrm{BER}_0 = 10^{-3}$).

Chapter 3

Channel Prediction with Antenna Diversity

The parts of this chapter considering calculations of BER under imperfect CSI is based on a paper presented at the conference *Mobile Communications Summit (IST)* (Hole, Holm, and Øien, 2001), and on an extended version which will appear in the Norwegian journal *Telektronikk* (Hole, Holm, and Øien, 2002). The parts considering linear prediction is based on a paper submitted to the *European Signal Processing Conference* (Øien, Holm, and Hole, 2002).

3.1 Introduction

The previous chapter described an adaptive coded modulation (ACM) system where the transmitter had perfect knowledge of the channel. A more practical scheme will have to incorporate some channel estimation technique and a feedback channel with nonzero delay. The model will be extended to take into account imperfect channel estimation and delay between the time when the channel is estimated and the time when the channel state information (CSI) can be utilized.[1]

To improve the reliability of signal detection, a technique called pilot symbol assisted modulation (PSAM) has been suggested as an aid in channel estimation (Cavers, 1991; Torrance and Hanzo, 1995; Tang *et al.*, 1999). Here, pilot symbols are regularly inserted into the data stream. PSAM is

[1]Note that the "feedback delay" does not consist of the actual transmission delay only; it will also incorporate the time it takes to perform the estimation and the processing time needed by the transmitter to activate the code fulfilling the BER requirements. For simplicity, the sum of these delays is referred to as feedback delay.

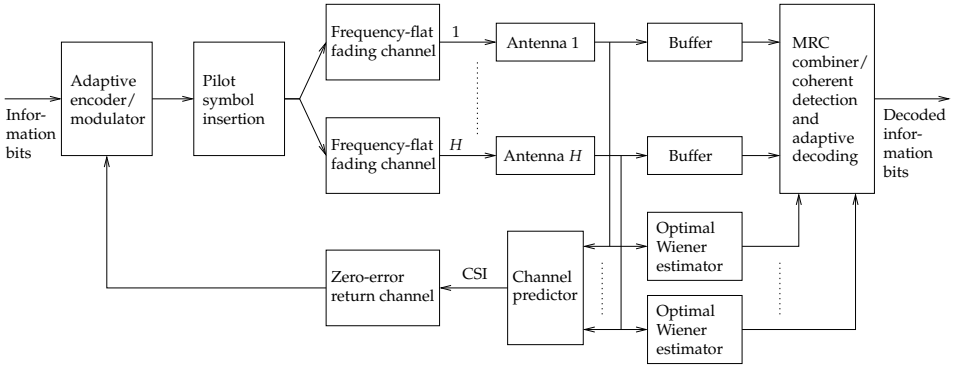

FIGURE 3.1: Adaptive coded modulation system with pilot symbol assisted channel estimation (for coherent detection purposes) and prediction (for transmitter adaptation purposes).

also well suited for channel estimation in an ACM system. The requirements of the estimation technique are then slightly different from the signal detection case. The feedback delay should be taken into account by estimating the channel-signal-to-noise ratio (CSNR) at the time in the future where it will be used—one is effectively implementing a channel predictor. Specifically, a system as shown in Figure 3.1 (baseband model) is assumed. The figure also covers the case where the receiver has more than one receive antenna, enabling a potential diversity combining gain.

When performing discrete rate adaptation by switching between the N available transmitter–receiver pairs, the transmitter must rely on the accuracy of CSI periodically fed back from the receiver end. The CSI in practice provides information about the CSNR *as predicted at the receiver* at the time of signal reception, which is denoted t. The *true* channel quality at the transmitter update time $t + \tau$, where τ is the return channel delay, may therefore deviate from the value available to the transmitter. The delay τ is a sum of the processing time used for CSNR prediction, transmission protocol delays, physical feedback transmission time, and time used for transmitter reconfiguration. The consequence is that the transmitter may make the wrong assumption about the channel quality, and thus transmit at either a too low, or a too high, information rate. This may lead to changes both in average BER and average information rate compared to the case of perfect CSI. Exactly what kind changes that will occur depends on several factors, the most important being the fading correlation, the delay τ, the average channel quality, the number of codes/signal constellations used (i.e., the degree of adaptivity), and how the CSNR is predicted. In this chapter we will analyze how these factors influence the effective bit error rate (BER),

the effective channel throughput (information rate, measured in average spectral efficiency—ASE), and the outage probability.

The rest of the chapter is organized as follows: In Section 3.2, a more in-depth description of the system model, and the assumptions made, is given. Section 3.3 discusses linear pilot-symbol-assisted channel prediction in general. Section 3.4 analyzes various features of the system—namely average spectral efficiency, outage probability, and BER—for an arbitrary linear prediction algorithm. In Section 3.5, the predictor which is optimal in the *maximum a posteriori* (MAP) sense is introduced, and the properties that are necessary to perform the analysis of the system are derived. Section 3.6 concerns experiments on a certain example set of codes. Finally, the contributions of the chapter are summarized in Section 3.7.

3.2 System Model and Problem Formulation

Denoting the transmitted complex baseband signal (after pilot symbol insertion) at time index k by $x(k)$, the received signal after transmission on a flat fading channel can be written as $y(k) = z(k) \cdot x(k) + n(k)$. For a diversity system like the one suggested in Figure 3.1, the received signal on the hth subchannel is denoted as $y_h(k) = z_h(k) \cdot x(k) + n_h(k)$. Here the random variable (RV) $z_h(k)$ is the *complex fading amplitude*, and $n_h(k)$ is complex-valued additive white Gaussian noise (AWGN) with statistically independent real and imaginary components. $x(k)$ is the information signal, except for time instants $k = mL$ ($m \in \mathbb{Z}$, $L \in \mathbb{Z}^+$), when deterministic *pilot symbols* are periodically transmitted, to be used on the receiver side as an aid towards efficient channel prediction and estimation. The size of L has to be determined as a trade-off between the requirement for adequate sampling of the fading process, calling for a large L, and the requirement for high spectral efficiency, calling for a small L. The absolute value and phase properties of the pilot symbols will not be scrutinized here to any other extent that the pilot symbols are all assumed to have the same (absolute) value, $|x(mL)| = a_p$. Note that the pilot symbols in practice will often be modulated according to a pseudo-random sequence, in order to avoid spectral peaks (See for instance ETSI, 1999, Sec. 4.5).

In order to be able to represent the results in closed-form, it is assumed that each subchannel is perturbed by flat Rayleigh fading. Then, $z_h(k)$ is a complex-valued Gaussian variable with zero mean. During our analysis, $z_h(k)$ is assumed to be constant between two successive pilot symbols (block fading). As shall be demonstrated, in practice a pilot symbol should be transmitted every 10th to 20th symbol or so, so this is not a restrictive as-

sumption. The channel is assumed to be wide-sense stationary (WSS). The fading power Ω is therefore time-invariant and the autocorrelation of z_h measured at two different time indices k_1 and k_2 is only dependent on the time difference. In practice, a wireless channel will not be WSS. Multipath fading is only one of the effects contributing to a varying CSNR; the two other main contributors are log-normal shadowing and path loss (Stüber, 2001). It is reasonable to assume that the CSNR variation due to multipath fading is considerably faster than the other CSNR perturbations. In addition, Abbas and Sheikh (1997) have performed measurements suggesting that the combined slow log-normal shadowing and fast Nakagami fading together fit the Nakagami distribution. Consequently the distinction between shadowing and fading might not be necessary. Assuming a WSS channel over the time span that is considered is therefore not a particularly restrictive assumption.

Furthermore a constant average transmit power P [W] and a one-sided power spectral density N_0 [W/Hz] of the complex AWGN in every subchannel is assumed. For a one-sided information bandwidth B [Hz]—the noise variance is consequently N_0B—the received CSNR on subchannel h at a given time k is then

$$\gamma_h(k) = \frac{|z_h(k)|^2 \cdot P}{N_0 B}, \tag{3.1}$$

with short-term expected value $E[\gamma_h] = \bar{\gamma}_h = \Omega P/(N_0 B)$.[2]

In addition to the time-invariance assumptions, it is also assumed that the subchannels are statistically independent and identically distributed. The variance of the channel gain $\Omega = E[|z_h|^2]$ is therefore independent of h, as is the short-term expectation of $\bar{\gamma}_h$. However, the latter is indexed by h anyway to indicate that this is not the *overall* expected CSNR on the channel. It is noted that the antenna elements must be spaced sufficiently far apart—at least half a wavelength λ—for the subchannels to be statistically independent. For transmission in the 2 GHz band, $\lambda/2$ is approximately 7.5 cm. The case of non-independent branches is considered for instance by Aalo (1995); Lombardo, Fedele, and Rao (1999).

Invoking the assumption of H statistically independent antenna branches, maximal ratio combining (MRC) can be implemented in the receiver. In this case, the channel gain $z_h(k)$ on each of the branches is assumed to be known. Each of the H branch signals is weighted by the corresponding

[2] $\gamma_h(k)$ is actually a short-short-term expectation of the CSNR. In a specific time instant, the noise part of the CSNR will itself be a stochastic variable, whereas it is the noise *power* that is referred to in Eq. (3.1).

channel gain, resulting in an overall received CSNR at time k (Jakes, Yeh, Gans, and Reudnik, 1994, Ch. 5; Stüber, 2001, Sec. 6.3):

$$\gamma(k) = \sum_{h=1}^{H} \gamma_h(k), \tag{3.2}$$

which corresponds to the following effective overall squared channel gain:

$$\alpha^2(k) = \sum_{h=1}^{H} \alpha_h^2(k), \tag{3.3}$$

where $\alpha_h = |z_h|$. Note that α_h is Rayleigh distributed with average power $E[|\alpha_h|^2] = \Omega$, i.e., its probability density function (PDF) is

$$f_{\alpha_h}(\alpha_h) = \frac{2\alpha_h}{\Omega} \cdot e^{-\alpha_h^2/\Omega} \qquad \text{for } \alpha_h \geq 0. \tag{3.4}$$

The squared channel gain $\alpha^2(k)$ is effectively a sum of $2H$ squared zero-mean, real-valued, independent Gaussian RVs, so the RV $\frac{2}{\Omega}\alpha^2(k)$ will possess a chi-square distribution with $2H$ degrees of freedom. Since a chi-square-distributed RV with ν degrees of freedom is equivalent to a gamma-distributed[3] RV with shape parameter $\nu/2$ and scale parameter 2, it can be concluded that $\alpha^2(k)$ will be described by the gamma distribution. In short, this will be written as

$$\alpha^2(k) \sim \mathcal{G}(H, \Omega). \tag{3.5}$$

Naturally, so will the overall CSNR: $\gamma(k) \sim \mathcal{G}(H, \bar{\gamma}_h)$—and the expectation is $E[\gamma] = \bar{\gamma} = H\bar{\gamma}_h$.[4] Thus, the overall channel in this case effectively behaves like a *Nakagami-H* channel, i.e., the effective overall channel gain $\alpha(k)$ obeys a Nakagami distribution with parameter H and with $E[\alpha^2(k)] = H\Omega$.

The task is now to perform periodical prediction of the CSNR at the receiver end, at a rate equal to (at least) the highest possible transmitter adaptation rate. We shall here simply assume that the CSNR is predicted and transmitted back to the transmitter every time a new pilot symbol arrives, and that the return channel delay (understood as the time delay between the time of CSNR prediction and the subsequent time of allowed transmitter update) is an integer number of pilot symbol intervals, i.e., $\tau = kLT_s$,

[3] see the definition of the gamma distribution in Section 4.2.2

[4] It is remarked that the the results will mainly be presented in terms of the branch mean CSNR $\bar{\gamma}_h$ and not the mean CSNR of the combined signal $\bar{\gamma} = H\bar{\gamma}_h$.

where $k \in \mathbb{Z}^+$ is the number of pilot symbol intervals and T_s [s] is the duration of one channel symbol. Finally, the return channel is assumed to be free of errors.

It is important to note that channel *prediction* is only necessary for the periodically fed back CSI. For the actual signal detection in the receiver, the signal may be buffered before detection (assuming that a certain receiver delay is acceptable, such as in data transmission)—cf. Figure 3.1. CSI estimation can then be accomplished using an optimal non-causal Wiener interpolator filter (Cavers, 1991; Torrance and Hanzo, 1995; Tang *et al.*, 1999; Øien and Hole, 2001), which will smooth the noise and improve CSI reliability beyond what can be achieved by a predictor, and it allows for true coherent detection to be used. In the 2001 paper, Øien and Hole show that the minimum non-causal estimation error variance in this case is given by

$$\sigma_e^2 = \frac{\Omega \cdot 2\frac{f_D}{B} L\sigma_n^2}{P\Omega + 2\frac{f_D}{B} L\sigma_n^2}, \tag{3.6}$$

where σ_n^2 is the noise variance, B is the signalling bandwidth, and $f_D = \frac{v}{c} f_c$ [Hz] is the Doppler spread due to terminal mobility (Stüber, 2001; Jamali and Le-Ngoc, 1994). The v is here the terminal speed, f_c is the carrier frequency, and c is the speed of light. Nyquist signalling will henceforth be assumed, rendering $B = 1/T_s$. Thus,

$$\sigma_e^2 = \frac{\Omega}{\bar{\gamma}_h/(2f_D T_s L) + 1} < \frac{\Omega}{\bar{\gamma}_h/(2f_D T_s L)} \leq \frac{\Omega}{\bar{\gamma}_h}. \tag{3.7}$$

The latter inequality stems from a result in the same paper by Øien and Hole; $2\frac{f_D}{B} L \leq 1$ in order to conform to the Nyquist condition. The minimum estimation error variance in each subchannel is consequently upper bounded by $\frac{\Omega}{\bar{\gamma}_h}$. Hence, unless the CSNR is very low, it can be assumed that the CSI used during detection in the receiver is perfect—as opposed to the CSI fed back to the transmitter.

3.3 Linear Pilot Symbol Assisted Channel Prediction

For any pilot symbol time instant $n - kL$ ($n = mL$, $m \in \mathbb{Z}$; $k \in \mathbb{Z}^\star$), define

$$\tilde{z}_h(n - kL) = z_h(n - kL) + \frac{n_h(n - kL)}{a_p} \tag{3.8}$$

which is the result of dividing the noisy signal received on one subchannel by the known pilot symbol value. As it will be shown in Section 3.5.1, this

can be interpreted as a memoryless maximum-likelihood (ML) estimate of $z_h(n-kL)$ based on one received observation (Meyr *et al.*, 1998). The two terms are statistically independent and are also both zero-mean complex Gaussian, so their sum is a complex Gaussian with variance equal to the sum of their variances. At time $n+j$ of transmitter update, a prediction of $z(n+j)$ can be made from K memoryless ML estimates $\tilde{z}_h(n), \tilde{z}_h(n-L), \tilde{z}_h(n-2L), \ldots, \tilde{z}_h(n-(K-1)L)$. Here, $K \in \mathbb{Z}^+$ is a designer-chosen constant. Due to the Gaussianity, the optimal predictor in the MAP or ML sense is known to be a linear function of these observations (Therrien, 1992). Allowing for complex predictor filter coefficients, any linear predictor of order K can be written on the form

$$\hat{z}_h(n+j) = \sum_{k=0}^{K-1} f^*_{j,h}(k) \cdot \tilde{z}_h(n-kL) = \mathbf{f}^{\mathsf{H}}_{j,h} \tilde{\mathbf{z}}_{h,n} \tag{3.9}$$

where $\mathbf{f}^{\mathsf{H}}_{j,h} = [f^*_{j,h}(0), \ldots, f^*_{j,h}(K-1)]$ the predictor filter coefficient vector corresponding to subchannel h and delay j, and where

$$\tilde{\mathbf{z}}_{h,n} = [\tilde{z}_h(n), \tilde{z}_h(n-L), \ldots, \tilde{z}_h(n-(K-1)L)]^{\mathsf{T}}. \tag{3.10}$$

is the vector of the K memoryless ML estimates of the complex fading amplitude—the latest estimate appearing first in the vector, with symbol index n—on which the MAP prediction at symbol index $n+j$ is based. The optimal filter coefficient vector shall be discussed in Section 3.5, but for the moment, we just assume that it is known. Due to the WSS assumption, the index n can be omitted. This will be done from now on when referring to $\tilde{\mathbf{z}}_{h,n}$ and other vectors where it is applicable.

The predicted linear fading envelope is a linear function of zero-mean, complex Gaussians, so it is itself also a complex Gaussian. Now define

$$\hat{\alpha}_h = |\hat{z}_h|. \tag{3.11}$$

which consequently is Rayleigh distributed, with PDF

$$f_{\hat{\alpha}_h}(\hat{\alpha}_h) = \frac{2\hat{\alpha}_h}{\widehat{\Omega}} \cdot e^{-\frac{\hat{\alpha}_h^2}{\widehat{\Omega}}} \qquad \text{for } \hat{\alpha}_h \geq 0. \tag{3.12}$$

Furthermore, for the moment, we assume that $E[\hat{\alpha}_h^2] = \widehat{\Omega}$ is known. It can then—following Tang *et al.* (1999)—be expressed as

$$\widehat{\Omega} = r \cdot \Omega \tag{3.13}$$

for some constant r. In Appendix B general expressions for $\widehat{\Omega}$ and r shall be derived as functions of the predictor coefficients and of the fading correlation properties.

Note that for the case when $r \neq 1$, the predictor in Eq. (3.9) is biased. It will be shown that for the MAP optimal prediction filter, $r < 1$—hence the bias is negative. This means that the CSNR will tend to be underestimated, and the bias will not contribute to an increase of the BER. The ASE will however be reduced compared to if the estimate was unbiased.

3.3.1 Maximal Ratio Combining

As discussed in Section 3.2, the receiver will implement MRC and the channel will consequently look like a Nakagami H channel. Having predicted the channel gain on each of the antenna branches, a reasonable estimate for the predicted squared overall channel gain is now

$$\hat{\alpha}^2 = \sum_{h=1}^{H} \hat{\alpha}_h^2 \tag{3.14}$$

Again, as was the case for the actual effective channel gain, we have a sum of squared Gaussian RVs. The effective predicted channel gain hence obeys a Nakagami-H distribution with $E[\hat{\alpha}^2] = H\widehat{\Omega} = rH\Omega$. The predicted overall CSNR $\hat{\gamma}$ is—as the actual overall CSNR—Gamma distributed with shape parameter H and expectation

$$E[\hat{\gamma}] = \bar{\hat{\gamma}} = H\bar{\hat{\gamma}}_h = rH\bar{\gamma}_h, \tag{3.15}$$

in short,

$$\hat{\gamma} \sim \mathcal{G}(H, r\bar{\gamma}_h). \tag{3.16}$$

Note that the parameter r can be viewed both as the ratio between the expectation of the predicted and the true CSNR γ and as the ratio between the variance of the predicted and the true complex fading amplitude z—and that r is independent on the number of receive antennas.

3.3.2 Correlation Coefficient

An important factor affecting the error performance in an ACM system is the correlation between the predicted and the true CSNR. Note that an ACM system always utilizes some kind of "prediction", even if an advanced predictor is not implemented. An ACM system which "isn't utilizing prediction"—like the one discussed in Chapter 2—must in fact use

some kind of causal estimate for the CSNR at any point of the transmission. It is therefore appropriate to consider the correlation between predicted and actual CSNR for any kind of ACM system. The BER expressions which will be developed in the next section will be functions of—amongst other parameters—the correlation coefficient ρ, i.e., In these expressions, the parameter ρ is the *normalized correlation coefficient* between the predicted and the true CSNR, i.e.,

$$\rho = \frac{\mathrm{Cov}(\hat{\gamma}, \gamma)}{\sqrt{\mathrm{Var}(\hat{\gamma})\,\mathrm{Var}(\gamma)}} \tag{3.17}$$

By replacing γ and $\hat{\gamma}$ by $\frac{\alpha^2 \cdot P}{N_0 B}$ and $\frac{\hat{\alpha}^2 \cdot P}{N_0 B}$, respectively

$$\rho = \frac{\mathrm{Cov}(\hat{\alpha}^2, \alpha^2)}{\sqrt{\mathrm{Var}(\hat{\alpha}^2)\,\mathrm{Var}(\alpha^2)}}. \tag{3.18}$$

Knowing that $\alpha^2 \sim \mathcal{G}(H, \Omega)$ and $\hat{\alpha}^2 \sim \mathcal{G}(H, r\Omega)$, it follows that $\mathrm{Var}(\alpha^2) = H\Omega^2$ and $\mathrm{Var}(\alpha^2) = H\Omega^2 r^2$. Consequently,

$$\rho = \frac{E[\hat{\alpha}^2\alpha^2] + H^2\Omega^2 r}{H\Omega^2 r}. \tag{3.19}$$

Concentrating for a moment on the correlation between α^2 and $\hat{\alpha}^2$,

$$E[\hat{\alpha}^2\alpha^2] = E\left[\sum_{h=1}^{H} \hat{\alpha}_h^2 \sum_{h=1}^{H} \alpha_h^2\right] = \sum_{h=1}^{H}\sum_{i=1}^{H} E[\hat{\alpha}_h^2\alpha_i^2],$$

and since the fading on each of the antenna branches are assumed independent,

$$\begin{aligned} &= \sum_{h=1}^{H} E[\hat{\alpha}_h^2\alpha_h^2] + \sum_{h=1}^{H}\sum_{i\neq h} E[\hat{\alpha}_h^2]E[\alpha_i^2] \\ &= HE[\hat{\alpha}_h^2\alpha_h^2] + H(H-1)\Omega^2 r. \end{aligned} \tag{3.20}$$

It then follows that ρ may be expressed as

$$\rho = \frac{E[\hat{\alpha}_h^2\alpha_h^2] - \Omega^2 r}{\Omega^2 r} = \rho_h, \tag{3.21}$$

i.e., for a given r, the overall correlation coefficient is independent of the number of receive antennas, and is therefore the same as the correlation coefficient for the channel between the transmitter and the hth receive antenna, where $h \in \{1, \ldots, H\}$ is arbitrary.

3.4 System Analysis

When assessing the system performance parameters, the following definition will be useful:

Definition 1 (The incomplete gamma function)
The incomplete gamma function and the normalized incomplete gamma function are defined as follows (Temme, 1996):

$$\Gamma(a,z) = \int_z^\infty t^{a-1}e^{-t}dt \tag{3.22a}$$

$$Q(a,z) = \Gamma(a,z)/\Gamma(a), \tag{3.22b}$$

respectively.

When $Q(a,z)$ (and also $\Gamma(a,z)$) appears here, a is often a positive integer. In that case, $Q(a,z)$ can be calculated in closed-form (Temme, 1996, Eq. 11.6):

$$Q(n,z) = e^{-z}\sum_{m=0}^{n-1}\frac{z^m}{m!} \tag{3.23}$$

3.4.1 BER Analysis

The BER (averaged over all codes and all CSNRs) is given as the average number of bits in error, divided by the average number of bits transmitted, i.e., the average spectral efficiency (ASE) (Alouini and Goldsmith, 2000; Hole *et al.*, 2002):

$$\overline{\text{BER}} = \frac{\sum_{n=1}^{N} R_n \cdot \overline{\text{BER}}_n}{\sum_{n=1}^{N} R_n P_n}, \tag{3.24}$$

where R_n is the information rate of code n, P_n is the probability that code n will be used, and $\overline{\text{BER}}_n$ is the average BER experienced when code n is used. The probability P_n is simply the probability that the predicted CSNR falls in the interval $[\gamma_n, \gamma_{n+1}\rangle$, i.e.,

$$P_n = \int_{\gamma_n}^{\gamma_{n+1}} f_{\hat{\gamma}}(\hat{\gamma})d\hat{\gamma}. \tag{3.25}$$

It can be shown (see e.g. Alouini and Goldsmith, 2000) that

$$P_n = Q\Big(H, \frac{\gamma_n}{r\bar{\gamma}_h}\Big) - Q\Big(H, \frac{\gamma_{n+1}}{r\bar{\gamma}_h}\Big) \tag{3.26}$$

where $Q(x,y)$ is the normalized incomplete gamma function as defined in the beginning of this section.

The average BER may now be written (Alouini and Goldsmith, 2000):

$$\overline{\mathrm{BER}}_n = \int_{\gamma_n}^{\gamma_{n+1}} \int_0^{\infty} \mathrm{BER}_n(\gamma \mid \hat{\gamma}) f_{\gamma,\hat{\gamma}}(\gamma, \hat{\gamma})\, d\gamma d\hat{\gamma}, \tag{3.27}$$

where $\mathrm{BER}_n(\gamma \mid \hat{\gamma})$ is the BER experienced when applying code n, where the choice of n is based on the belief that the CSNR is $\hat{\gamma}$, while it actually is γ. That is, n—and therefore all functions of n—should be viewed as dependent on $\hat{\gamma}$ in the expressions to follow. Furthermore, $f_{\gamma,\hat{\gamma}}(\gamma, \hat{\gamma})$ is the joint distribution of the actual and the predicted CSNR. In our case this will be a bivariate gamma distribution (Nagao and Kadoya, 1971) (see also Definition 5 in Section 4.3).

The key to further analysis of the general BER expression (3.24) is to approximate the BER–CSNR relationship for code n by an analytical expression which will make the integral (3.27) solvable. Hole *et al.* (2000) demonstrated that a very good fit to the actual BER–CSNR relationship for *multidimensional trellis codes* on AWGN channels could be found by applying the expression

$$\mathrm{BER}_n(\gamma \mid \hat{\gamma}) = \begin{cases} a_n \cdot \exp\left(-\frac{b_n \gamma}{M_n}\right) & \text{when } \gamma \geq \gamma_n^l \\ \frac{1}{2} & \text{when } \gamma < \gamma_n^l \end{cases} \tag{3.28}$$

where a_n and b_n are code-dependent constants which may be found by least-squares curve fitting to simulated BER–CSNR data on AWGN channels. M_n is the number of points in the symbol constellation used by the trellis code, and $\gamma_n^l = \ln(2a_n)M_n/b_n$. In the subsequent analysis, we assume that multidimensional trellis codes are used as component codes in the adaptive coder/modulator. Eq. (3.28) will therefore be employed.

For a $2G$-dimensional ($2G$-D) trellis code, one $2G$-D symbol is transmitted as a sequence of G consecutive complex (i.e., 2-D) coded symbols. The G coded symbols have been generated from R_n input information bits when code n is utilized, as previously explained in Chapter 2. In addition, pilot symbols are inserted in between the coded sequence so that every Lth channel symbol does not convey information. The information rate of code n is consequently expressed as follows:

$$R_n = (\log_2(M_n) - 1/G) \cdot \frac{L-1}{L}. \tag{3.29}$$

This expression will be used in Eq. (3.24) when evaluating the average BER. Note that L will not contribute to the BER via this expression, since R_n appears both in the numerator and in the denominator of Eq. (3.24). (However, L will be affecting the ratio r, thus, the average BER will certainly be affected by L.)

In Appendix C, the BER–CSNR relation (3.28) is applied, together with the bivariate gamma distribution, to derive a general closed-form expression for the average BER of an ACM system when trellis code n is used (i.e., Eq. (3.27)) on a Rayleigh fading channel with MRC receive combining. It is shown that the result can be expressed as a sum of three integrals,

$$\begin{aligned}\overline{\mathrm{BER}}_n &= \int_{\gamma_m}^{\gamma_{n+1}} \{\mathcal{J}1(n,\hat{\gamma}) - (\mathcal{J}21(n,\hat{\gamma}) - \mathcal{J}22(n,\hat{\gamma}))\}\, d\hat{\gamma} \\ &= \mathcal{I}1(n) - (\mathcal{I}21(n) - \mathcal{I}22(n)),\end{aligned} \tag{3.30}$$

where

$$\mathcal{J}1(n,\hat{\gamma}) = \int_0^{\infty} a_n \exp\left(-\frac{b_n\gamma}{M_n}\right) f_{\gamma,\hat{\gamma}}(\gamma,\hat{\gamma})\, d\gamma \tag{3.31}$$

$$\mathcal{J}21(n,\hat{\gamma}) = \int_0^{\gamma_n^l} a_n \exp\left(-\frac{b_n\gamma}{M_n}\right) f_{\gamma,\hat{\gamma}}(\gamma,\hat{\gamma})\, d\gamma \tag{3.32}$$

$$\mathcal{J}22(n,\hat{\gamma}) = \frac{1}{2}\int_0^{\gamma_n^l} f_{\gamma,\hat{\gamma}}(\gamma,\hat{\gamma})\, d\gamma. \tag{3.33}$$

and $\mathcal{I}1(n)$, $\mathcal{I}21(n)$, and $\mathcal{I}22(n)$ are the integrals—over the range of $\hat{\gamma}$—of $\mathcal{J}1(n,\hat{\gamma})$, $\mathcal{J}21(n,\hat{\gamma})$, and $\mathcal{J}22(n,\hat{\gamma})$, respectively. Manipulations as shown in Appendix C yield closed-form expressions for these three integrals. The expressions involve two special functions, the *Gamma function* $\Gamma(\cdot)$, and the earlier introduced $Q(\cdot,\cdot)$. The Gamma function is evaluated only for strictly positive integer arguments k , so $\Gamma(k) = (k-1)!$. We refer to Eq. (3.22) for the definition of $Q(x,y)$, which can be found in standard mathematical software packages such as Matlab, Mathematica, or Maple.

The three integrals of interest can now be expressed as follows:

$$\begin{aligned}\mathcal{I}1(n) = a_n &\left(\frac{1}{\frac{b_n\bar{\gamma}_h}{M_n}+1}\right)^H \\ &\times\left[Q\left(H, \frac{\gamma_n}{\bar{\gamma}_h r}\cdot\frac{\frac{b_n\bar{\gamma}_h}{M_n}+1}{(1-\rho)\frac{b_n\bar{\gamma}_h}{M_n}+1}\right) - Q\left(H, \frac{\gamma_{n+1}}{\bar{\gamma}_h r}\cdot\frac{\frac{b_n\bar{\gamma}_h}{M_n}+1}{(1-\rho)\frac{b_n\bar{\gamma}_h}{M_n}+1}\right)\right],\end{aligned} \tag{3.34}$$

$$\mathcal{I}21(n) = a_n \sum_{k=0}^{\infty} \frac{\Gamma(k+H)}{\Gamma(k+1)\Gamma(H)} \left(\frac{\rho}{1-\rho}\right)^k \left(\frac{1}{\frac{b_n \bar{\gamma}_h}{M_n} + \frac{1}{1-\rho}}\right)^{k+H} \times \left[1 - Q\left(k+H, \gamma_n^l \left(\frac{b_n}{M_n} + \frac{1}{(1-\rho)\bar{\gamma}_h}\right)\right)\right] \times \left[Q\left(k+H, \frac{\gamma_n}{(1-\rho)\bar{\gamma}_h r}\right) - Q\left(k+H, \frac{\gamma_{n+1}}{(1-\rho)\bar{\gamma}_h r}\right)\right], \quad (3.35)$$

and

$$\mathcal{I}22(n) = \frac{1}{2} \sum_{k=0}^{\infty} \frac{\Gamma(k+H)}{\Gamma(k+1)\Gamma(H)} \rho^k (1-\rho)^H \times \left[1 - Q\left(k+H, \frac{\gamma_n^l}{(1-\rho)\bar{\gamma}_h}\right)\right] \times \left[Q\left(k+H, \frac{\gamma_n}{(1-\rho)\bar{\gamma}_h r}\right) - Q\left(k+H, \frac{\gamma_{n+1}}{(1-\rho)\bar{\gamma}_h r}\right)\right]. \quad (3.36)$$

Note that $\mathcal{I}1(n)$, $\mathcal{I}21(n)$, and $\mathcal{I}22(n)$ are dependent on the value of the ratio r of the expectations and of the correlation coefficient ρ of the predicted and the true CSNR. In addition, these are all functions of the number of receive antennas H and of the short-term expected value $\bar{\gamma}_h$ of the CSNR. Other parameters affecting the average BER are a_n, b_n, M_n, γ_n^l, and the CSNR interval boundaries γ_n; note, however, that the latter parameters are constant for a given set of transmitter–receiver pairs.

We are now in a position to finally combine Eqs. (3.26), (3.29), (3.30) and (3.34)–(3.36), to obtain the average BER from Eq. (3.24).

3.4.2 Average Spectral Efficiency

The ASE is defined as the transmission rate divided by the bandwidth, and it can be calculated as the average number of bits per channel symbol; i.e., the denominator of Eq. (3.24):

$$\begin{aligned} \text{ASE} &= \sum_{n=1}^{N} R_n P_n \\ &= \sum_{n=1}^{N} \left(\log_2(M_n) - 1/G\right) \cdot \left(\frac{L-1}{L}\right) \cdot \left(Q\left(H, \frac{\gamma_n}{r\bar{\gamma}_h}\right) - Q\left(H, \frac{\gamma_{n+1}}{r\bar{\gamma}_h}\right)\right) \end{aligned} \quad (3.37)$$

3.4.3 Outage Probability

In a situation where the delay constraints are relatively mild, the outage probability is not too much of a concern—the main system parameters are throughput (measured by the ASE) and error resilience (measured by the BER). Real-time systems are in different in this context. If for instance speech is to be transmitted, the system will work in an acceptable manner only when there is a continuous flow of data. An outage is not permitted. Related to the system discussed here, the consequence is that the CSNR must be higher than γ_1. The outage probability (P_{out}) can then be expressed as follows,

$$P_{out} = P_0 = 1 - Q\Big(H, \frac{\gamma_1}{r\bar{\gamma}_h}\Big). \tag{3.38}$$

3.5 Optimal MAP Prediction

For a PSAM system, Torrance and Hanzo (1995) have through simulations shown that a wiener interpolator, albeit optimal in the minimum-mean-square-error sense, is not necessarily the interpolator that will result in the lowest BER. However, for an ACM system aided by pilot symbols, it is important to have a very good prediction of the future CSNR. Since the goal of this work is to suggest bounds for the possible BER, ASE, and P_{out}, a computationally intensive MAP optimal predictor is chosen.

The following notation is introduced for the normalized correlation vector, which contains the covariance between the fading at the pilot symbol instants and the fading to be predicted at time instant $n + j$:

$$\mathbf{r}_j = \frac{1}{\Omega} E[\mathbf{z}_h z_h^*(n+j)] \tag{3.39}$$

where $\mathbf{z}_h = [z_h(n), z_h(n-L), \ldots, z_h(n-(K-1)L)]^\mathsf{T}$ is a companion of the vector $\tilde{\mathbf{z}}_{h,n}$ from Eq. (3.10), this one containing the true complex fading amplitude at the time instants of the pilot symbols, for channel h. Since the signals are zero-mean, the covariance between time indices i_1 and i_2 will be $\mathrm{Cov}(z(i_1), z(i_2)) = E[z(i_1)z(i_2)^*]$, thus, $\mathbf{r}_j$ also represents correlation. The components of $\mathbf{z}_h$ and $z_h(n, j)$ are naturally instances of the same process; $\mathbf{r}_j$ can therefore be looked upon as a punctured autocorrelation vector—"skew-punctured" if $j \neq mL$. It is also remarked that $\mathbf{r}_j$ is real-valued, since the imaginary and real-valued parts of the fading process are independent and zero-mean.

Since the channel is assumed to be WSS, the time index n is omitted in the notation for $\mathbf{z}_h$. In addition, since all the subchannels have the same

fading properties, the channel index h is omitted from $\mathbf{r}_j$. An element $[\mathbf{r}_j]_k$ of $\mathbf{r}_j$ will thus be a function of the lag between the relevant pilot symbol time instant $n - kL$ and of the time $n + j$ of the CSNR to be predicted only. It is advantageous to introduce and utilize the notion of a general normalized correlation function $R(\tau)$, which describes the normalized correlation between two instances of the fading amplitude as a function of the time delay between them,

$$[\mathbf{r}_j]_k = \frac{1}{\Omega} E[z_h(n+j)z_h(n-kL)] = R((j+kL)T_s). \tag{3.40}$$

It will be shown that the optimal filter depends only on the feedback delay when all subchannels have the same fading properties. The predictor filter coefficient vector $\mathbf{f}_{j,h}$ is therefore also redefined to disregard the subchannel index h as shown in the following equation:

$$\mathbf{f}_j = [f_j(0), \ldots, f_j(K-1)]^{\mathsf{T}} \tag{3.41}$$

is the row vector of predictor filter coefficients for an arbitrary subchannel. Lastly, the normalized autocovariance matrix of the fading at the pilot symbol instants is defined as follows:

$$\mathbf{R} = \frac{1}{\Omega} \mathrm{Cov}(\mathbf{z}_h, \mathbf{z}_h) = \frac{1}{\Omega} E[\mathbf{z}_h \mathbf{z}_h^{\mathsf{H}}] \tag{3.42}$$

Similarly to $\mathbf{r}_j$, $\mathbf{R}$ is real-valued and can be viewed as a punctured autocorrelation matrix of the fading process, each element $[\mathbf{R}]_{kl}$ being a function of the lag between the two pilot symbol time instants $n - lL$ and $n - kL$ only,

$$[\mathbf{R}]_{kl} = R(|k-l|LT_s). \tag{3.43}$$

$\mathbf{R}$ is therefore a symmetric Toeplitz matrix.

3.5.1 MAP Optimal Prediction Filter

Meyr *et al.* (1998) have developed MAP optimal predictors and estimators is in the case of Gaussian channel perturbation and noise. Since those results are very general—and rather difficult to grasp at first sight—the expressions relevant to MAP optimal prediction in the case of white, zero-mean (Gaussian) noise and zero-mean fading are re-developed here.

The notation is slightly extended as follows: The $K \times K$ diagonal matrix $\mathbf{A}$ holds the transmitted pilot symbols:

$$\mathbf{A} = \begin{bmatrix} x(n) & & & \\ & x(n-L) & & \\ & & \ddots & \\ & & & x(n-(K-1)L) \end{bmatrix} \tag{3.44}$$

For the case when all the pilot symbols are equal, $x(mL) = a_p$,

$$\mathbf{A} = a_p \mathbf{I} \tag{3.45}$$

The noise at the time instants of pilot symbol transmission is gathered in the vector $\mathbf{n}$ with covariance matrix $\mathbf{C}_n = N_0 B\mathbf{I} = \sigma_n^2 \mathbf{I}$, thus the collection of received signals after transmission of the K pilot symbols can be written as

$$\mathbf{y}_h = \mathbf{A}\mathbf{z}_h + \mathbf{n}_h = a_p \mathbf{z}_h + \mathbf{n}_h \tag{3.46}$$

The ML-optimal estimate of a set of memoryless or static channel parameters $\mathbf{z}$ on the basis of observations $\mathbf{y}$ is the estimate that maximizes the likelihood function $f_{y|z}(\mathbf{y} \mid \mathbf{z})$,[5] i.e.,

$$\tilde{\mathbf{z}} = \arg\max_{\mathbf{z}} f_{y|z}(\mathbf{y} \mid \mathbf{z}) \tag{3.47}$$

For a Gaussian likelihood function, the estimator that accomplishes the maximization can be shown to be (Meyr *et al.*, 1998, Eq. 12.27)

$$\tilde{\mathbf{z}} = (\mathbf{A}^{\mathsf{H}} \mathbf{R}_n^{-1} \mathbf{A})^{-1} \cdot (\mathbf{A}^{\mathsf{H}} \mathbf{R}_n^{-1} \mathbf{y}) = \mathbf{A}^{-1} \mathbf{y} \tag{3.48}$$

(where $\mathbf{R}_n$ is the noise correlation matrix) which, in the case that all the elements of $\mathbf{A}$ are equal to a_p, reduces to

$$\tilde{\mathbf{z}} = \mathbf{y}/a_p = \mathbf{z} + \frac{1}{a_p}\mathbf{n} \tag{3.49}$$

which can be recognized as the noisy fading amplitude vector stated in Eq. (3.10).

[5] The antenna branch index h has here been removed for notational simplicity. However, it should be noted that both $\mathbf{z}$ and $\mathbf{n}$—and therefore $\mathbf{y}$—are dependent on the antenna branch.

The MAP-optimal estimate of a channel parameter z based on a set of observations $\mathbf{y}$ is the estimate that maximizes the PDF $f_{z|y}(z \mid \mathbf{y})$

$$\hat{z}_{\text{MAP}} = \arg\max_{z} f_{z|y}(z \mid \mathbf{y}) \tag{3.50}$$

Considering the zero-mean Gaussian RVs z and $\mathbf{y}$, their variance, covariance matrix, and cross correlation vector can be determined as follows:

$$\sigma_z^2 = E[|z|^2] = \Omega \tag{3.51}$$

$$\mathbf{R}_y = E[\mathbf{y}\mathbf{y}^{\mathsf{H}}] = a_p^2 E[\mathbf{z}\mathbf{z}^{\mathsf{H}}] + E[\mathbf{n}\mathbf{n}^{\mathsf{H}}] = a_p^2 \Omega \mathbf{R} + \sigma_n^2 \mathbf{I} \tag{3.52}$$

$$\mathbf{r}_{z,y} = E[\mathbf{y}z^*] = a_p E[\mathbf{z}z^*] = a_p \Omega \mathbf{r}_j, \tag{3.53}$$

where $\mathbf{R}$ and $\mathbf{r}_j$ are as defined earlier. It follows that $\mathbf{r}_{z,y}$ and $\mathbf{R}_y$ are both real-valued, and that the latter is a symmetric Toeplitz matrix.

When z and $\mathbf{y}$ are jointly Gaussian RVs, it is known that the conditional PDF $f_{z|\mathbf{y}}(z \mid \mathbf{y})$ is also Gaussian; the expectation of z conditioned on $\mathbf{y}$ is then (Therrien, 1992; Meyr *et al.*, 1998)

$$E[z \mid \mathbf{y}] = \mathbf{r}_{z,y}^{\mathsf{T}} \mathbf{R}_y^{-1} \mathbf{y}, \tag{3.54}$$

and the variance is

$$\text{Var}(z \mid \mathbf{y}) = \sigma_z^2 - \mathbf{r}_{z,y}^{\mathsf{T}} \mathbf{R}_y^{-1} \mathbf{r}_{z,y}, \tag{3.55}$$

For Gaussian RVs, the optimal MAP estimate obtained by maximizing the conditional PDF in Eq. (3.50) is equivalent to the conditional mean, thus,

$$\begin{aligned} \hat{z}_{\text{MAP}} = E[z \mid \mathbf{y}] &= a_p \Omega \mathbf{r}_j^{\mathsf{T}} (a_p^2 \Omega \mathbf{R} + \sigma_n^2 \mathbf{I})^{-1} \mathbf{y} \\ &= \mathbf{r}_j^{\mathsf{T}} \left(\mathbf{R} + \frac{\sigma_n^2}{a_p^2 \Omega} \mathbf{I} \right)^{-1} \frac{\mathbf{y}}{a_p}. \end{aligned} \tag{3.56}$$

It is now assumed that the power of the pilot symbol a_p is kept constant at the average transmission power, thus, $a_p^2 = P$. Recognizing the rightmost fraction as $\frac{\mathbf{y}}{a_p} = \tilde{\mathbf{z}}$, the MAP-optimal filter coefficient vector on a Rayleigh fading channel can be deduced:

$$\mathbf{f}_{j,\text{MAP}}^{\mathsf{T}} = \mathbf{r}_j^{\mathsf{T}} \left(\mathbf{R} + \frac{1}{\bar{\gamma}_h} \mathbf{I} \right)^{-1}. \tag{3.57}$$

The error variance of the MAP-optimal estimator is

$$\text{Var}(z - \hat{z}_{\text{MAP}} \mid \mathbf{y}) = \text{Var}\left(z - E[z \mid \mathbf{y}] \mid \mathbf{y}\right) \tag{3.58}$$

which—since $E[z \mid \mathbf{y}]$ can be regarded as a constant when $\mathbf{y}$ is given—equals

$$\begin{aligned}\mathrm{Var}(z \mid \mathbf{y}) &= \Omega - a_p \Omega \mathbf{r}_j^{\mathsf{T}} (a_p^2 \Omega \mathbf{R} + \sigma_n^2 \mathbf{I})^{-1} a_p \Omega \mathbf{r}_j \\ &= \Omega\big(1 - \mathbf{r}_j^{\mathsf{T}} (\mathbf{R} + \tfrac{1}{\bar{\gamma}_h}\mathbf{I})^{-1} \mathbf{r}_j\big) \\ &= \Omega(1 - \mathbf{f}_{j,\mathrm{MAP}}^{\mathsf{T}} \mathbf{r}_j) \end{aligned} \tag{3.59}$$

This finally yields the MAP-optimally predicted fading amplitude at symbol index $n + j$,

$$\hat{z}_{h,\mathrm{MAP}}(n + j) = \mathbf{f}_{j,\mathrm{MAP}}^{\mathsf{T}} \tilde{\mathbf{z}}_{h,n}. \tag{3.60}$$

and the error variance is

$$\sigma_{e(j)}^2 = \Omega(1 - \mathbf{f}_{j,\mathrm{MAP}}^{\mathsf{T}} \mathbf{r}_j). \tag{3.61}$$

3.5.2 Ratio and Correlation Coefficient

Following Tang *et al.* (1999), it is shown in Appendix B (assuming $a_p = \sqrt{P}$), that the ratio r of the expectations and the correlation coefficient ρ between the estimated and the true squared channel gain can be expressed as:

$$r = \frac{\widehat{\Omega}}{\Omega} = \mathbf{f}_j^{\mathsf{H}} \mathbf{R} \mathbf{f}_j + \frac{1}{\bar{\gamma}_h} \|\mathbf{f}_j\|^2 \tag{3.62}$$

$$\rho = \frac{|\mathbf{f}_j^{\mathsf{H}} \mathbf{r}_j|^2}{r} = \frac{|\mathbf{f}_j^{\mathsf{H}} \mathbf{r}_j|^2}{\mathbf{f}_j^{\mathsf{H}} \mathbf{R} \mathbf{f}_j + \frac{1}{\bar{\gamma}_h} \|\mathbf{f}_j\|^2}. \tag{3.63}$$

Note that the parameter ρ, which will be shown to govern the BER expression, is directly dependent on the type of predictor filter used, which is again dependent on the feedback delay (expressed through j).

It is finally remarked that a consequence of using the MAP-optimal set of predictor coefficients is that $\rho = r$. This can be seen by introducing the expression for $\mathbf{f}_{j,\mathrm{MAP}}$ from Eq. (3.57) into the expression for r from Eq. (3.62), having in mind that the MAP-optimal $\mathbf{f}_{j,\mathrm{MAP}}$ is real-valued:

$$\begin{aligned} r &= \mathbf{f}_{j,\mathrm{MAP}}^{\mathsf{T}} \mathbf{R} \mathbf{f}_{j,\mathrm{MAP}} + \tfrac{1}{\bar{\gamma}_h} \|\mathbf{f}_{j,\mathrm{MAP}}\|^2 = \mathbf{f}_{j,\mathrm{MAP}}^{\mathsf{T}} (\mathbf{R} + \tfrac{1}{\bar{\gamma}_h}\mathbf{I}) \mathbf{f}_{j,\mathrm{MAP}} \\ &= \mathbf{r}_j^{\mathsf{T}} (\mathbf{R} + \tfrac{1}{\bar{\gamma}_h}\mathbf{I})^{-1} (\mathbf{R} + \tfrac{1}{\bar{\gamma}_h}\mathbf{I}) (\mathbf{r}_j^{\mathsf{T}} (\mathbf{R} + \tfrac{1}{\bar{\gamma}_h}\mathbf{I})^{-1})^{\mathsf{T}} \\ &= \mathbf{r}_j^{\mathsf{T}} (\mathbf{R} + \tfrac{1}{\bar{\gamma}_h}\mathbf{I})^{-1} \mathbf{r}_j. \end{aligned} \tag{3.64}$$

By inserting Eq. (3.57) into the numerator of Eq. (3.63),

$$(\mathbf{f}_{j,\mathrm{MAP}}^{\mathsf{T}}\mathbf{r}_j)^2 = \left(\mathbf{r}_j^{\mathsf{T}}(\mathbf{R} + \tfrac{1}{\bar{\gamma}_h}\mathbf{I})^{-1}\mathbf{r}_j\right)^2 = r^2, \tag{3.65}$$

and it is concluded that

$$\rho = \mathbf{r}_j^{\mathsf{T}}(\mathbf{R} + \tfrac{1}{\bar{\gamma}_h}\mathbf{I})^{-1}\mathbf{r}_j = r. \tag{3.66}$$

3.5.3 Jakes Spectrum

From here on, it is assumed that the the fading process is described by the much-used *Jakes spectrum* (see for instance Meyr *et al.* (1998, Sec. 12.2.3), Alouini and Goldsmith (2000, Sec. 5), or Stüber (2001, Sec. 2.1)). This implies that the fading experienced is due to terminal mobility (and thus Doppler effects) in an isotropic scattering environment. The autocorrelation of the fading is given by the following expression:

$$E[z_h(n+j)z_h^*(n-kL)] = \Omega \cdot J_0(2\pi f_D(j+kL)T_s), \tag{3.67}$$

where $J_0(x)$ is the 0th order Bessel function of the first kind. Henceforth,

$$[\mathbf{r}_j]_k = R((j+kL)T_s) = J_0(2\pi f_D(j+kL)T_s) \tag{3.68}$$

and

$$[\mathbf{R}]_{kl} = R(|k-l|LT_s) = J_0(2\pi f_D|k-l|LT_s) \tag{3.69}$$

3.5.4 Illustration of the Prediction Advantage

The discussion here will be concerned with the correlation coefficient ρ. Since ρ and r are shown to be equal in the MAP optimal case, it will apply to both of them.

An illustration of the advantage of employing a predictor is is shown in Figure 3.2. The correlation coefficient is there plotted as a function of the normalized delay $f_D T_s \cdot j$ for the MAP optimal predictor (solid) and for the case when the last received pilot symbol—divided by the pilot symbol value—is used as a prediction (dash-dotted). The latter is also shown when there is no noise on the channel (dashed). Relevant parameters are the carrier frequency $f_c = 2\,\mathrm{GHz}$ and a terminal velocity $v = 30\,\mathrm{m/s}$; the resulting Doppler spread is consequently $f_D = 200\,\mathrm{Hz}$. Assuming a transmission bandwidth of $B = 400\,\mathrm{kHz}$ and Nyquist signalling, the symbol duration is $T_s = 2.5\,\mu\mathrm{s}$—the normalized Doppler spread will be $f_D T_s = 5 \cdot 10^{-4}$. Hanzo

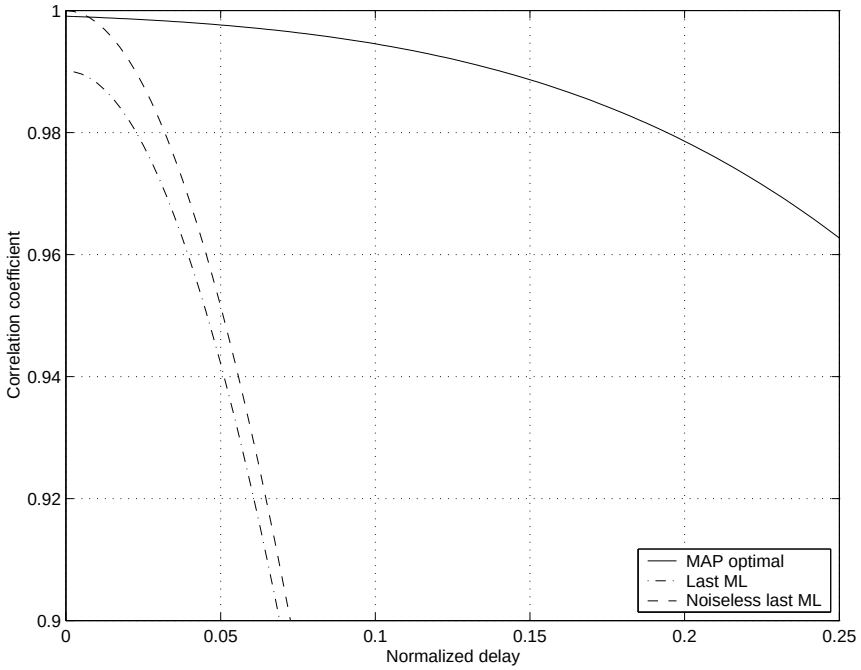

FIGURE 3.2: The correlation coefficient as a function of normalized delay $f_D T_s \cdot j$.

et al. (2000, Ch. 13) suggest that a mobile speed of 30 mph and a carrier frequency of 1.9 GHz calls for a symbol rate of at least $512 \cdot 10^3$ Ksymbols/s, corresponding to a normalized Doppler spread of approximately $6 \cdot 10^{-4}$. The parameters considered here consequently lead to a sufficiently low normalized Doppler spread. Other parameters employed in Figure 3.2 is an expected CSNR $\bar{\gamma}_h = 20$ dB and a prediction filter length of $K = 1000$. The pilot symbols are inserted every 10th channel symbol, i.e., $L = 10$.

The expression for ρ in Eq. (3.66) is easily seen to be dependent on $\bar{\gamma}_h$—an increase in the expected CSNR will naturally cause an increase of ρ, as is illustrated in Figure 3.3 by letting $\bar{\gamma}_h$ run from 0 dBto 20 dB.

The pilot symbol transmission and detection can be viewed as sampling of a band-limited process. The Jakes spectrum is strictly band-limited to f_D (Stüber, 2001, Ch. 2), and the pilot symbols should be transmitted at a rate which is at least $2 \cdot f_D$ (according to the sampling theorem), hence, $L \leq 1/(2 f_D T_s)$. However, this is only valid when the pilot symbols are not corrupted by noise. In a noise-free environment, any $L \leq 1000$ would yield adequate sampling when the Doppler spread is $f_D T_s = 5 \cdot 10^{-4}$. Meyr *et al.* (1998, Sec. 14.2.2) suggest that pilot symbols need to be transmitted at

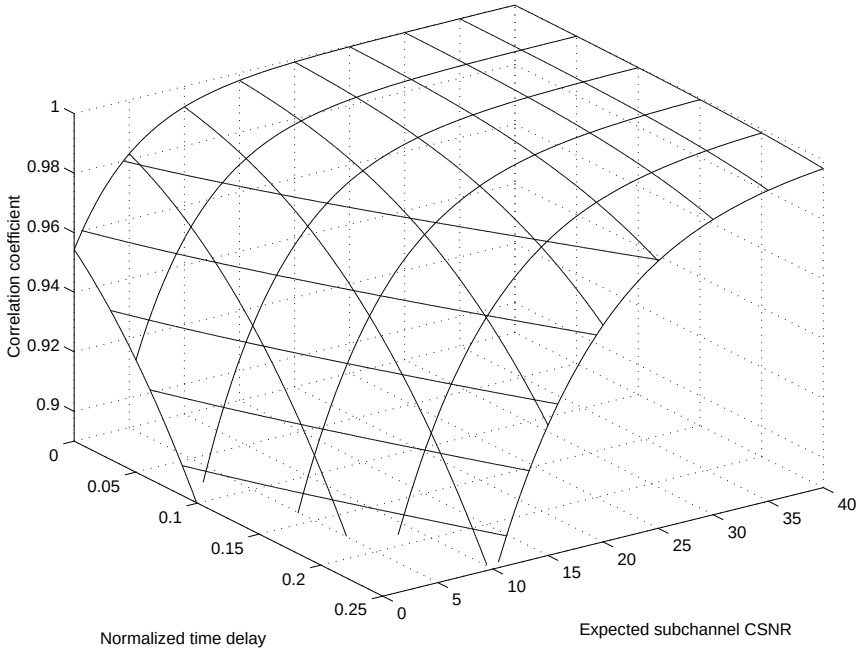

FIGURE 3.3: The correlation coefficient as a function of normalized delay $f_D T_s \cdot j$ and expected CSNR $\bar{\gamma}_h$

a much greater pace. As Figure 3.4 illustrates, relatively small variations of L yields substantial improvement of ρ—even when L is several orders of magnitude smaller than 1000. Note that the variations in correlation are most notable for the smaller CSNRs. For $\bar{\gamma}_h = 0$ or 10 dB, the relative gain of decreasing the pilot symbol spacing from $L = 15$ to 5 is substantial compared to when the CSNR is more advantageous. As it shall be shown in the next section, also the BER performance benefits from the oversampling following from a smaller L.

The number of pilot symbols upon which the prediction is done must of course be limited, yet remain sufficiently high. Meyr *et al.* (1998, Sec. 14.2.2) claims that, for non-causal detection, quasi-optimal performance will be achieved if $(K/2)L \gg 1/(f_D T_s)$. A practical problem is then that the filter order K can easily become very large if L is to be kept small. For instance, with parameters from the discussion above—$f_D T_s = 5 \cdot 10^{-4}$ and $L = 10$, $K \gg 400$. For $L = 5$, $K \gg 800$. Fortunately, the results indicate that L may be decreased without necessarily increasing K correspondingly; note for instance that K is kept steady at $K = 1000$ in Figure 3.4. The effect of increasing the filter order while keeping L steady is shown in Figure 3.5. Several authors have viewed the fading as an auto-regressive (AR) process

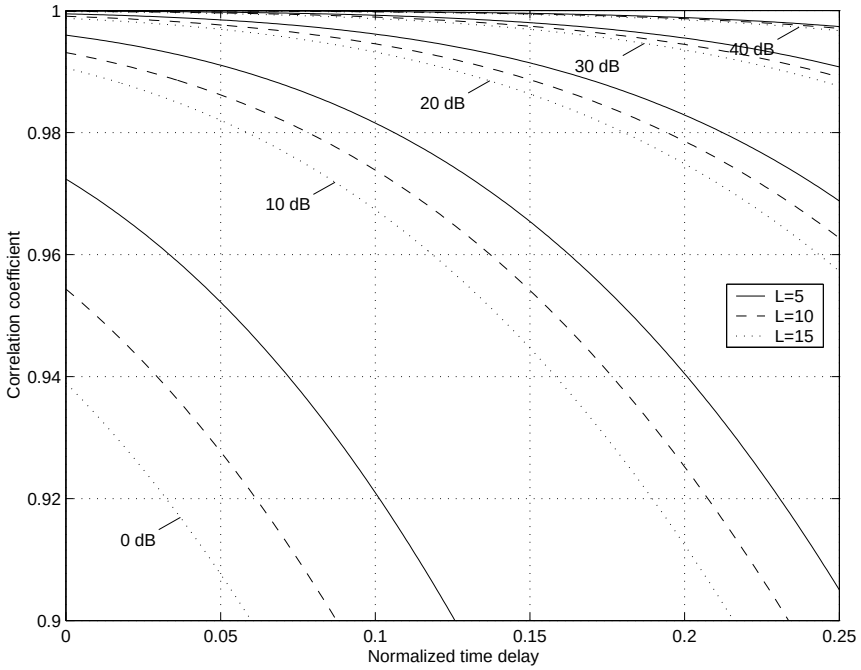

FIGURE 3.4: Correlation coefficient ρ as a function of delay, plotted for expected branch CSNR $\bar{\gamma}_h = 0, 10, \ldots 40$, and for pilot symbol spacing $L = 5$, 10, and 15. The prediction filter length is $K = 1000$.

(Aghamohammadi, Meyr, and Ascheid, 1989; Zhang, Fritz, and Gelfand, 1997), which may explain the minute advantage of increasing K compared to the improvement resulting from decreasing L shown in Figure 3.4. When making a linear prediction of an AR process, an optimal filter order K equal to the order of the AR process should be used. In the examples below, it is chosen to keep the filter order constant at $K = 1000$.

3.6 Example System

In order to assess bounds for the performance of a system incorporating antenna diversity and channel prediction as suggested in the previous sections, a specific system similar to the one in Chapter 2 is investigated. The system under consideration employs the same codes; however, the path length of the Viterbi decoder is set to 16 while is was 9 for the system considered in Chapter 2. This leads to slightly different performance merits. In addition, the BER requirement is here set to $\text{BER}_0 = 10^{-4}$ whereas it was before $\text{BER}_0 = 10^{-3}$; resulting in slightly higher values for the thresholds.

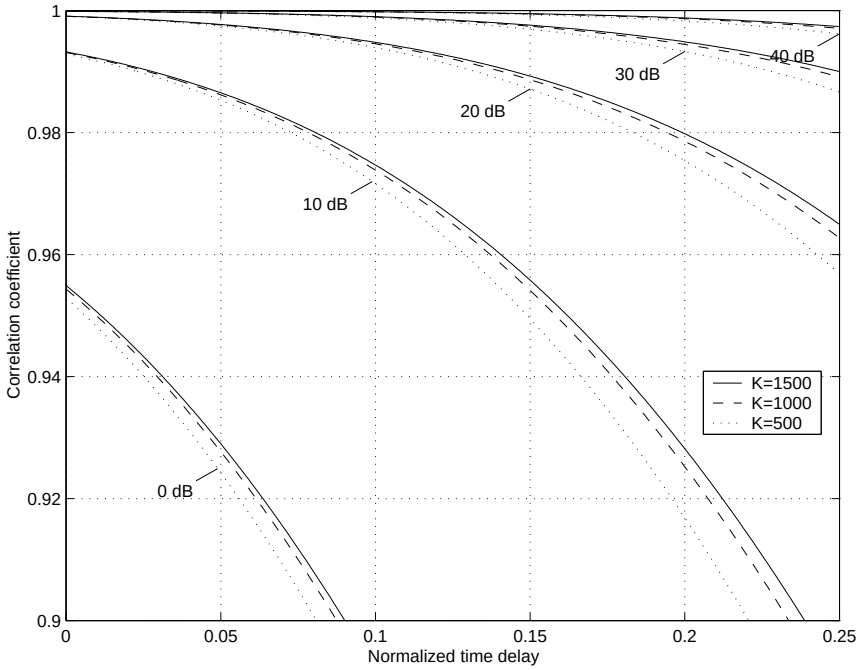

FIGURE 3.5: Correlation coefficient plotted analogous to Figure 3.4, however, the pilot symbol spacing is kept still at $L = 10$ and the filter order is varied from $K = 500$ to $K = 1500$.

The a_n and b_n parameters for the BER expression of the individual codes are summarized in Table 3.1, along with the calculated thresholds.

Parameters not directly tied to the codes, albeit dependent on the implementation, are the carrier frequency $f_c = 2\,\text{GHz}$, a bandwidth of $B = 400\,\text{kHz}$, and a terminal velocity of $v = 30\,\text{m/s}$—the same parameters as the ones chosen in the previous section. Similarly, a prediction filter length of $K = 1000$ is utilized.

3.6.1 BER Performance

In order to calculate the average BER, the expressions from Section 3.4.1 are employed. In Figure 3.6, the BER has been plotted as a function of channel CSNR and of feedback delay, for a pilot symbol spacing of $L = 10$. It is assumed that the system uses two receive antennas and combines the signals with MRC. Since a target BER_0 is decided, the operation of the system will be acceptable whenever $\text{BER} < \text{BER}_0$. When $\text{BER} > \text{BER}_0$, the system does not operate properly. The shape of the BER surface is therefore not significant, except for the contour at $\text{BER}_0 = 10^{-4}$. In Figure 3.7, the

TABLE 3.1: Parameters a_n and b_n for the example codec, along with thresholds γ_n for $\mathrm{BER}_0 = 10^{-4}$.

n	M_n	a_n	b_n	γ_n (dB)
1	4	188.7471	9.81182	7.7
2	8	288.8051	6.8792	12.4
3	16	161.6898	7.8862	14.6
4	32	142.6920	7.8264	17.6
5	64	126.2118	7.4931	20.8
6	128	121.5189	7.7013	23.7
7	256	79.8360	7.1450	26.9
8	512	34.6128	6.9190	29.7

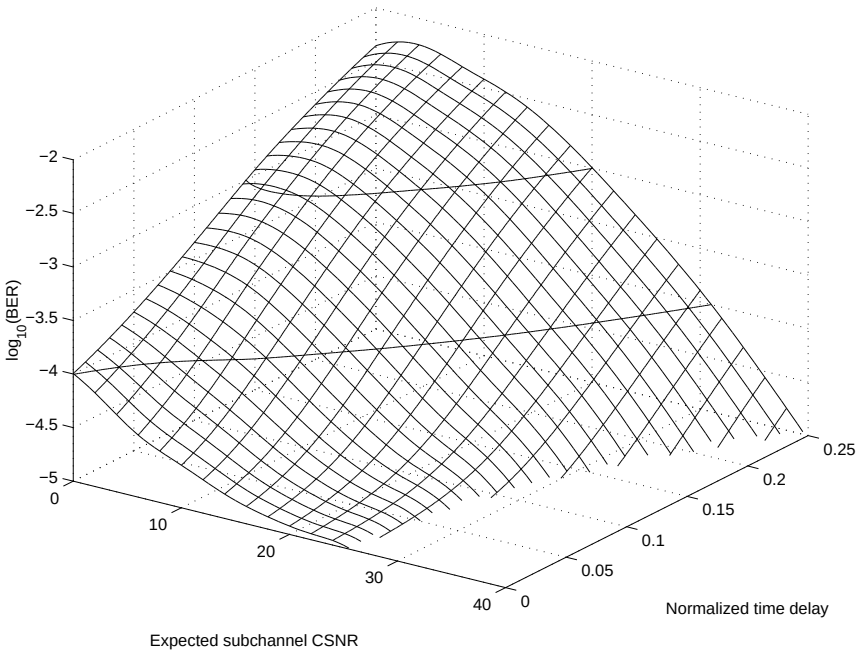

FIGURE 3.6: BER as a function of feedback delay and of expected subchannel CSNR. $H = 2$ receive antennas are utilized and the pilot symbol spacing is $L = 10$. In this plot—as in all subsequent plots—the prediction filter length is kept steady at $K = 1000$.

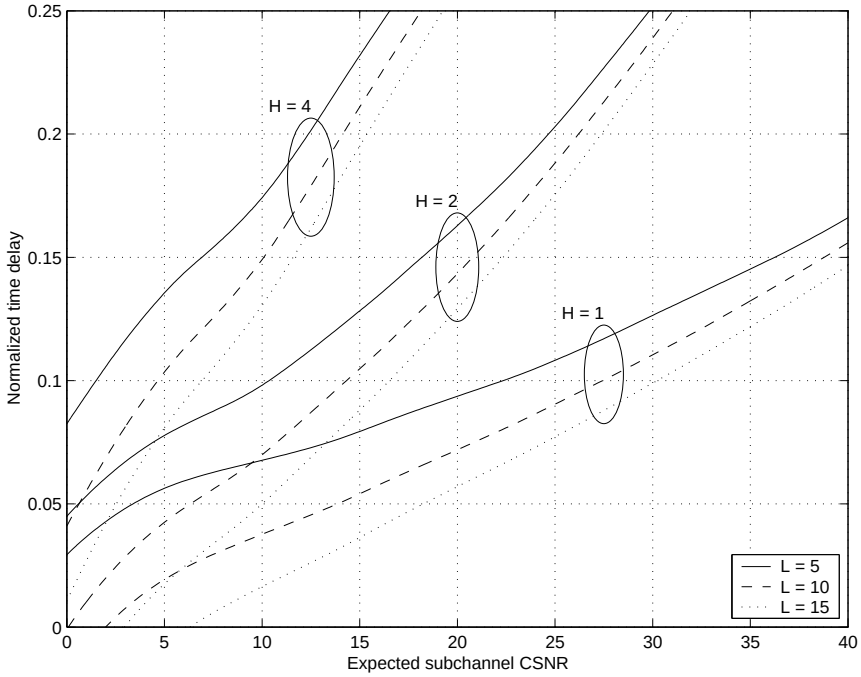

FIGURE 3.7: Regions for which system performance is acceptable, plotted for pilot symbol spacing $L = 5, 10, 15$, and for $H = 1, 2$, and 4 receive antennas. The curves indicate largest delay that is allowed in order to achieve the BER requirements, for a given expected CSNR. Thus, acceptable performance results when the point specified by a CSNR/delay combination is below and to the right of the curve for system parameters L and H.

contour lines at BER $= 10^{-4}$ have been plotted for pilot symbol spacing $L = 5, 10, 15$, and for $H = 1, 2$, and 4 receive antennas. The middle stippled line corresponds to the contour curve at BER $= 10^{-4}$ in Figure 3.6. The figure shows that a large improvement (in the form of lowering the CSNR requirements, or equivalently, allowing for a longer delay) can be achieved by using more than one receive antenna. Naturally, lowering the pilot symbol spacing will also lead to some performance gain since the quality of the predicted instantaneous CSNR is increased.

The parameters utilized in the simulations incorporate a vehicle speed of 30 m/s and a carrier frequency of 2 GHz. When the CSNR is 10 dB and when every $L = 10$th channel symbol is a pilot symbol, $H = 1$ receive antenna lead to an acceptable normalized delay of $j \cdot f_D T_s = 0.038$. This corresponds to an actual delay of $j \cdot T_s = 190\,\mu$s. Increasing the number of receive antennas to $H = 2$ leads to an acceptable delay of 350 μs. Note

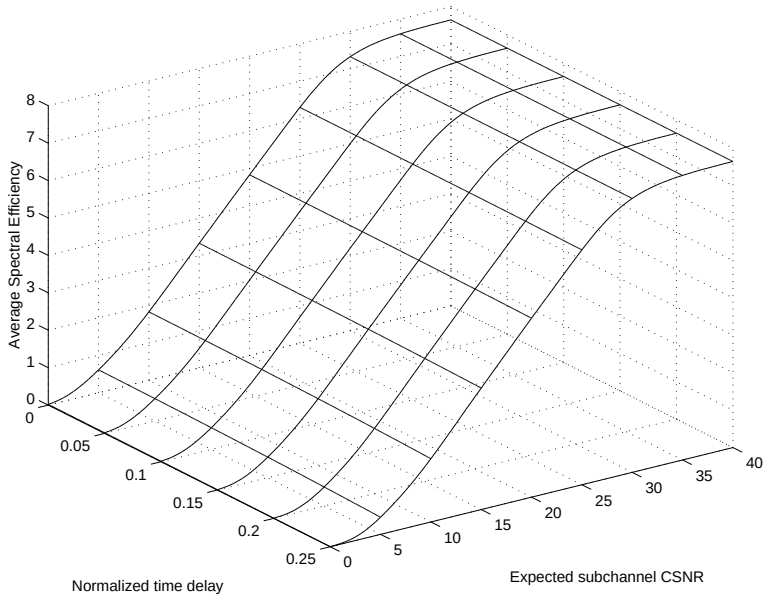

FIGURE 3.8: ASE as a function of feedback delay and expected subchannel CSNR. $L = 10$, $H = 2$. Note that the ASE is almost independent on the feedback delay when normalized delay is in the region 0–0.25 (the biggest delay corresponding to an actual delay of 1.25 ms.)

that the CSNR here is the CSNR *per antenna branch*, and the CSNR after MRC will be approximately 13 dB. Addition of a second antenna branch causes the power consumption to be doubled. When considering a system where low power consumption is a requirement, it might be reasonable to reduce the power in each antenna branch accordingly, effectively reducing the branch CSNR. For the sake of comparison, assuming that the branch CSNR on each of the two branches is 7 dB will reduce the acceptable delay to 270 μs.

3.6.2 ASE Performance

As explained in the previous section, the BER can largely be divided into two regions—acceptable (smaller than BER_0) and unacceptable (larger than BER_0). The BER analysis is therefore significant mainly for determining allowable operation regions. The ASE is more of a key feature of a system like the one under consideration here. Using the expression in Eq. (3.37), the ASE is in Figure 3.8 plotted as a function of CSNR and of delay (similarly to in Figure 3.6). The dependence on the delay is minimal. This is reasonable, since the delay only affects the expected value $r\bar{\gamma}_h$ of the pre-

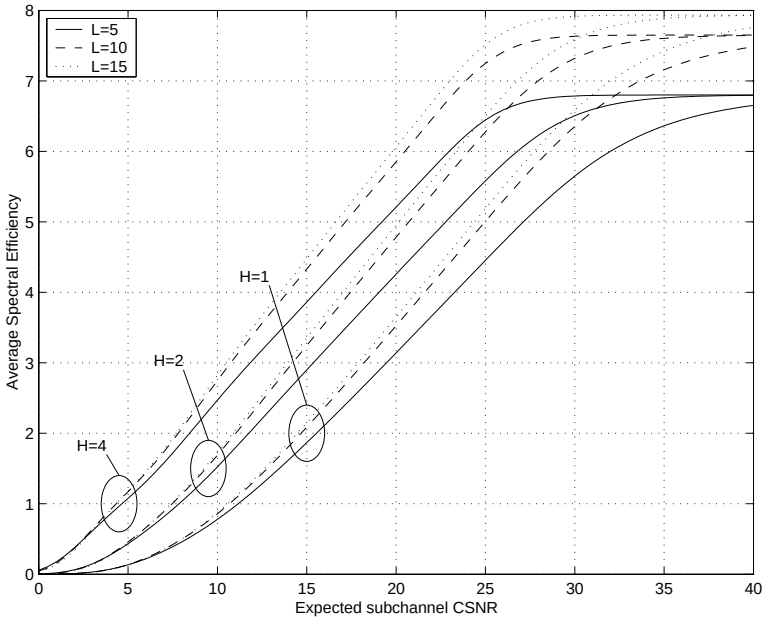

FIGURE 3.9: ASE as a function of expected subchannel CSNR, plotted for various L and H, for a normalized delay of 0.25.

dicted CSNR, which appears in the second argument to the normalized incomplete gamma function in Eq. (3.37). In Figure 3.9, the ASE is plotted for a delay of 0.25, as a function of the expected CSNR. Plots have been made for $L = 5$, 10, 15, and for $H = 1$, 2, and 4 receive antennas. Note that plotting the ASE (and later the P_{out}) on a constant large delay of 0.25 is not in correspondence with the results encountered in the previous section when dealing with the BER performance: Those results clearly show that the system will not operate properly at such a large delay. However, the 0.25 delay is considered anyway since staying within the delay limits determined by the BER performance plotted in Figure 3.7 can only lead to improved results.

It is apparent that the ASE reaches a ceiling when the CSNR grows large, the ceiling being dependent on L. The reason is that the $2G$-dimensional codes have a spectral efficiency of $\log_2 M_n - 1/G$—for the system considered here, $G = 2$. The spectral efficiency of the largest code—and hence the largest possible spectral efficiency for the set of codes—is consequently 8.5. But the spectral efficiency of the system under consideration is also affected by the pilot symbol spacing L. A smaller L naturally leads to a smaller relative part of the transmission time available for transmission

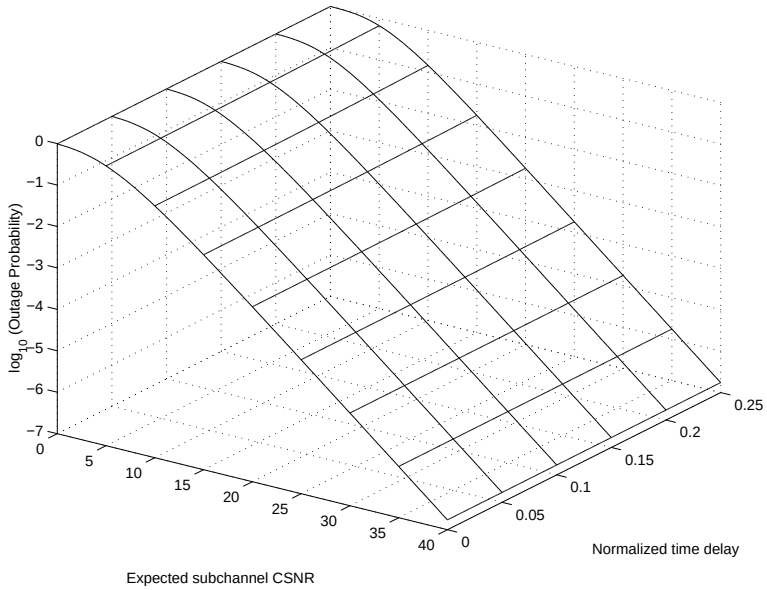

FIGURE 3.10: P_{out} as a function of feedback delay and expected subchannel CSNR. $L = 10$, $H = 2$. Similarly to the ASE, P_{out} is virtually independent on delay in the region under consideration.

of information. Thus the maximal possible ASE—utilized when the CSNR is at the highest—is $R_8 = 8.5 \cdot (L-1)/L$. For $L = 15$ the maximal possible ASE is 7.933, decreasing to 6.8 for $L = 5$.

It is here emphasized that the CSNR under consideration is again the subchannel CSNR, thus most of the difference between the $H = 1$, 2, and 4 curve bundles in Figure 3.9 stems from the $\bar{\gamma} = H\bar{\gamma}_h$ gain. Even if the results for the BER in Figure 3.7 were also affected by the beneficial total CSNR of an MRC system when increasing the number of antennas, the BER takes advantage of the lower variance of the underlying gamma distribution when H is increased. This is not the case for the ASE.

3.6.3 P_{out} Performance

The last figure of merit considered here is the outage probability. Similarly to the ASE, P_{out} is also only slightly dependent on the delay, as is shown in Figure 3.10. As it can be predicted from Eq. (3.38), the pilot symbol spacing does not affect the outage probability very much. Both the delay and the pilot symbol spacing only affect the expected value $r\bar{\gamma}_h$ of the predicted CSNR, appearing in the second argument to the normalized incomplete gamma function.

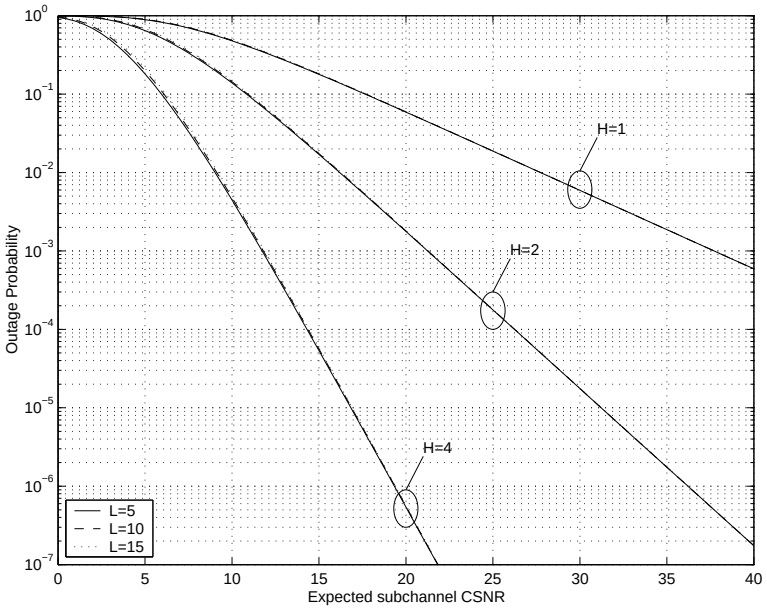

FIGURE 3.11: P_{out} as a function of expected subchannel CSNR, plotted for various L and H, for a normalized delay of 0.25.

Note again that Figures 3.8–3.11 can be challenged since not the full CSNR range is relevant at normalized delay 0.25 (cf. Figure 3.7). Nevertheless, it is here chosen to plot at such a big delay. It is again emphasized—as the three-dimensional plots (Figures 3.8 and 3.10) indicate—that the effect upon ASE and P_{out} of varying delay is very slight. In addition, reducing the delay will only lead to better ASE and P_{out} performance.

3.7 Conclusions

The results considered in this chapter reveal that delay in the feedback channel and erroneous CSI due to noise have a big impact on the BER in an ACM system. The increased BER limits the region where the system can operate reliably with respect to permitted delay and average CSNR. In order to combat the harmful effects of delay, using channel prediction seems to be a promising tool. The predictor considered in this chapter results in MAP-optimal correlation between the predicted fading and the actual fading. In an implementation of an ACM system, it might be more feasible to utilize a less complex sub-optimal predictor. The trade-off between complexity and optimality is a subject for further research.

The ASE and P_{out} of the system are relatively independent on the feedback delay. This is natural, since the only effect of increasing the delay is a slightly lowered expected value of the CSNR due to the biased predictor.

The system under consideration utilizes a pilot tone with fixed power. Whether this is optimal has not been considered—more power to the pilot tone could yield a better estimate, whereas less pilot tone power would leave more to the actual transmission of data. A system where the pilot tone power is adapted to the channel quality should also be considered. Similar arguments apply to the pilot symbol spacing. Decreasing the pilot symbol spacing under adverse channel condition might yield a better channel estimate which in turn could cause a lower overall BER—or equivalently a bigger operable region—and a lower outage probability.

Part II

Statistical Methods

Chapter 4

Sum and Difference of Two Correlated Gamma-distributed Random Variables

This chapter is based on a paper presented at the *35th Annual Conference on Information Sciences and Systems* (Holm and Alouini, 2001), and on an extended journal version submitted for possible publication in *IEEE Trans. Commun. Theory* (Holm and Alouini).

4.1 Introduction

The wide versatility, computational tractability, and experimental consistency (Sheikh *et al.*, 1993) of the Nakagami-*m* distribution (Nakagami, 1960) has made it popular as a fading model when analyzing the performance of wireless systems (see for example Abu-Dayya and Beaulieu, 1991; Yao and Sheikh, 1992; Eng and Milstein, 1995; Aalo, 1995; Alouini and Simon, 1998; Lombardo *et al.*, 1999; Win and Winters, 1999)). One of the important features of the distribution is that the power of a signal perturbed by Nakagami fading is gamma-distributed. In performance evaluation involving Nakagami fading, one can therefore often rely on established results (in the statistics literature) about the gamma distribution. An important special case of the Nakagami distribution is the Rayleigh distribution, which arises in the situation of multipath transmission with no direct component, i.e., when all of the received power stems from scattered components. The corresponding distribution for the signal power is the exponential distribution. Another often employed distribution when modelling wireless channels is the Rice distribution, which considers the multipath signal as a sum

of a direct component and a reflected component. When the magnitude of the direct component is zero, the Rice also reduces to the Rayleigh distribution. Although the Nakagami-m and the Rice distributions are not equal, except in the common Rayleigh special case, their probability density functions (PDFs) can be close when a proper mapping is used between the m parameter and the Rice-factor K (Stüber, 2001, Eqs. 2.53 and 2.54). However, as mentioned in the introduction chapter, an advantage of the Nakagami-m over the Rice model is the relatively simple expression for its PDF and joint PDF for the signal power. Indeed, while the gamma PDF contains no complicated special functions, the signal power in the Rician case is described by a non-central chi-square distribution with two degrees of freedom, which contains a modified Bessel function. On the other hand, the bivariate distribution of two squared correlated Nakagami-m random variables (RVs) (or equivalently two correlated gamma RVs) has a relatively simple closed-form expression, while (to the best of our knowledge) no simple formula is yet known for the joint PDF of two correlated non-central chi-square RVs.

Many of the performance analysis problems in wireless communication systems over Nakagami-m channels require determination of the statistics of functions of the squared envelope of Nakagami-m faded signals. In the classical 1960 paper (Nakagami, 1960), relying on a series of papers (Nakagami and Nishio, 1955; Ōta, 1956; Nakagami and Ōta, 1957) appearing in Japanese journals, Nakagami cites expressions for the distribution of the sum, the ratio, and the product of squares of two correlated Nakagami-m RVs (or equivalently, sum, ratio, and product of two correlated gamma RVs). However, no expression for the PDF of the difference between two gamma RVs is provided. This PDF can not be derived from the PDF of a sum, and it has a slightly different form since the sum of gamma RVs (always positive) naturally is positive—while the difference can clearly be negative. Apparently, even in the specialized statistics literature only the difference between two *uncorrelated* gamma RVs has been investigated (McKay, 1932; Pearson, Stouffer, and David, 1932; Laha, 1954; Springer, 1979; Johnson *et al.*, 1994). One of the main contributions of this chapter is to show that starting from the bivariate gamma distribution, we are able to derive a closed-form expression for the PDF, moments, and in certain particular cases the cumulative distribution function (CDF) of the difference between two correlated not necessarily identically distributed gamma-distributed RVs.

Much effort has been made in finding general statistical distributions, or systems of distributions, for the purpose of fitting sample data to a distribution. The Pearson system (Pearson *et al.*, 1932; Johnson *et al.*, 1994)

is an example of one of the most general systems of distributions. As an addition to the Pearson system, McKay (1932) provides what he calls "A Bessel Function Distribution", which is a distribution with particularly simple expressions for the moment-generating function and for the cumulants. This distribution splits naturally in two forms—depending on the value of one of the parameters—where one of them describes a RV that can be only positive while the other describes a RV that can take on all values. The two forms of this distribution will together be referred to as "The McKay Distributions". Since the sum and difference of two uncorrelated gamma-distributed RVs are described by these two forms, respectively (Johnson *et al.*, 1994), they will be of particular interest in the context of this chapter. In particular, another main contribution of this chapter is to show that the sum and difference of *correlated* gamma RVs are also described by McKay's distributions.

The chapter is organized as follows. Section 4.2 defines the two McKay distributions. Expressions for the moments of these distributions are stated as theorems, as are the PDFs of the sum and difference between two uncorrelated gamma RVs. Lastly, an important special case—relevant to Rayleigh fading—is investigated. Section 4.3 introduces the bivariate gamma distribution and derives the distributions of the sum and difference of correlated gamma RVs. An application of this new result relevant to the calculation of outage probability in presence of self-interference is presented in Section 4.4. Finally, a conclusion summarizing the main results is given in Section 4.5.

4.2 McKay's Bessel Function Distribution

In this section, we define McKay's distributions and provide expressions for the moments of these distributions. Next, we remind the reader about the basic definition of the gamma distribution. Some previously known results regarding the sum and difference between independent gamma RVs are stated before an important special case is considered.

McKay defines his distribution in terms of one function with different forms due to different values of one of the parameters, namely, the c parameter. However, we find it more convenient to treat the two forms as separate distributions; called $f_\Sigma(\sigma)$ and $f_\Delta(\delta)$, respectively.

Definition 2 (Type I McKay Distribution)

Σ follows the type I McKay distribution with parameters $a > -\frac{1}{2}$, $b > 0$,

and $c > 1$,[1] when the PDF of Σ is given by

$$f_\Sigma(\sigma) = \frac{\sqrt{\pi}(c^2-1)^{a+1/2}\sigma^a}{2^a b^{a+1}\Gamma(a+1/2)} e^{-\sigma\frac{c}{b}} I_a\Big(\frac{\sigma}{b}\Big) H(\sigma), \tag{4.1}$$

where $\Gamma(\cdot)$ is the gamma function, $I_a(\cdot)$ is the Modified Bessel function of the first kind and of order a, and $H(\cdot)$ is the Heaviside unit step function (Gradshteyn and Ryzhik, 2000, page xliv).

Definition 3 (Type II McKay Distribution)
Δ follows the type II McKay distribution with parameters $a > -\frac{1}{2}$, $b > 0$, and $|c| < 1$, when the PDF of Δ is given by

$$f_\Delta(\delta) = \frac{(1-c^2)^{a+1/2}|\delta|^a}{\sqrt{\pi}2^a b^{a+1}\Gamma(a+1/2)} e^{-\delta\frac{c}{b}} K_a\Big(\frac{|\delta|}{b}\Big), \qquad \delta \neq 0 \tag{4.2}$$

where $K_a(\cdot)$ is the Modified Bessel function of the second kind and of order a.

$K_a(\cdot)$ is not defined when the argument is equal to zero. However, with the aid of an approximation of $K_a(x)$ valid for small x, we provide an expression for the type II McKay distribution for $x = 0$, valid when $a > 0$:

Proposition:
When $a > 0$, and b and c are as in Definition 3,

$$f_\Delta(0) = \frac{(1-c^2)^{a+1/2}}{\sqrt{\pi}2b} \frac{\Gamma(a)}{\Gamma(a+1/2)}. \tag{4.3}$$

Proof: Use the formula $\lim_{x\to 0} x^a K_a(x) = 2^{a-1}\Gamma(a)$ (Abramowitz and Stegun, 1972, Eq. 9.6.9) to find the limit of Eq. (4.2). □

Note that when $-\frac{1}{2} < a < 0$, then $f_\Delta(\delta)$ is negative and thus undefined as a PDF value. When $a = 0$, $f_\Delta(\delta)$ is undefined ($f_\Delta(\delta) \xrightarrow{\delta\to 0} \infty$). However, plotting of Eq. (4.2) indicates that the PDF, with a in the range $-\frac{1}{2} < a \leq 0$, approaches a Dirac "delta" distribution.

4.2.1 Moments

McKay provides expressions for the moment-generating function and for the cumulants of his distribution functions (McKay, 1932, Eqs. (10) and (19), respectively). As will be shown, it is also possible to find general closed-form expressions for the moments of the McKay distributions.

[1] The third parameter to the first McKay distribution can also be $c < -1$. Then, the distribution function is defined for negative, instead of positive, x.

Theorem 1 (Moments of McKay's Type I Distribution)
Let Σ be distributed according to the type I McKay distribution (Definition 2). Then the moments of Σ can be expressed as

$$E[\Sigma^n] = \frac{(c^2-1)^{a+\frac{1}{2}} b^n}{c^{2a+n+1}} \frac{\Gamma(2a+n+1)}{\Gamma(2a+1)} \times {}_2F_1\Big(\frac{2a+n+1}{2}, \frac{2a+n+2}{2}; a+1; \frac{1}{c^2}\Big), \tag{4.4}$$

where ${}_2F_1(\cdot,\cdot;\cdot;\cdot)$ is Gauss' hypergeometric function (quoted for instance by Gradshteyn and Ryzhik, 2000, Section 9.1).

Proof: See Appendix D.1. □

As indicated, the previous theorem applies solely to McKay's distribution of the first kind, i.e., when $c > 1$. For $|c| < 1$, the type II McKay distribution is the appropriate distribution function—and then the moments must be expressed as in the following theorem:

Theorem 2 (Moments of McKay's Type II Distribution)
Let Δ follow the type II McKay distribution (Definition 3). Then the moments of Δ can be expressed as:

$$\begin{aligned} E[\Delta^n] = {} & \frac{b^n}{(1-c^2)^{a+n+\frac{1}{2}}} \frac{\Gamma(2a+n+1)\Gamma(n+1)}{\Gamma(a+n+\frac{3}{2})\Gamma(a+\frac{1}{2})} \\ & \times \Big[(-1)^n (1+c)^{2a+n+1} {}_2F_1\Big(2a+n+1, a+\tfrac{1}{2}; a+n+\tfrac{3}{2}; -\frac{1+c}{1-c}\Big) \\ & + (1-c)^{2a+n+1} {}_2F_1\Big(2a+n+1, a+\tfrac{1}{2}; a+n+\tfrac{3}{2}; -\frac{1-c}{1+c}\Big)\Big]. \end{aligned} \tag{4.5}$$

Proof: See Appendix D.2. □

The hypergeometric function is commonly available in numerical software, so the moments can be calculated easily. Expressions for the moments can also be found by utilizing multiple derivatives of the moment-generating function. In addition, it is always possible to find an expression for the n-th moment in terms of the n first cumulants (Kendall, 1947, Chapter 3), and vice versa. As an example, utilizing (McKay, 1932, Eq. 19) gives the following expression for the mean and the variance:

$$\begin{aligned} \mu_Z &= \frac{(2a+1)bc}{c^2-1}, \\ \sigma_Z^2 &= \frac{(2a+1)b^2(c^2+1)}{(c^2-1)^2}. \end{aligned} \tag{4.6}$$

The second moment can now be found as $\mu_Z^2 + \sigma_Z^2$.

Before concluding this section, we mention that in the special case that arises when a is restricted to $a = 1/2$, the formulas (4.4) and (4.5) for the type I and II, respectively become particularly simple, as shown in Appendix D.3.

4.2.2 Sum and Difference of Two Independent Gamma RVs

Definition 4 (Gamma Distribution)
X follows a gamma distribution with shape parameter $\alpha > 0$ and scale parameter $\beta > 0$ when the PDF of X is given by

$$f_X(x) = \frac{x^{\alpha-1}e^{-x/\beta}}{\Gamma(\alpha)\beta^\alpha} H(x). \tag{4.7}$$

We use the short hand notation $X \sim \mathcal{G}(\alpha, \beta)$ to denote that X follows a gamma distribution with shape parameter α and scale parameter β. Note that the mean of X $E[X] = \alpha\beta$.

As mentioned before, the gamma distribution is related to the Nakagami distribution. Namely, when a signal is Nakagami distributed with Nakagami fading parameter m and average fading power $\bar{S}$, then the power (i.e., the square) of the signal is gamma-distributed with shape parameter $\alpha = m$ and scale parameter $\beta = \bar{S}/m$.

Theorem 3 (Sum of Two Independent Gamma RVs)
Let X_1, X_2 be mutually independent random variables, distributed as $X_1 \sim \mathcal{G}(\alpha, \beta_1)$ and $X_2 \sim \mathcal{G}(\alpha, \beta_2)$, respectively. Then $\Sigma = X_1 + X_2$ is distributed according to the first of McKay's forms with parameters:

$$\begin{aligned} a &= \alpha - 1/2, \\ b &= 2\beta_1\beta_2/|\beta_1 - \beta_2|, \\ c &= (\beta_1 + \beta_2)/|\beta_1 - \beta_2|. \end{aligned} \tag{4.8}$$

Thus $b > 0$ and $c > 1$ so the restrictions that applies to the McKay distribution I are fulfilled.

This result is provided without proof in the classical textbook by Johnson *et al.* (1994, Sect. 12-4.4), but we could not trace where the result was originally derived and presented.

Theorem 4 (Difference Between Two Independent Gamma RVs)
Let X_1, X_2 be mutually independent random variables, distributed as $X_1 \sim \mathcal{G}(\alpha, \beta_1)$ and $X_2 \sim \mathcal{G}(\alpha, \beta_2)$, respectively. Then $\Delta = X_1 - X_2$ is distributed according to the second of McKay's forms with parameters:

$$\begin{aligned} a &= \alpha - 1/2, \\ b &= 2\beta_1\beta_2/(\beta_1+\beta_2), \\ c &= -(\beta_1-\beta_2)/(\beta_1+\beta_2), \end{aligned} \tag{4.9}$$

where we see that the requirements $b > 0$ and $|c| < 1$ are met since β_1, β_2 are positive.

This result is also provided without proof in the classical textbook by Johnson *et al.* (1994, Sect. 12-4.4) and again we could not trace where the result was originally derived and presented.

Since the shape parameter/Nakagami parameter $\alpha = m \geq 1/2$, the interesting range of values for the a parameter in the McKay distributions (for these applications) is $a \geq 0$.

4.2.3 Special Case of $a = 1/2$

In the important special case of Rayleigh fading, the previous PDF and moment expressions can be used by simply setting $m = \alpha = 1$. As can be seen from Eqs. (4.8) and (4.9), this means that the a parameter in the McKay distributions is $a = 1/2$. It turns out that this restriction leads to particularly simple expressions for both the PDFs and the moments, involving only elementary functions (i.e., no special functions like the hypergeometric function or modified Bessel functions.) It is also possible to find simple closed-form expressions for the CDFs.

Corollary 1 (McKay Type I, $a = 1/2$)
When $a = 1/2$, the type I McKay distribution reduces to the following expression:

$$f_\Sigma(\sigma) = \frac{c^2-1}{2b}(e^{-\frac{\sigma}{b}(c-1)} - e^{-\frac{\sigma}{b}(c+1)})H(\sigma), \tag{4.10}$$

Proof: Insert $a = 1/2$ in Eq. (4.1), use the identity $\sqrt{x\pi/2}\cdot I_{1/2}(x) = \sinh(x)$ (Abramowitz and Stegun, 1972, Eq. 10.2.13) and the hyperbolic sine property $\sinh(x) = (e^z - e^{-z})/2$ (Barnett and Cronin, 1986, Eq. 2.8.2), and collect terms. □

Like Definition 2, Definition 3 can be simplified when $a = 1/2$. The following Corollary is a counterpart to Corollary 1.

Corollary 2 (McKay Type II, $a = 1/2$)
When $a = 1/2$, the type II McKay distribution reduces to the following expression:

$$f_\Delta(\delta) = \frac{1-c^2}{2b}e^{-\frac{1}{b}(\delta c + |\delta|)} \tag{4.11}$$

Proof: Insert $a = 1/2$ (equivalent to $\alpha = 1$) in Eq. (4.2), use the identity $\sqrt{x/(2\pi)} \cdot K_{1/2}(x) = e^{-x}/2$ (Abramowitz and Stegun, 1972, Eq. 10.2.17), and collect terms. □

The hypergeometric functions appearing in Eqs. (4.4) and (4.5) are also possible to simplify when $a = 1/2$, as is displayed in the following corollary:

Corollary 3 (Moments when $a = 1/2$)
Let $a = 1/2$. Then the expression for the moments of both McKay distributions can be written as follows:

$$E[Z^n] = \frac{n!}{2} \frac{b^n}{(c^2-1)^n} \left((c+1)^{n+1} - (c-1)^{n+1} \right) \tag{4.12}$$

Proof: See Appendix D.3. □

Because of the simple PDFs when $a = 1/2$, it is possible to find closed-form expressions for the CDFs of both McKay distributions.

Corollary 4 (CDF of McKay Type I)
When $a = 1/2$, and when restricting, as before, $c > 1$, the CDF of the McKay type I distribution can be written as follows:

$$F_\Sigma(\sigma) = \frac{1}{2} \left((c-1) e^{-\frac{\sigma}{b}(c+1)} - (c+1) e^{-\frac{\sigma}{b}(c-1)} + 2 \right). \tag{4.13}$$

Proof: Integrate Eq. (4.10) from $\sigma = 0$ to σ and collect terms. □

Corollary 5 (CDF of McKay Type II)
When $a = 1/2$, and when restricting $|c| < 1$, the CDF of the McKay type II distribution can be written as follows:

$$F_\Delta(\delta) = \begin{cases} \frac{1+c}{2} \exp\left(\frac{1-c}{b} \delta \right), & \text{for } \delta < 0 \\ 1 - \frac{1-c}{2} \exp\left(-\frac{1+c}{b} \delta \right), & \text{for } \delta \geq 0. \end{cases} \tag{4.14}$$

Proof: For $\delta < 0$: Integrate Eq. (4.11) from $\delta = -\infty$ to δ and collect terms. For $\delta \geq 0$: Find $1 - F_\Delta(\delta)$ by integrating Eq. (4.11) from $\delta = \delta$ to ∞ and collecting terms. □

4.3 Sum and Difference of Correlated Gamma RVs

When the gamma-distributed RVs are correlated, the bivariate gamma distribution—which takes into account the correlation—must be employed.

Definition 5 (Bivariate Gamma Distribution)

X_1 and X_2 are described by a bivariate gamma distribution with common shape parameter $\alpha > 0$, scale parameters $\beta_1 > 0$, $\beta_2 > 0$, respectively, and correlation coefficient $\rho = \frac{\mathrm{Cov}(X_1,X_2)}{\sqrt{\mathrm{Var}(X_1)\,\mathrm{Var}(X_2)}}$ $(0 \leq \rho \leq 1)$ if their joint PDF is given by

$$\begin{aligned} f_{X_1X_2}(x_1,x_2) = {} & \frac{(x_1x_2)^{(\alpha-1)/2}}{\Gamma(\alpha)(\beta_1\beta_2)^{(\alpha+1)/2}(1-\rho)\rho^{(\alpha-1)/2}} \\ & \times \exp\Big(-\frac{x_1/\beta_1 + x_2/\beta_2}{1-\rho}\Big) \\ & \times I_{\alpha-1}\Big(\frac{2\sqrt{\rho}}{1-\rho}\sqrt{\frac{x_1x_2}{\beta_1\beta_2}}\Big)H(x_1)H(x_2), \end{aligned}$$

We use the shorthand notation $X_1, X_2 \sim \mathcal{G}(\alpha,\beta_1,\beta_2,\rho)$ to denote that X_1 and X_2 follow a bivariate gamma distribution. When $\rho \to 0$, the joint PDF reduces to the product of two univariate gamma PDFs (with the aid of Abramowitz and Stegun, 1972, Eq. 9.6.7).

4.3.1 Sum of Two Correlated Gamma RVs

Theorem 5 (Sum of Two Correlated Gamma RVs)

Let $X_1, X_2 \sim \mathcal{G}(\alpha,\beta_1,\beta_2,\rho)$. The sum $\Sigma = X_1 + X_2$ follows the type I McKay distribution with parameters

$$\begin{aligned} a &= \alpha - 1/2, \\ b &= \frac{2\beta_1\beta_2(1-\rho)}{\sqrt{(\beta_1+\beta_2)^2 - 4\beta_1\beta_2(1-\rho)}}, \\ c &= \frac{\beta_1+\beta_2}{\sqrt{(\beta_1+\beta_2)^2 - 4\beta_1\beta_2(1-\rho)}}, \end{aligned} \tag{4.15}$$

where, since $0 \leq \rho < 1$, the restrictions $b > 0$ and $c > 1$ are met.

Proof: See Appendix D.4. □

It can be concluded that Nakagami and Nishio's result (Nakagami and Nishio, 1955; Nakagami, 1960) is in fact on the McKay form. McKay's first form which is known to be valid for the sum of independent gamma-distributed variates, is hence also valid for the sum of correlated ones.

Corollary 6 (Sum of Two Correlated Exponential RVs)
Let $X_1, X_2 \sim \mathcal{G}(1, \beta_1, \beta_2, \rho)$. The sum $\Sigma = X_1 + X_2$ has a PDF as follows:

$$f_\Sigma(\sigma) = \left[\exp\left(-\frac{\beta_1+\beta_2-\sqrt{(\beta_1+\beta_2)^2-4\beta_1\beta_2(1-\rho)}}{2\beta_1\beta_2(1-\rho)}\cdot\sigma\right)\right.$$
$$\left. - \exp\left(-\frac{\beta_1+\beta_2+\sqrt{(\beta_1+\beta_2)^2-4\beta_1\beta_2(1-\rho)}}{2\beta_1\beta_2(1-\rho)}\cdot\sigma\right)\right]$$
$$\times \left(\sqrt{(\beta_1+\beta_2)^2-4\beta_1\beta_2(1-\rho)}\right)^{-1}\cdot H(\sigma). \tag{4.16}$$

Proof: Insert values for b and c from Eq. (4.15) in Eq. (4.10), and collect terms. □

Of course, the previous corollary also applies to the uncorrelated case by inserting corresponding values for b and c (from Eq. (4.8)) in Eq. (4.10), or by inserting $\rho = 0$ in Eq. (4.16).

4.3.2 Difference Between Two Correlated Gamma RVs

Theorem 6 (Difference Between Two Correlated Gamma RVs)
Let $X_1, X_2 \sim \mathcal{G}(\alpha, \beta_1, \beta_2, \rho)$. The difference $\Delta = X_1 - X_2$ follows the PDF given by

$$f_\Delta(\delta) = \frac{|\delta|^{\alpha-1/2}}{\Gamma(\alpha)\sqrt{\pi}\sqrt{\beta_1\beta_2(1-\rho)}}\left(\frac{1}{(\beta_1+\beta_2)^2-4\beta_1\beta_2\rho}\right)^{\frac{2\alpha-1}{4}}$$
$$\times \exp\left(\frac{\delta/2}{1-\rho}\left(\frac{1}{\beta_2}-\frac{1}{\beta_1}\right)\right)$$
$$\times K_{\alpha-1/2}\left(|\delta|\frac{\sqrt{(\beta_1+\beta_2)^2-4\beta_1\beta_2\rho}}{2\beta_1\beta_2(1-\rho)}\right), \quad \text{for } \delta \neq 0. \tag{4.17a}$$

When $\alpha > 1/2$, there exists an expression for the special case $\delta = 0$:

$$f_\Delta(0) = \frac{\Gamma(\alpha-\frac{1}{2})}{\sqrt{\pi}\Gamma(\alpha)}\frac{\left(4\beta_1\beta_2(1-\rho)\right)^{\alpha-1}}{\left((\beta_1+\beta_2)^2-4\beta_1\beta_2\rho\right)^{\alpha-1/2}}. \tag{4.17b}$$

Proof: See Appendix D.5. □

Corollary 7 (Relation to McKay's Distribution Function)
The difference between two correlated gamma RVs is distributed according to the type II McKay distribution with parameters:

$$\begin{aligned} a &= \alpha - 1/2, \\ b &= \frac{2\beta_1\beta_2(1-\rho)}{\sqrt{(\beta_1-\beta_2)^2 + 4\beta_1\beta_2(1-\rho)}}, \\ c &= -\frac{\beta_1-\beta_2}{\sqrt{(\beta_1-\beta_2)^2 + 4\beta_1\beta_2(1-\rho)}}, \end{aligned} \tag{4.18}$$

where the conditions $b > 0$ and $|c| < 1$ are met, as long as $\rho < 1$.

Proof: Can be readily seen by inserting the parameters a, b, and c from Eq. (4.18) in Eq. (4.2). □

Corollary 8 (Difference Between Two Correlated Exponential RVs)
This corollary is a counterpart to Corollary 6.

Let $X_1, X_2 \sim \mathcal{G}(1, \beta_1, \beta_2, \rho)$. The difference $\Delta = X_1 - X_2$ has a PDF as follows:

$$f_\Delta(\delta) = \frac{\exp\left(\dfrac{\delta\cdot(\beta_1-\beta_2) - |\delta|\cdot\sqrt{(\beta_1-\beta_2)^2 + 4\beta_1\beta_2(1-\rho)}}{2\beta_1\beta_2(1-\rho)}\right)}{\sqrt{(\beta_1-\beta_2)^2 + 4\beta_1\beta_2(1-\rho)}} \tag{4.19}$$

Proof: Insert values for b and c from Eq. (4.18) in Eq. (4.11), and collect terms. □

This implies, of course, that an expression for the CDF of the difference between two exponentially distributed RVs can be expressed similarly to Eq. (4.14), with values for b and c from Eq. (4.18) inserted.

4.3.3 Numerical Validation

Monte Carlo simulation is well suited for checking the results derived in the previous section. Correlated gamma-distributed random variables can be generated as described by Ko and Alouini or by Tellambura and Jayalath (2000). We used the algorithm described by Ko and Alouini to generate 10 000 pairs $\{X_1, X_2\} \sim \mathcal{G}(\alpha, \beta_1, \beta_2, \rho)$ and computed the difference. A normalized histogram of this difference was plotted and is shown in Fig. 4.1 for the special case of $\alpha = 2$, $\beta_1 = 20$, $\beta_2 = 10$, and $\rho = 0.5$. As can be seen from this figure the analytical and the simulation results are in perfect agreement.

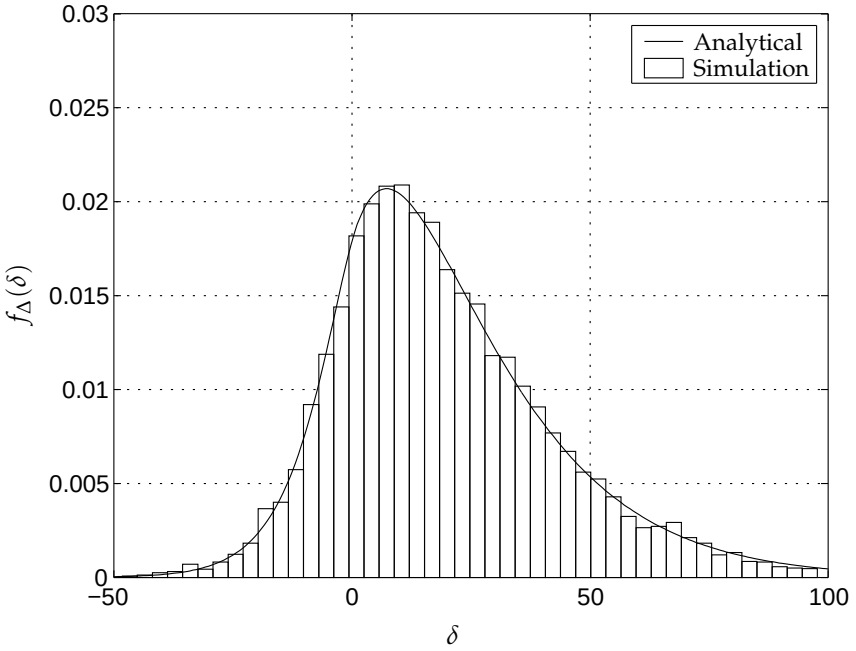

FIGURE 4.1: Comparison between the analytical PDF and the PDF obtained via Monte Carlo simulation, for $\alpha = 2$, $\beta_1 = 20$, $\beta_2 = 10$, and $\rho = 0.5$.

4.4 Application to Outage Probability with Self-Interference

4.4.1 System Model

When transmitting in a multipath fading environment, one will receive reflections that appear as delayed, in average down-scaled, and correlated versions of the desired signal. If the reflections are not handled properly, they will degrade the quality of the decoded signal because of the self-interference, as pointed out by Ligeti (2000) for multicarrier systems. A measure for the effect of interference and noise is the signal-to-interference-and-noise ratio (SINR).

We consider a single carrier system where there is one self-interfering signal and define the SINR as follows:

Definition 6 (SINR)

Let S_D be the instantaneous power of the desired signal, S_I the instantaneous power of the reflected signal, and N the additive noise variance. We

define the SINR as

$$\gamma = \text{SINR} = \frac{S_D}{S_I + N}.$$

4.4.2 Outage Probability

If the SINR falls below a predetermined protection ratio γ_{th}, an outage is declared. Denoting the outage probability by P_{out}, we have

$$\begin{aligned} P_{out} &= \Pr\{\gamma \leq \gamma_{th}\} = \Pr\Big\{\frac{S_D}{S_I + N} \leq \gamma_{th}\Big\} \\ &= \Pr\{\Delta \leq N\gamma_{th}\}, \end{aligned}$$

where we have defined $\Delta = S_D - \gamma_{th} S_I$.

In a Nakagami fading environment with Nakagami parameter m, S_D will be gamma-distributed, $S_D \sim \mathcal{G}(m, \frac{\bar{S}_D}{m})$ where $\bar{S}_D$ is the short-term average of the desired faded signal power. The self-interfering signal S_I is also gamma distributed, i.e., $S_I \sim \mathcal{G}(m, \frac{\bar{S}_I}{m})$. The desired and interfering signals S_D, S_I are correlated with correlation coefficient ρ so that the pair $\{S_D, S_I\} \sim \mathcal{G}(m, \frac{\bar{S}_D}{m}, \frac{\bar{S}_I}{m}, \rho)$. Multiplication of a gamma RV with a constant results in a new gamma RV with mean scaled by the multiplication factor, so S_D and $\gamma_{th} S_I$ are correlated with correlation coefficient $\rho' = \frac{\text{Cov}(S_D, \gamma_{th} S_I)}{\sqrt{\text{Var}(S_D)\,\text{Var}(\gamma_{th} S_I)}} = \rho$ and the pair of signals S_D and $\gamma_{th} S_I$ are consequently gamma-distributed, $\{S_D, \gamma_{th} S_I\} \sim \mathcal{G}(m, \frac{\bar{S}_D}{m}, \frac{\gamma_{th}\bar{S}_I}{m}, \rho)$. The random variable Δ is the difference of two correlated gamma-distributed RVs, and it follows the distribution $f_\Delta(\delta)$ given in Eq. (4.17). The outage probability can then be expressed as the CDF of Δ evaluated at $N\gamma_{th}$:

$$P_{out} = F_\Delta(N\gamma_{th}) = \int_{-\infty}^{N\gamma_{th}} f_\Delta(\delta)\, d\delta = 1 - \int_{N\gamma_{th}}^{\infty} f_\Delta(\delta)\, d\delta. \tag{4.20}$$

In the general case of Nakagami fading, we are not able to find a closed-form solution for this integral, but because of the smooth tails, numerical integration over the PDF as given in Eq. (4.20) can be easily performed with standard mathematical software such as Matlab or Mathematica. However, the CDF can be found in closed-form for the following two special cases.

Rayleigh Fading Case

For the special case of Rayleigh fading, (i.e., $m = 1$), there exists a closed-form expression for the CDF of Δ—and hence the outage probability—

namely Eq. (4.14) with the parameters b and c defined as follows:

$$\begin{aligned} b &= \frac{2\bar{S}_D\bar{S}_I\gamma_{th}(1-\rho)}{\sqrt{(\bar{S}_D-\bar{S}_I\gamma_{th})^2+4\bar{S}_D\bar{S}_I\gamma_{th}(1-\rho)}}, \\ c &= -\frac{\bar{S}_D-\bar{S}_I\gamma_{th}}{\sqrt{(\bar{S}_D-\bar{S}_I\gamma_{th})^2+4\bar{S}_D\bar{S}_I\gamma_{th}(1-\rho)}}. \end{aligned} \tag{4.21}$$

Note that $N\gamma_{th}$ is positive, so the second line of Eq. (4.14) should be used.

Interference Limited Case

In the case of interference-limited transmission the noise is negligible and the noise variance is approximated by zero. In this case a solution to the integral in Eq. (4.20) can be found in terms of Gaussian hypergeometric functions (by means of Gradshteyn and Ryzhik, 2000, Eq. 6.621-3). After some manipulations and with the help of some transformations (Eqs. (15.3.7), (15.3.3), and (6.6.8) from Abramowitz and Stegun, 1972), it can be shown that the outage probability can be put in the following compact closed-form:

$$P_{out} = I_x(m,m), \tag{4.22}$$

where $x = \frac{1}{1+\frac{1-c}{1+c}}$ (with c given in Eq. (4.21)) and $I_x(\cdot,\cdot)$ is the normalized incomplete Beta function (defined in Abramowitz and Stegun, 1972, Eq. 6.6.2 and tabulated by Pearson, 1932). In the case that the correlation $\rho = 0$, $\frac{1-c}{1+c} = \frac{\bar{S}_D}{\bar{S}_I\gamma_{th}}$. Once substituted in (4.22), this leads to a result which is in agreement with the results of Abu-Dayya and Beaulieu (1991, Eq. 6a) and Yao and Sheikh (1992, Eq. 13) for the outage probability of cellular systems when the number of co-channel interferers in the latter equations is set to one. In the case of m integer, it can be shown that Eq. (4.22) reduces to the following finite sum

$$P_{out} = \left(1+\frac{1-c}{1+c}\right)^{1-2m}\sum_{k=0}^{m-1}\binom{2m-1}{k}\left(\frac{1-c}{1+c}\right)^k. \tag{4.23}$$

4.4.3 Numerical Examples

The outage probability depends on a number of factors; γ_{th}, $\bar{S}_D$, $\bar{S}_I$, N, ρ, and m. When $\bar{S}_I$ is more than approximately three orders of magnitude larger than N, it turns out that P_{out} basically only depends on $\frac{\bar{S}_D}{(\bar{S}_I+N)\gamma_{th}}$, ρ, and m. However, when the magnitude of $\bar{S}_I$ decreases in comparison to N,

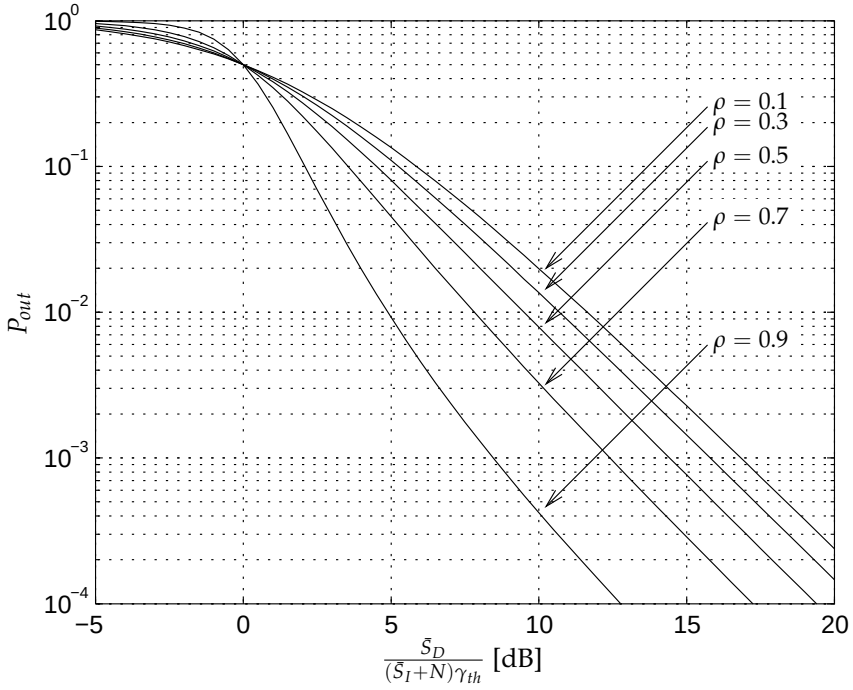

FIGURE 4.2: Outage probability as a function of $\frac{\bar{S}_D}{(\bar{S}_I+N)\gamma_{th}}$ for $m = 2$ and for $\rho = 0.1, 0.3, 0.5, 0.7$, and 0.9.

the effect of ρ on the outage probability diminishes. We will focus in our numerical examples on the former case.

The outage probability was calculated from the formula in Eq. (4.20) by using numerical integration, for various values of the parameters; plots of P_{out} as a function of $\frac{\bar{S}_D}{(\bar{S}_I+N)\gamma_{th}}$ are shown in Figs. 4.2–4.3 and as a function of ρ in Figs. 4.4–4.5. Note that, for $\frac{\bar{S}_D}{(\bar{S}_I+N)\gamma_{th}} > 0\,\text{dB}$, P_{out} decreases as ρ increases. Also; for $\frac{\bar{S}_D}{(\bar{S}_I+N)\gamma_{th}} = 0\,\text{dB}$, $P_{out} \approx 0.5$, regardless of the value of the other parameters.

4.5 Conclusions

This chapter offered general formulas for the PDF of the sum and the difference of two correlated not necessarily identically distributed squared Nakagami RVs and established connections between these PDFs and the McKay "Bessel function" distributions. Additional formulas for the moments of these distributions in terms of the Gauss' hypergeometric function were derived. As an illustration of the mathematical formalism, an applica-

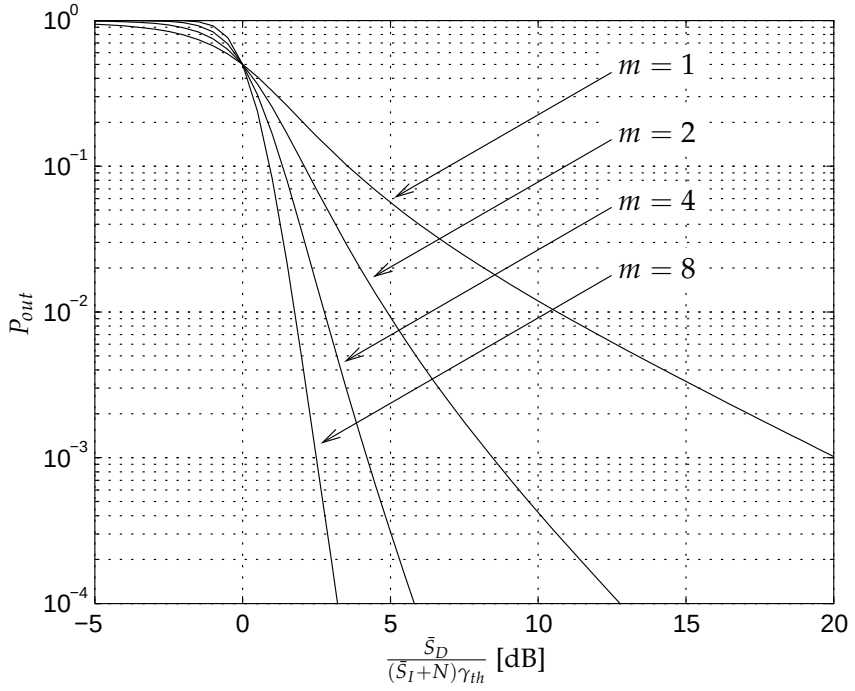

FIGURE 4.3: Outage probability as a function of $\frac{\bar{S}_D}{(\bar{S}_I+N)\gamma_{th}}$ for $m = 1$, 2, 4, and 8; and for $\rho = 0.9$.

tion of these new results relevant to the calculation of outage probability in presence of self-interference was presented and some numerical examples were provided and discussed.

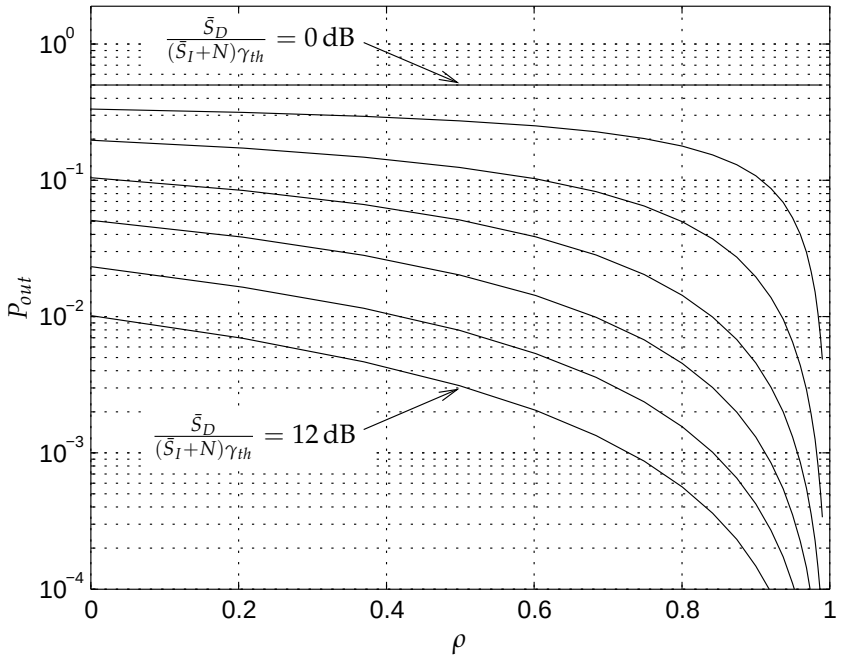

FIGURE 4.4: Outage probability as a function of ρ for $m = 2$ and for $\frac{\bar{S}_D}{(\bar{S}_I+N)\gamma_{th}} = 0, 2, \cdots, 10, 12\,\text{dB}$.

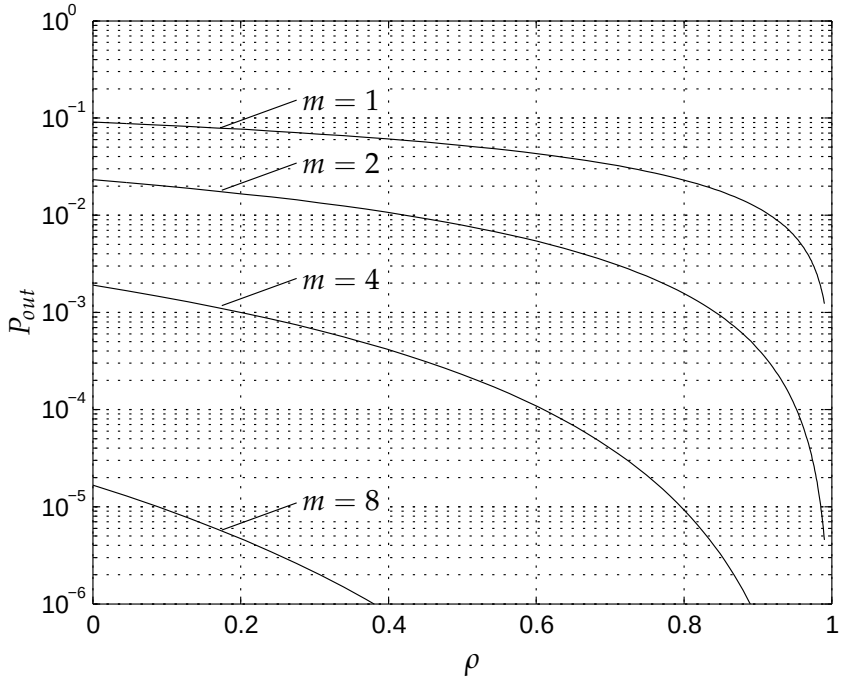

FIGURE 4.5: Outage probability as a function of ρ for $m = 1$, 2, 4, and 8; and for $\frac{\bar{S}_D}{(\bar{S}_I+N)\gamma_{th}} = 10\,\text{dB}$.

Chapter 5

CSNR Estimation Error in Rayleigh Fading Channels

This chapter is based on a paper presented at the conference *NORSIG* (Holm, 2001).

5.1 Introduction

In mobile and wireless communication, the channel is frequently perturbed by fading, which leads to varying channel signal-to-noise ratio (CSNR). In order to compensate for the fading, several schemes have been proposed—among them is fast power control (Hashem and Sousa, 1997), pilot symbol assisted modulation (Tang *et al.*, 1999) and adaptive (coded) modulation (Alouini and Goldsmith, 2000; Hole *et al.*, 2000). In all these methods, knowledge of the instantaneous channel quality, the CSNR, is essential for good performance. An inaccurate CSNR estimate will degrade the performance of adaptive modulation and coding systems. For instance, the rate-adaptive scheme of Hole *et al.* (2000) employs a set of channel codes, each designed for a specific CSNR. Updated information on the channel state enables the transmitter to frequently change the code, thus using the code best suited for the instantaneous CSNR. A too low estimate will cause the rate to be less than what the channel actually is able to convey under the bit error rate (BER) requirements, while a too high estimate will cause the BER to be larger than required.

In order to gain control over the BER, to calculate bounds for the probability of failure, and to maximize the spectral efficiency, it is advantageous to know the statistical properties of the estimation error. The purpose of this chapter is to describe the characteristics of the error when using pi-

lot symbol assisted channel estimation on a Rayleigh fading channel. We denote the true CSNR by γ and its estimate by $\hat{\gamma}$. The error can then be defined as the difference $\Delta = \hat{\gamma} - \gamma$ between the CSNR estimate and the true CSNR in natural units. In the previous chapter, we provided general expressions for the statistical properties of the difference between two gamma-distributed random variables (RVs) and related the expressions to McKay's Bessel function distribution (McKay, 1932). In this chapter, we utilize those expressions to find closed-form expressions for the probability density function (PDF) and the cumulative distribution function (CDF) of the natural unit error measure. It is also desirable to investigate the difference in decibel $\Delta_{\text{dB}} = \hat{\gamma}_{\text{dB}} - \gamma_{\text{dB}}$ (Wong and Cox, 1999). Expressions for the PDF and CDF of the dB estimation error measure are provided in this chapter.

The McKay distribution was defined in Section 4.2. For convenience, the definition is recited in Section 5.2. The Rayleigh fading model is given in Section 5.3, followed by Section 5.4 where the pilot symbol technique which is used for CSNR estimation is described. Closed-form expressions for the PDF and CDF of the natural units difference error Δ are derived in Section 5.5. In this section, a general expression for the nth moment of the PDF is also computed, and the PDF is verified by simulation. Section 5.6 is devoted to finding the PDF of the error in decibel, and conclusions follow in Section 5.7.

5.2 The McKay Distributions

McKay (1932) defines the following "Bessel Function Distribution":

Definition 7 (McKay Distributions)
X follows the McKay distribution with parameters $a > -\frac{1}{2}$, $b > 0$, and c, when the PDF of X is given by

$$f_X(x) = \frac{|1-c^2|^{a+1/2}\,|x|^a e^{-x\frac{c}{b}}}{\sqrt{\pi}2^a b^{a+1}\Gamma(a+1/2)} \times \begin{cases} \pi I_a\left(\frac{|x|}{b}\right) H(x) & \text{Type I—for } c > 1, \\ K_a\left(\frac{|x|}{b}\right) & \text{Type II—for } |c| < 1, \end{cases} \tag{5.1}$$

where $I_a(\cdot)$ and $K_a(\cdot)$ are the Modified Bessel functions of the first and second kind, respectively, (both of order a) and $H(\cdot)$ is the Heaviside (unit step) function.

The value of c decides the one that should be used of the two forms of the distribution. Note that, for convenience, we have defined the first form for positive x only. However—if the parameter c is negative ($c < -1$), the first form will be defined for negative, instead of positive x.

It is known that the sum and difference of two independent gamma-distributed RVs follow the McKay distribution—see (Johnson *et al.*, 1994, Sect. 12-4.4). However, it is shown in Chapter 4 that also the sum and difference of correlated gamma-distributed RVs are described by the McKay distribution.

5.2.1 Special case for $a = 1/2$

It is shown in Chapter 4 that the sum or difference of gamma-distributed random variables with shape factor m is McKay-distributed with the parameter $a = m - \frac{1}{2}$. Note also that the square of a Rayleigh-distributed random variable is distributed according to a gamma distribution with shape factor 1. The gamma distribution with shape factor 1 is equivalent to the exponential distribution. Considering the sum or difference of the power (or square) of two Rayleigh-distributed RVs, it can be concluded that this sum or difference will be distributed according to the McKay distribution. In this important special case, the expression for the McKay Distribution reduces to the following one:

$$f_X(x) = \frac{|1-c^2|}{2b} \times \begin{cases} (e^{-\frac{x}{b}(c-1)} - e^{-\frac{x}{b}(c+1)})H(x) & \text{Type I,} \\ e^{-\frac{1}{b}(xc+|x|)} & \text{Type II.} \end{cases} \tag{5.2}$$

involving no special functions.

5.3 System Model

We assume a frequency nonselective Rayleigh fading channel—also denoted as a flat fading channel. When using a QAM modulation technique, the transmitted signal can be viewed as a complex signal. In this manner, the channel can be modeled as attenuation of the transmitted signal with a complex zero-mean Gaussian random variable $z(k) = \alpha(k)e^{j\theta(k)}$ with amplitude $\alpha(k)$ and phase $\theta(k)$ followed by addition of complex Gaussian noise $n(k)$. This means that when the information-bearing signal is $x(k)$, the received symbol at time instant k is $y(k) = z(k)x(k) + n(k)$. The channel model is illustrated in Fig. 5.1.

The noise variance is $\sigma_n^2 = N_0 B$ where N_0 is the spectral density of the noise and B is the bandwidth of the signal. We assume coherent detection, such that the phase θ is detected and corrected in the receiver. Thus, only the fading envelope will contribute to the CSNR. If we denote the average transmit power by P, the instantaneous CSNR is $\gamma = \alpha^2 \frac{P}{N_0 B}$ where the

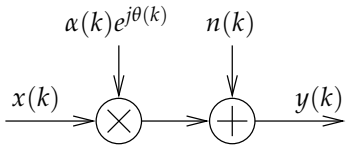

FIGURE 5.1: Flat fading.

time index k is omitted. For notational simplicity, the time index will be suppressed in the rest of the chapter.

As the CSNR is the square of a Rayleigh-distributed random variable, it is distributed according to an exponential distribution with mean $E[\gamma] = \bar{\gamma}$, or, equivalently, to a gamma distribution with shape factor 1 and scale factor $\bar{\gamma}$.

5.4 Fading Envelope and CSNR Estimation

PSAM estimation of the fading envelope is discussed by Tang *et al.* (1999), where the $\hat{\alpha}$ is a linear combination of preceding and subsequent known pilot symbols. Clearly, such an estimator can only be used for post-processing of received symbols. In the case of adaptive modulation, which requires feedback of channel state information (Alouini and Goldsmith, 2000; Hole *et al.*, 2000), a predictor would be used. For simplicity, we consider the special case of Tang *et al.* (1999) where the $\hat{\alpha}$ is based on one pilot symbol only, and we also only consider the instant of reception of the pilot symbol. The analysis can be readily extended to the more general case of a longer-memory linear estimator or predictor.

The information-bearing signal is grouped in clusters, and $L-1$ symbols plus a pilot symbol a_p of known phase and with power P_0 constitute a frame. From here on, it is assumed that the pilot symbol power is the average transmission power P. At the time the pilot symbol plus the channel perturbation is received, the fading can be estimated by dividing with the known a_p:

$$\hat{z} = \frac{y}{a_p} = z + \frac{n}{a_p}. \tag{5.3}$$

An estimate of the envelope at the time the pilot symbol arrives is then $\hat{\alpha} = |\hat{z}|$, and in the simplified case where only one pilot symbol is considered, an apparent estimator for γ is $\hat{\gamma} = \hat{\alpha}^2 \frac{P}{N_0 B}$. It must be emphasized that this estimator is very simple and not a very good one; for instance, it is biased.

However, we choose to use it for the sake of simplicity, since the results are easily generalized to more advanced linear estimators.

Since $\hat{z}$ is a sum of zero-mean complex Gaussian random variables, it will itself be a zero-mean complex Gaussian random variable. The estimate of the CSNR will accordingly be exponentially distributed with mean $E[\hat{\gamma}] = \bar{\hat{\gamma}}$. Naturally, γ and $\hat{\gamma}$ will be correlated, and they are as such described by a bivariate gamma distribution with shape factor 1. Thus,

$$f_{\gamma,\hat{\gamma}}(\gamma,\hat{\gamma}) = \frac{1}{(1-\rho)\bar{\gamma}\bar{\hat{\gamma}}}\, I_0\left(\frac{2\sqrt{\rho}}{(1-\rho)}\sqrt{\frac{\gamma\hat{\gamma}}{\bar{\gamma}\bar{\hat{\gamma}}}}\right)\exp\left(-\frac{1}{1-\rho}\left(\frac{\gamma}{\bar{\gamma}}+\frac{\hat{\gamma}}{\bar{\hat{\gamma}}}\right)\right) \quad (5.4)$$

where $I_0(\cdot)$ is the modified Bessel function of the first kind and zeroth order and the term

$$\rho = \frac{\mathrm{Cov}(\gamma,\hat{\gamma})}{\sqrt{\mathrm{Var}(\gamma)\,\mathrm{Var}(\hat{\gamma})}}, \qquad 0 \le \rho < 1, \quad (5.5)$$

is the power correlation coefficient.

The parameters $\bar{\hat{\gamma}}$ and ρ can both be expressed in terms of γ, by noting that

$$\bar{\hat{\gamma}} = \frac{P}{N_0 B}E[|\hat{z}|^2] = E[\gamma] + \frac{P}{N_0 B}E[|n/a_p|^2] = \bar{\gamma} + 1. \quad (5.6)$$

Note also that, since $E[\hat{\gamma}] \neq E[\gamma]$, $\hat{\gamma}$ is a biased estimator. For the case of the correlation factor, observe that

$$\mathrm{Var}(\gamma) = \bar{\gamma}^2, \quad (5.7)$$

$$\mathrm{Var}(\hat{\gamma}) = \bar{\hat{\gamma}}^2 = (\bar{\gamma}+1)^2 \quad (5.8)$$

and

$$\begin{aligned}\mathrm{Cov}(\gamma,\hat{\gamma}) &= E[\gamma\hat{\gamma}] - \bar{\gamma}\bar{\hat{\gamma}} \\ &= E[\gamma^2] + E[\gamma]\frac{P}{N_0 B}E[|n/a_p|^2] - \bar{\gamma}\bar{\hat{\gamma}} \\ &= 2\bar{\gamma}^2 + \bar{\gamma} - \bar{\gamma}(\bar{\gamma}+1) \\ &= \bar{\gamma}^2. \end{aligned} \quad (5.9)$$

Thus,

$$\rho = \frac{\bar{\gamma}^2}{\bar{\gamma}\bar{\hat{\gamma}}} = \frac{\bar{\gamma}}{1+\bar{\gamma}}. \quad (5.10)$$

5.5 PDF of the Error $\Delta = \hat{\gamma} - \gamma$

As shown in Chapter 4, the difference Δ between two correlated gamma-distributed random variables is described by the type I McKay distribution (McKay, 1932). A particularly simple special case arises when the two variables are exponentially distributed; then, the PDF of the difference is expressed as in Eq. (5.2)—recited here for convenience:

$$f_\Delta(\delta) = \frac{1-c^2}{2b} e^{-\frac{1}{b}(\delta c + |\delta|)}, \tag{5.11}$$

where b and c are given in terms of the scale factors β_1, β_2, and the correlation coefficient ρ of the random variables:

$$\begin{aligned} b &= \frac{2\beta_1\beta_2(1-\rho)}{\sqrt{(\beta_1-\beta_2)^2 + 4\beta_1\beta_2(1-\rho)}}, \\ c &= -\frac{\beta_1-\beta_2}{\sqrt{(\beta_1-\beta_2)^2 + 4\beta_1\beta_2(1-\rho)}}, \end{aligned} \tag{5.12}$$

where $\beta_1 = \bar{\hat{\gamma}}$ and $\beta_2 = \bar{\gamma}$. For the simple estimator defined in Section 5.4, we found that $\bar{\hat{\gamma}} = \bar{\gamma} + 1$ and $\rho = \frac{\bar{\gamma}}{1+\bar{\gamma}}$, so that b and c reduces to

$$b = \frac{2\bar{\gamma}}{\sqrt{4\bar{\gamma}+1}}, \qquad c = \frac{-1}{\sqrt{4\bar{\gamma}+1}}, \tag{5.13}$$

and Eq. (5.11) consequently becomes:

$$f_\Delta(\delta) = \exp\left(\frac{\delta - |\delta| \cdot \sqrt{4\bar{\gamma}+1}}{2\bar{\gamma}}\right) \Big/ \sqrt{4\bar{\gamma}+1} \tag{5.14}$$

A histogram of the estimation error has been obtained by Monte-Carlo simulation of the channel. The result, compared with plots of Eq. (5.14) for different values of $\bar{\gamma}$, is shown in Fig. 5.2.

5.5.1 CDF of Δ

The CDF of the McKay distribution can be calculated in closed-form in the special case (as shown in Section 4.2.3):

$$F_\Delta(\delta) = \begin{cases} \frac{1+c}{2}\exp\left(\frac{1-c}{b}\delta\right), & \text{for } \delta < 0 \\ 1 - \frac{1-c}{2}\exp\left(-\frac{1+c}{b}\delta\right), & \text{for } \delta \geq 0. \end{cases} \tag{5.15}$$

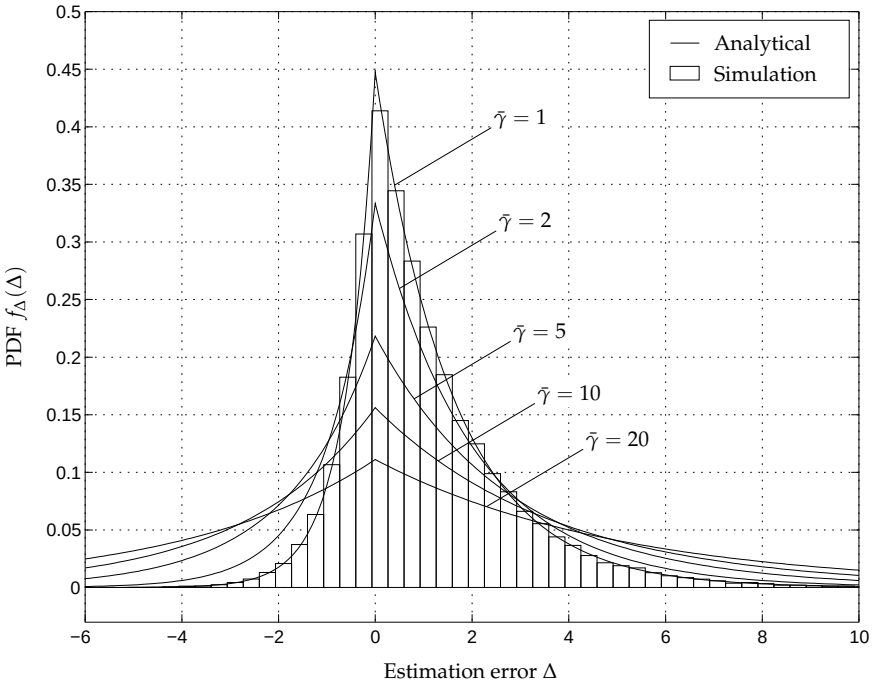

FIGURE 5.2: Monte-Carlo Simulation of the Estimation Error Δ for $\bar{\gamma} = 1$, along with plots of the PDF of Δ from Eq. (5.14) for $\bar{\gamma} = 1, 2, 5, 10$ and 20. Comparison of the simulation results and the closed-form expression of the PDF indicate that the expression is valid.

As before, b and c are inserted from Eq. (5.13),

$$F_\Delta(\delta) = \begin{cases} \frac{\sqrt{4\bar{\gamma}+1}-1}{2\sqrt{4\bar{\gamma}+1}} \exp\left(\frac{\sqrt{4\bar{\gamma}+1}+1}{2\bar{\gamma}}\delta\right), & \delta < 0 \\ 1 - \frac{\sqrt{4\bar{\gamma}+1}+1}{2\sqrt{4\bar{\gamma}+1}} \exp\left(-\frac{\sqrt{4\bar{\gamma}+1}-1}{2\bar{\gamma}}\delta\right), & \delta \geq 0. \end{cases} \tag{5.16}$$

5.5.2 Moments

In Chapter 4, an expression for the moments of a McKay-distributed random variable is also provided. In the special case that applies to the difference between exponentially distributed random variables, the moments (of any order) are:

$$E[\Delta^n] = \frac{n!}{2} \frac{b^n}{(c^2-1)^n} \left((c+1)^{n+1} - (c-1)^{n+1}\right) \tag{5.17}$$

and by inserting b and c from Eq. (5.13) and collecting terms, we arrive at the following expression for the moments of the estimation error δ:

$$E[\Delta^n] = \frac{n!}{2^{n+1}\sqrt{4\bar{\gamma}+1}}\left((1+\sqrt{4\bar{\gamma}+1})^{n+1} - (1-\sqrt{4\bar{\gamma}+1})^{n+1}\right) \tag{5.18}$$

From Eq. (5.18) we calculate $E[\Delta] = 1$ and $E[\Delta^2] = 2\bar{\gamma}+2$ which leads to $\mathrm{Var}(\Delta) = 2\bar{\gamma}+1$. This result is supported by Fig. 5.2 in which plots of the PDF of Δ for several values of $\bar{\gamma}$ indicate that the variance increases as the mean CSNR $\bar{\gamma}$ increases.

5.6 PDF of the Error in Decibel $\Delta_{\mathrm{dB}} = \hat{\gamma}_{\mathrm{dB}} - \gamma_{\mathrm{dB}}$

We define $\Phi = \hat{\gamma}/\gamma$. The PDF of the ratio of two correlated gamma-distributed random variables is provided by Nakagami (1960, Eq. 145). Nakagami's formula includes, as a special case, exponentially distributed random variables. Accordingly, by using the simplifications in Eqs. (5.6) and (5.10), we find the PDF of Φ:

$$f_\Phi(\phi) = \frac{1}{\bar{\gamma}} \frac{\left(\phi + \frac{1+\bar{\gamma}}{\bar{\gamma}}\right)}{\left(\left(\phi + \frac{1+\bar{\gamma}}{\bar{\gamma}}\right)^2 - 4\phi\right)^{3/2}} H(\phi). \tag{5.19}$$

By change of variables (since $\Delta_{\mathrm{dB}} = 10\log_{10}\Phi$,) the PDF of the difference in decibel can be derived as follows,

$$f_{\Delta_{\mathrm{dB}}}(\delta_{\mathrm{dB}}) = \frac{1}{\bar{\gamma}}\frac{\ln 10}{10} \frac{10^{\frac{\delta_{\mathrm{dB}}}{10}}\left(10^{\frac{\delta_{\mathrm{dB}}}{10}} + \frac{1+\bar{\gamma}}{\bar{\gamma}}\right)}{\left(\left(10^{\frac{\delta_{\mathrm{dB}}}{10}} + \frac{1+\bar{\gamma}}{\bar{\gamma}}\right)^2 - 4\cdot 10^{\frac{\delta_{\mathrm{dB}}}{10}}\right)^{3/2}}. \tag{5.20}$$

Eq. (5.20) is plotted for several values of $\bar{\gamma}$, along with a Monte-Carlo Simulation in Fig. 5.3. The plots indicate that the main lobe of $f_{\Delta_{\mathrm{dB}}}(\delta_{\mathrm{dB}})$ becomes narrower and approaches 0 dB as the mean CSNR $\bar{\gamma}$ increases. However, closed-form expressions for $E[\Delta_{\mathrm{dB}}]$ and $\mathrm{Var}(\Delta_{\mathrm{dB}})$ have not been found.

5.6.1 CDF of Δ_{dB}

By integrating Eq. (5.19) from 0 to ϕ, the CDF of Φ can be found and expressed as follows:

$$F_\Phi(\phi) = \frac{1}{2}\frac{\phi - \frac{\bar{\gamma}+1}{\bar{\gamma}}}{\sqrt{\left(\phi + \frac{\bar{\gamma}+1}{\bar{\gamma}}\right)^2 - 4\phi}} + \frac{1}{2}. \tag{5.21}$$

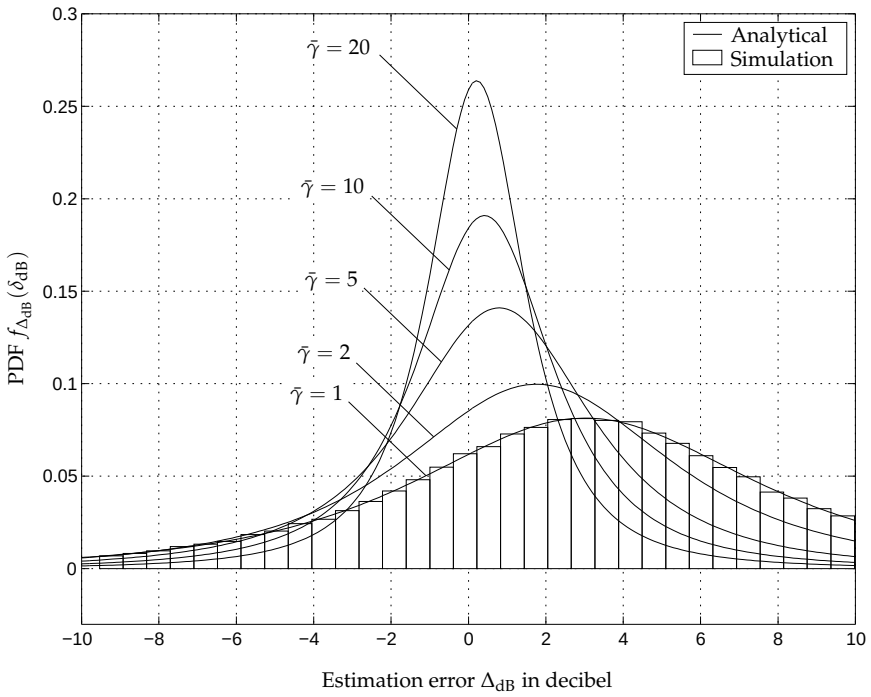

FIGURE 5.3: Monte-Carlo Simulation of the Estimation Error Δ_{dB} for $\bar{\gamma} = 1$, along with plots of the PDF of Δ_{dB} from Eq. (5.20) for $\bar{\gamma} = 1$, 2, 5, 10 and 20 (0, 3, 7, 10 and 13 dB, respectively.)

Thus, the CDF of Δ_{dB} can be found as:

$$F_{\Delta_{\mathrm{dB}}}(\delta_{\mathrm{dB}}) = F_{\Phi}(10^{\frac{\delta_{\mathrm{dB}}}{10}}) = \frac{1}{2}\frac{10^{\frac{\delta_{\mathrm{dB}}}{10}} - \frac{\bar{\gamma}+1}{\bar{\gamma}}}{\sqrt{\left(10^{\frac{\delta_{\mathrm{dB}}}{10}} + \frac{\bar{\gamma}+1}{\bar{\gamma}}\right)^2 - 4 \cdot 10^{\frac{\delta_{\mathrm{dB}}}{10}}}} + \frac{1}{2}. \tag{5.22}$$

5.7 Conclusions

We have found closed-form expressions for the PDF and CDF of two different measures for the estimation error when using a pilot tone fading estimation system on a Rayleigh channel. The two error measures are the error defined as the difference $\Delta = \hat{\gamma} - \gamma$ between the CSNR estimate and the true CSNR measured in natural units, and the error $\Delta_{\mathrm{dB}} = \hat{\gamma}_{\mathrm{dB}} - \gamma_{\mathrm{dB}}$ when the true CSNR and the estimate is given in decibel. The expressions have been verified by Monte-Carlo simulations.

For the natural units difference, a closed-form expression for the moments of the distribution has also been derived. The expression indicates

that the variance of Δ increases linearly as the mean CSNR increases. This somewhat surprising result can be explained by considering that, since the instantaneous CSNR γ and $\hat{\gamma}$ are exponentially distributed, the variance of both increase with the square of $\bar{\gamma}$. It is reasonable that the variance of the difference $\hat{\gamma} - \gamma$ also increases, even if they are correlated.

For the difference in decibel values, the mean and variance have not been found. However, plots of the $f_{\Delta_{\mathrm{dB}}}(\delta_{\mathrm{dB}})$ for several values of $\bar{\gamma}$ indicate that the main lobe becomes narrower and that it tends towards 0 dB as $\bar{\gamma}$ increases.

The estimator considered in this chapter is a very simple one, based on the currently received pilot symbol only. A natural and simple extension of this work would be to incorporate a more general estimator, where $\hat{z}$ is a linear combination of several pilot symbols, as explained for instance by Tang *et al.* (1999). Specifically, incorporating the predictor described in Chapter 3 would yield results that are more applicable to a system that could be implemented.

Chapter 6

Conclusions

In order to give an outline of the major achievements described in this dissertation, the next section will state the main contributions. The chapter will end with some suggestions for further research.

Main Contributions of the Thesis

- A method for assessing performance merits of an adaptive coded modulation (ACM) system was developed by Hole, Holm, and Øien (2000) as an extension to an earlier method which applies to uncoded systems only. The new method has in Chapter 2 been employed to evaluate the average spectral efficiency of a coding scheme utilizing any set of multi-dimensional trellis codes originally designed for additive white Gaussian noise channels.

- A system based on the set of codes discussed in Chapter 2 has been extended to take into consideration the effect of feedback delay and inaccurate estimation of channel state information (CSI).

- Use of linear prediction based on pilot symbols has been proposed as a technique for combating the harmful effects of feedback delay, and a predictor which is optimal in the maximum a posteriori (MAP) sense has been considered. The advantage of employing a MAP optimal predictor in the previously discussed system has been assessed.

- McKay's probability distribution (McKay, 1932) has been scrutinized, obtaining expressions for the moments of the distribution.

- The relation between the McKay distribution and the distribution of sum and difference of gamma-distributed random variables (RVs) has been stated.
- For an important special case of the McKay distribution, related to Rayleigh fading, closed-form expressions have been found for the moments and also for the cumulative distribution function.
- A new expression for the probability density function (PDF) of the difference between two correlated gamma-distributed RVs has been found. Nakagami (1960) provides a toolbox, from which the PDF of the product, ratio, and sum of correlated gamma-distributed RVs can be deduced. However, the expression for the PDF of the difference between two such RVs is—to the best of the author's knowledge—previously unknown. The PDF is shown to be on the form of McKay's distribution.
- It is also shown that the sum of correlated gamma-distributed RVs is described by a PDF (originally provided by Nakagami and Nishio, 1955; Nakagami, 1960) is in fact on the McKay form.
- An application of the new result, relevant to outage probability calculation, is investigated. The new PDF enables calculation of the outage probability in an environment with self-interference. For the interference-limited case (when the Gaussian noise is negligible) a closed-form expression is found.
- The new result has also been shown to have significance in assessing the quality of certain channel estimators.
- Nakagami's (1960) expression for the PDF of the ratio between two gamma-distributed RVs has been utilized to find the PDF of the difference in decibel of two gamma-distributed RVs.

Suggestions for Further Research

The research presented in this dissertation has been concentrated on single-user systems. A natural extension is to examine ACM schemes in multi-user access systems, for instance cellular systems. Also, the fading has been assumed to be flat, i.e., the considerations are restricted to narrow-band transmission. The use of multicarrier/orthogonal frequency division multiplexing (OFDM) systems could be investigated in order to extend the methods to wideband transmission. "Bandwidth-Efficient and Adaptive

Transmission Schemes for Wireless Multimedia Communications" (BEATS) is a project which is financed by the Research Council of Norway. One of the subtopics considered by this project is rate-adaptive OFDM; ACM in cellular networks is another.

In the chapter concerned with linear prediction, the pilot symbols are assumed to be transmitted with the same average power as the information symbols. It is not known whether this is optimal. Adapting the pilot symbol power to the channel quality is a possibility for increasing the performance of a pilot symbol assisted ACM system. In addition, the spacing between the pilot symbols has been assumed to be constant. Adapting the pilot symbol spacing might also contribute to a more efficient and reliable system.

In order to perform thorough simulation of an ACM system in a Nakagami fading environment, it is necessary to generate a set of Nakagami-distributed RVs with arbitrary correlation. Although a method has been devised for generating pairs of such RVs (Tellambura and Jayalath, 2000), this method is not readily extendable to generation of a bigger set. Generation of an arbitrarily large set of such RVs is another subject for further research.

The Jakes Doppler spectrum with corresponding autocorrelation function is a model for the autocorrelation of a signal under the influence of flat fading (Stüber, 2001). The model (also known as Clarke's 2-D isotropic scattering model) is while widely used in analysis of systems perturbed by flat fading (see for instance Meyr *et al.*, 1998; Tang *et al.*, 1999). However, the model is restricted to the case of isotropic scattering and is possibly not very well suited for the case when the received signal has a line-of-sight component. Hence, there is a need for studying candidates for more realistic scattering models.

An ACM system will suffer from low throughput during periods of small CSNR, and a buffer is therefore required at the transmitter. The appropriate size of this buffer is a subject for further research.

Appendix A

Average Energy of QAM Constellations

We calculate the average energy of QAM signal constellations with size $M = 2^k$, $k \geq 2$. For even k, the constellation is square, while for odd k, the constellation is cross-shaped. Examples of such constellations are shown in Fig. 2.1, where the distance between two adjacent symbols is denoted by d_0.

Sterian (1997) has determined exact expressions for the average energy for $d_0 = 2$. We provide an alternative derivation of the expressions for arbitrary value of d_0.

The first quadrant of a general constellation is as shown in Fig. A.1. A square constellation consists of the crosses in the middle, while the cross constellation also contains the circles. The number P is associated with the

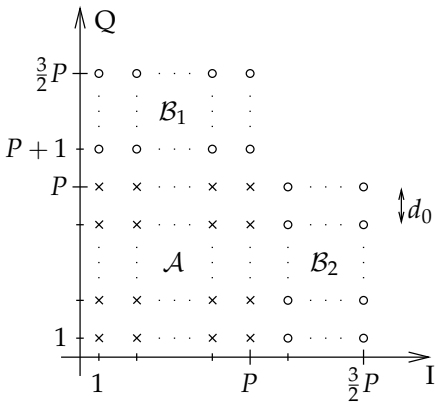

FIGURE A.1: First quadrant of a square/cross constellation.

number of symbols along each quadrature component. It is defined slightly differently for square and cross constellations,

$$P = \begin{cases} \sqrt{M/4} & \text{for } k \text{ even} \\ \sqrt{M'/4} = \sqrt{M/8} & \text{for } k \text{ odd} \end{cases} \tag{A.1}$$

where we have defined $M' = M/2$ as the size of the largest square constellation contained in the cross constellation.

A.1 Square Constellations

We first determine the average energy for even $k \geq 2$, i.e., for square constellations. Due to symmetry, the average energy of the whole constellation is equal to the average energy of one of the quadrants.

The number of symbols in each quadrant is $M/4$. For each symbol i, the energy E_i is given in terms of its first and second coordinates (x_i, y_i), $E_i = x_i^2 + y_i^2$. The average energy E_{sq} is given by

$$E_{sq} = \frac{1}{M/4} \sum_{i=1}^{M/4} E_i = \frac{1}{M/4} \sum_{i=1}^{M/4} \left(x_i^2 + y_i^2\right) \tag{A.2}$$

As indicated in Eq. (A.1), the number of symbols in each of the quadrature components is $P = \sqrt{M/4}$. The symbols have coordinates (x_i, y_i) where $\{x_i\} = \{y_i\} = \{\frac{1}{2}d_0, \frac{3}{2}d_0, \frac{5}{2}d_0, \ldots, \frac{2P-1}{2}d_0\}$, and E_{sq} is thus given by

$$\begin{aligned} E_{sq} &= \frac{1}{P^2} \sum_{m=1}^{P} \sum_{n=1}^{P} \left\{ \left(\tfrac{d_0}{2}(2m-1)\right)^2 + \left(\tfrac{d_0}{2}(2n-1)\right)^2 \right\} \\ &= \frac{d_0^2}{4P^2} \left\{ P \sum_{m=1}^{P} (2m-1)^2 + P \sum_{n=1}^{P} (2n-1)^2 \right\} \\ &= \frac{d_0^2}{2P} \sum_{n=1}^{P} (2n-1)^2. \end{aligned} \tag{A.3}$$

There exist a closed-form expression for the sum in Eq. (A.3); to calculate it, we use the following formulas (Gradshteyn and Ryzhik, 2000, Eq. 0.121):

$$\begin{aligned} \sum_{n=1}^{P} n &= \frac{P(P+1)}{2} \\ \sum_{n=1}^{P} n^2 &= \frac{P(P+1)(2P+1)}{6}. \end{aligned} \tag{A.4}$$

Thus,

$$\begin{aligned}\sum_{n=1}^{P}(2n-1)^2 &= \sum_{n=1}^{P}(4n^2-4n+1)\\ &= 4\sum_{n=1}^{P}n^2 - 4\sum_{n=1}^{P}n + \sum_{n=1}^{P}1\\ &= 4\frac{P(P+1)(2P+1)}{6} - 4\frac{P(P+1)}{2} + P\\ &= \tfrac{1}{3}P(4P^2-1).\end{aligned} \tag{A.5}$$

Using Eq. (A.5) in Eq. (A.3), and inserting $P = \sqrt{M/4}$, we obtain

$$\begin{aligned}E_{sq} &= \tfrac{1}{6}d_0^2(4P^2-1)\\ &= \tfrac{1}{6}d_0^2(M-1).\end{aligned} \tag{A.6}$$

A.2 Cross Constellations

For the cross constellations, when $k \geq 5$ is odd, each of the quadrants consists of 3 regions denoted by $\mathcal{A}$, $\mathcal{B}_1$, and $\mathcal{B}_2$, as indicated in Fig. A.1, with average energies $E_{\mathcal{A}}$, $E_{\mathcal{B}_1}$, and $E_{\mathcal{B}_2}$, respectively. Regions $\mathcal{B}_1$ and $\mathcal{B}_2$ are mirror images of each other, thus $E_{\mathcal{B}_1} = E_{\mathcal{B}_2}$.

When calculating the total average energy, the contribution from both $\mathcal{B}_1$ and $\mathcal{B}_2$ must be counted. But each of them consists of half as many symbols as $\mathcal{A}$, hence

$$E_{cr} = \tfrac{1}{2}E_{\mathcal{A}} + \tfrac{1}{4}E_{\mathcal{B}_1} + \tfrac{1}{4}E_{\mathcal{B}_2} = \tfrac{1}{2}(E_{\mathcal{A}} + E_{\mathcal{B}_1}). \tag{A.7}$$

A.2.1 Region $\mathcal{A}$

The square region $\mathcal{A}$ consists of $P \times P = M/8$ symbols, and is actually the first quadrant of the squared constellation of size $M' = M/2$. Thus, the average energy is

$$\begin{aligned}E_{\mathcal{A}} &= E_{sq}\big|_{M=M'}\\ &= \tfrac{1}{6}d_0^2(M'-1)\\ &= \tfrac{1}{6}d_0^2(M/2-1).\end{aligned} \tag{A.8}$$

A.2.2 Regions $\mathcal{B}_1$ and $\mathcal{B}_2$

The $\mathcal{B}_1$ region consists of $P/2 \times P = M'/8 = M/16$ symbols (see Fig. A.1). As for the square constellation, we calculate the average energy

$$E_{\mathcal{B}_1} = \frac{1}{M/16} \sum_{i=1}^{M/16} (x_i^2 + y_i^2). \tag{A.9}$$

The points in the $\mathcal{B}_1$ region have the following coordinates:

$$\{x_i\} = \{\frac{1}{2}d_0, \frac{3}{2}d_0, \ldots, \frac{2P-1}{2}d_0\} \tag{A.10a}$$

$$\{y_i\} = \{\frac{2P+1}{2}d_0, \frac{2P+3}{2}d_0, \ldots, \frac{3P-1}{2}d_0\} \tag{A.10b}$$

Thus,

$$\begin{aligned}
E_{\mathcal{B}_1} &= \frac{2}{P^2} \sum_{m=1}^{P} \sum_{n=P+1}^{\frac{3}{2}P} \left\{ \left(\tfrac{d_0}{2}(2m-1)\right)^2 + \left(\tfrac{d_0}{2}(2n-1)\right)^2 \right\} \\
&= \frac{d_0^2}{2P^2} \left\{ P \sum_{n=P+1}^{\frac{3}{2}P} (2n-1)^2 + \frac{P}{2} \sum_{m=1}^{P} (2m-1)^2 \right\} \\
&= \frac{d_0^2}{2P} \left\{ \sum_{n=1}^{\frac{3}{2}P} (2n-1)^2 - \sum_{n=1}^{P} (2n-1)^2 + \tfrac{1}{2} \sum_{m=1}^{P} (2m-1)^2 \right\} \\
&= \frac{d_0^2}{2P} \left\{ \sum_{n=1}^{\frac{3}{2}P} (2n-1)^2 - \tfrac{1}{2} \sum_{m=1}^{P} (2m-1)^2 \right\} \\
&= \frac{d_0^2}{2P} \left\{ \tfrac{1}{3}(\tfrac{3}{2}P)\left(4(\tfrac{3}{2}P)^2 - 1\right) - \tfrac{1}{2} \cdot \tfrac{1}{3}P(4P^2-1) \right\}.
\end{aligned} \tag{A.11}$$

Gathering the last terms, we obtain

$$\begin{aligned}
E_{\mathcal{B}_1} &= \tfrac{1}{6}d_0^2(\tfrac{23}{2}P^2 - 1) \\
&= \tfrac{1}{6}d_0^2(\tfrac{23}{16}M - 1).
\end{aligned} \tag{A.12}$$

We insert Eq. (A.8) and Eq. (A.12) into Eq. (A.7) to obtain

$$E_{cr} = \tfrac{1}{2}(E_{\mathcal{A}} + E_{\mathcal{B}_1}) = \tfrac{1}{6}d_0^2(\tfrac{31}{32}M - 1). \tag{A.13}$$

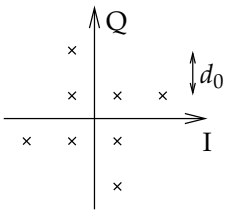

FIGURE A.2: Illustration of the 8-cross constellation

A.2.3 8-cross Constellation

For $k = 3$, we cannot obtain a constellation of the form in Fig. A.1. Instead, a constellation formed as indicated in Fig. 2.1 is employed. This constellation is called 8-cross; an enlarged view of it is shown in Fig. A.2.

Again, due to symmetry, the average energy will be equal to the average energy in the first quadrant. It is readily seen that this is

$$\begin{aligned} E_{8\text{-}cross} &= \tfrac{1}{2}\Big(\big((\tfrac{d_0}{2})^2 + (\tfrac{d_0}{2})^2\big) + \big((3\tfrac{d_0}{2})^2 + (\tfrac{d_0}{2})^2\big)\Big) \\ &= \tfrac{3}{2}d_0^2 \\ &= \tfrac{1}{6}d_0^2(\tfrac{40}{32}M - 1). \end{aligned} \tag{A.14}$$

The average energy is written on the form (A.14) to correspond with the expressions for average energy of the larger constellations.

To summarize, we have found that the energy of QAM-constellations are,

$$E_{avg} = \begin{cases} \tfrac{1}{6}d_0^2(M-1) & \text{for even } k \geq 2 \\ \tfrac{1}{6}d_0^2\big(\tfrac{40}{32}M - 1\big) & \text{for } k = 3 \\ \tfrac{1}{6}d_0^2\big(\tfrac{31}{32}M - 1\big) & \text{for odd } k \geq 5 \end{cases} \tag{A.15}$$

where the size of the constellation is $M = 2^k$. Even k corresponds to square constellations, $k = 3$ corresponds to the special 8-cross constellation while odd $k \geq 5$ corresponds to the larger cross constellations.

Appendix B

Statistical Properties of the Predicted Fading Amplitude

Tang *et al.* (1999) derive general formulas for the expectation of the square of a linear, non-causal estimate of the fading amplitude, and for the power correlation coefficient between the estimate and the true fading amplitude. It is here demonstrated that the formulas also apply to the case of linear prediction.

B.1 Expectation of $\hat{\alpha}^2$

$$\begin{aligned}\widehat{\Omega} = E[\hat{\alpha}^2] = E[|\hat{z}_h|^2] = E[|\mathbf{f}_j^{\mathsf{H}}\tilde{\mathbf{z}}_h|^2] = \mathbf{f}_j^{\mathsf{H}} E[\tilde{\mathbf{z}}_h\tilde{\mathbf{z}}_h^{\mathsf{H}}]\mathbf{f}_j \\ = \mathbf{f}_j^{\mathsf{H}}\left(E[\mathbf{z}_h\mathbf{z}_h^{\mathsf{H}}] + \frac{1}{a_p^2}E[\mathbf{n}_h\mathbf{n}_h^{\mathsf{H}}]\right)\mathbf{f}_j \end{aligned} \tag{B.1}$$

where $\mathbf{n}_h$ is the noise accompanying the fading $\mathbf{z}_h$. Since the noise is assumed to be white, its covariance matrix is simply the $K \times K$ identity matrix multiplied by the noise variance $N_0 B$. Thus,

$$\widehat{\Omega} = \Omega\mathbf{f}_j^{\mathsf{H}}\mathbf{R}\mathbf{f}_j + \frac{N_0 B}{a_p^2}\|\mathbf{f}_j\|^2 \tag{B.2}$$

Defining r as the ratio of the $\widehat{\Omega}$ to the Ω, and assuming that $a_p = \sqrt{P}$ where P is the average transmit power, we obtain

$$r = \frac{\widehat{\Omega}}{\Omega} = \mathbf{f}_j^{\mathsf{H}}\mathbf{R}\mathbf{f}_j + \frac{\|\mathbf{f}_j\|^2}{\bar{\gamma}_h}. \tag{B.3}$$

B.2 Correlation Coefficient

In calculating an expression for the correlation coefficient $\rho = \frac{E[\hat{\alpha}_h^2 \alpha_h^2] - \Omega^2 r}{\Omega^2 r}$ between the predicted and the true value of the CSNR at time index $(n+j)$, it is advantageous to concentrate on the correlation between $\hat{\alpha}_h^2$ and α_h^2:

$$\begin{aligned} E[\hat{\alpha}_h^2 \alpha_h^2] &= E[|\mathbf{f}_j^{\mathsf{H}} \tilde{\mathbf{z}}_h|^2 \cdot |z_h(n+j)|^2] \\ &= \mathbf{f}_j^{\mathsf{H}} E[(\mathbf{z}_h + \frac{1}{a_p}\mathbf{n})(\mathbf{z}_h^{\mathsf{H}} + \frac{1}{a_p}\mathbf{n}^{\mathsf{H}}) \cdot |z_h(n+j)|^2]\mathbf{f}_j \end{aligned} \tag{B.4}$$

and since noise and fading are statistically independent and both zero-mean,

$$\begin{aligned} E[\hat{\alpha}_h^2 \alpha_h^2] &= \mathbf{f}_j^{\mathsf{H}} E[\mathbf{z}_h \mathbf{z}_h^{\mathsf{H}} \cdot |z_h(n+j)|^2 + \frac{1}{a_p^2}\mathbf{n}\mathbf{n}^{\mathsf{H}} \cdot |z_h(n+j)|^2]\mathbf{f}_j \\ &= \mathbf{f}_j^{\mathsf{H}} E[\mathbf{z}_h \mathbf{z}_h^{\mathsf{H}} \cdot |z_h(n+j)|^2]\mathbf{f}_j + \Omega \frac{N_0 B}{a_p^2}\|\mathbf{f}_j\|^2 \end{aligned} \tag{B.5}$$

still assuming that $a_p = \sqrt{P}$, using $\bar{\gamma}_h = \frac{\Omega \cdot P}{N_0 B}$, and introducing $\mathbf{z}_{r,h} = \mathrm{Re}(\mathbf{z}_h)$ (and similarly for the scalar $z_h(n+j)$), where $\mathrm{Re}(\cdot)$ indicates the real part (in-phase or I-component) of a complex baseband symbol.

$$\begin{aligned} E[\hat{\alpha}_h^2 \alpha_h^2] &= 2\mathbf{f}_j^{\mathsf{H}} E[\mathbf{z}_{r,h} \mathbf{z}_{r,h}^{\mathsf{T}} \cdot z_{r,h}^2(n+j)]\mathbf{f}_j \\ &\quad + 2\mathbf{f}_j^{\mathsf{H}} E[\mathbf{z}_{r,h} \mathbf{z}_{r,h}^{\mathsf{T}}] E[z_{r,h}^2(n+j)]\mathbf{f}_j + \frac{\Omega^2}{\bar{\gamma}_h}\|\mathbf{f}_j\|^2. \end{aligned} \tag{B.6}$$

Since $E[\mathbf{z}_h \mathbf{z}_h^{\mathsf{H}}] = E[\mathbf{z}_{r,h} \mathbf{z}_{r,h}^{\mathsf{T}}] + E[\mathbf{z}_{i,h} \mathbf{z}_{i,h}^{\mathsf{T}}] = \Omega \mathbf{R}$, and $E[\mathbf{z}_{r,h} \mathbf{z}_{r,h}^{\mathsf{T}}] = E[\mathbf{z}_{i,h} \mathbf{z}_{i,h}^{\mathsf{T}}]$,

$$E[\mathbf{z}_{r,h} \mathbf{z}_{r,h}^{\mathsf{T}}] = \frac{\Omega}{2}\mathbf{R}, \tag{B.7a}$$

and it turns out that similar expressions exist for the scalar variance/cross-correlation expressions, namely,

$$E[\mathbf{z}_{r,h} z_{r,h}(n+j)] = \frac{\Omega}{2}\mathbf{r}_j \qquad \text{and} \qquad E[z_{r,h}^2(n+j)] = \frac{\Omega}{2}. \tag{B.7b}$$

Thus it can be concluded that,

$$E[\hat{\alpha}_h^2 \alpha_h^2] = 2\mathbf{f}_j^{\mathsf{H}} E[\mathbf{z}_{r,h} \mathbf{z}_{r,h}^{\mathsf{T}} \cdot z_{r,h}^2(n+j)]\mathbf{f}_j + \frac{1}{2}\Omega^2 \mathbf{f}_j^{\mathsf{H}} \mathbf{R} \mathbf{f}_j + \frac{\Omega^2}{\bar{\gamma}_h}\|\mathbf{f}_j\|^2 \tag{B.8}$$

This equation contains a fourth-order moment, and in order to complete the solution, the following Lemma will be utilized:

Lemma 1 (Fourth order moment of a Gaussian process)
It is known (see for instance Papoulis, 1991, Sec. 8-2) that, for zero-mean, real, Gaussian RVs a, b, c, and d, the following formula can be used to find the fourth-order moment:

$$E[abcd] = E[ab]E[cd] + E[ac]E[bd] + E[ad]E[bc]. \tag{B.9}$$

The above formula may also be used when two of the RVs are vectors, as can be demonstrated by letting $\mathbf{c} = [x\ y]^\mathsf{T}$ and $\mathbf{d} = [w\ z]^\mathsf{T}$:

$$\begin{aligned}
E[ab\mathbf{c}\mathbf{d}^\mathsf{T}] &= E\left[ab\begin{bmatrix}x\\y\end{bmatrix}\begin{bmatrix}w & z\end{bmatrix}\right] = \begin{bmatrix}E[abxw] & E[abxz]\\ E[abyw] & E[abyz]\end{bmatrix}\\
&= \begin{bmatrix}E[ab]E[xw] + E[ax]E[bw] + E[aw]E[bx] & \\ & E[ab]E[xz] + E[ax]E[bz] + E[az]E[bx]\\ E[ab]E[yw] + E[ay]E[bw] + E[aw]E[by] & \\ & E[ab]E[yz] + E[ay]E[bz] + E[az]E[by]\end{bmatrix}\\
&= E[ab]\begin{bmatrix}E[xw] & E[xz]\\ E[yw] & E[yz]\end{bmatrix}\\
&\quad + \begin{bmatrix}E[ax]\\E[ay]\end{bmatrix}\begin{bmatrix}E[bw] & E[bz]\end{bmatrix} + \begin{bmatrix}E[bx]\\E[by]\end{bmatrix}\begin{bmatrix}E[aw] & E[az]\end{bmatrix}\\
&= E[ab]E\left[\begin{bmatrix}x\\y\end{bmatrix}\begin{bmatrix}w & z\end{bmatrix}\right]\\
&\quad + E\left[a\cdot\begin{bmatrix}x\\y\end{bmatrix}\right]E\left[b\cdot\begin{bmatrix}w & z\end{bmatrix}\right] + E\left[b\cdot\begin{bmatrix}x\\y\end{bmatrix}\right]E\left[a\cdot\begin{bmatrix}w & z\end{bmatrix}\right]
\end{aligned} \tag{B.10}$$

and it is concluded that

$$E[ab\mathbf{c}\mathbf{d}^\mathsf{T}] = E[ab]E[\mathbf{c}\mathbf{d}^\mathsf{T}] + E[a\mathbf{c}]E[b\mathbf{d}^\mathsf{T}] + E[b\mathbf{c}]E[a\mathbf{d}^\mathsf{T}]. \tag{B.11}$$

With Lemma 1 in mind, and utilizing the expression for r from Eq. (B.3),

$$\begin{aligned}
E[\hat{\alpha}_h^2\alpha_h^2] &= 2\mathbf{f}_j^\mathsf{H}\Big(E[\mathbf{z}_{r,h}\mathbf{z}_{r,h}^\mathsf{T}]E[z_{r,h}^2(n+j)] + 2E[\mathbf{z}_{r,h}z_{r,h}(n+j)]E[\mathbf{z}_{r,h}^\mathsf{T}z_{r,h}(n+j)]\Big)\mathbf{f}_j\\
&\quad + \frac{1}{2}\Omega^2\mathbf{f}_j^\mathsf{H}\mathbf{R}\mathbf{f}_j + \frac{\Omega^2}{\bar{\gamma}_h}\|\mathbf{f}_j\|^2\\
&= 4\mathbf{f}_j^\mathsf{H}\Big(\frac{\Omega}{2}\mathbf{r}_j\frac{\Omega}{2}\mathbf{r}_j^\mathsf{T}\Big)\mathbf{f}_j + \Omega^2\mathbf{f}_j^\mathsf{H}\mathbf{R}\mathbf{f}_j + \frac{\Omega^2}{\bar{\gamma}_h}\|\mathbf{f}_j\|^2\\
&= \Omega^2|\mathbf{f}_j^\mathsf{H}\mathbf{r}_j|^2 + \Omega^2 r
\end{aligned} \tag{B.12}$$

By inserting Eq. (B.12) in Eq. (3.21), the final expression for the correlation coefficient is obtained as follows:

$$\rho = \frac{|\mathbf{f}_j^\mathsf{H}\mathbf{r}_j|^2}{r} = \frac{|\mathbf{f}_j^\mathsf{H}\mathbf{r}_j|^2}{\mathbf{f}_j^\mathsf{H}\mathbf{R}\mathbf{f}_j + \frac{1}{\bar{\gamma}_h}\|\mathbf{f}_j\|^2} \tag{B.13}$$

Appendix C

Derivation of $\overline{\text{BER}}_\eta$

C.1 Useful Formulas

We now provide a useful integral related to the incomplete gamma function.

Lemma 2 (Integration rule: Incomplete gamma function)
From the definition of the normalized incomplete gamma function (Definition 1, Section 3.4) and from Gradshteyn and Ryzhik (2000, Eq. 3.381-3), the following integration formula is deduced:

$$\int_x^y t^{a-1} e^{-t\cdot\mu} dt = \frac{\Gamma(a)}{\mu^a} \left[Q(a, x\mu) - Q(a, y\mu)\right] \tag{C.1}$$

Lemma 3 (The Nuttall function)
We have the following relationship involving the Nuttall function (Nuttall, 1974), AKA the generalized Marcum Q-function, AKA the non-central chi-square distribution (Temme, 1996, Sec. 11.4)[1] $Q_H(\cdot,\cdot)$:

$$\int_y^\infty u^{\frac{H-1}{2}} e^{-u\alpha} I_{H-1}\left(\sqrt{u}2\beta\right) du = \frac{\beta^{H-1}}{\alpha^H} \cdot e^{\frac{\beta^2}{\alpha}} \cdot Q_H\left(\frac{\beta^2}{\alpha}, y\alpha\right) \tag{C.2}$$

This can be seen by making the substitution $z = u\alpha$ and using $x = \frac{\beta^2}{\alpha}$, and then applying the definition of the generalized Marcum Q-function as provided by Temme (1996, Eq. 11.63).

A different definition of the Nuttall function is in terms of the following series of normalized incomplete gamma functions (Temme, 1996, Eq. 11.61):

$$Q_\mu(x, y) = e^{-x} \sum_{n=0}^{\infty} \frac{x^n}{n!} Q(\mu + n, y) \tag{C.3}$$

[1] Note that Temme and Nuttall utilize slightly different definitions of this function.

It follows from Eq. (3.22) that $Q(z,0) = 1$ so that $Q_\mu(x,0) = 1$. An integration rule, slightly different from Eq. (C.2), follows:

$$\int_0^y u^{\frac{H-1}{2}} e^{-u\alpha} I_{H-1}\left(\sqrt{u}2\beta\right) du = \frac{\beta^{H-1}}{\alpha^H} \cdot e^{\frac{\beta^2}{\alpha}} \cdot \left(1 - Q_H\left(\frac{\beta^2}{\alpha}, y\alpha\right)\right) \quad \text{(C.4)}$$

The following formula is a series definition analogous to Eq. (C.3):

$$1 - Q_\mu(x,y) = e^{-x} \sum_{n=0}^{\infty} \frac{x^n}{n!} \left(1 - Q(\mu + n, y)\right) \quad \text{(C.5)}$$

C.2 Calculations

We want to calculate the following integral:

$$\overline{\text{BER}}_n = \int_{\gamma_m}^{\gamma_{n+1}} \int_0^{\infty} \text{BER}_n(\gamma \mid \hat{\gamma}) f_{\gamma,\hat{\gamma}}(\gamma, \hat{\gamma})\, d\gamma\, d\hat{\gamma} \quad \text{(C.6)}$$

Here, we use the approximation

$$\text{BER}_n(\gamma \mid \hat{\gamma}) = \begin{cases} a_{n(\hat{\gamma})} \exp\left(-\frac{b_{n(\hat{\gamma})}\gamma}{M_{n(\hat{\gamma})}}\right), & \gamma \geq \gamma^l_{n(\hat{\gamma})} \\ 1/2, & \gamma < \gamma^l_{n(\hat{\gamma})} \end{cases} \quad \text{(C.7)}$$

for $\gamma^l_n = \ln(2a_n)M_n/b_n$, and $\gamma, \hat{\gamma} \sim \mathcal{G}(H, \bar{\gamma}_h, \bar{\hat{\gamma}}_h, \rho)$ are jointly gamma-distributed RVs. The index n is dependent on $\hat{\gamma}$. However, in the integral kernel—when the boundaries γ_m, γ_{n+1} are given—n is a constant. Thus, $a_{n(\hat{\gamma})} = a_n$, $b_{n(\hat{\gamma})} = b_n$, and $M_{n(\hat{\gamma})} = M_n$.

We now define the following integrals,

$$\mathcal{J}1(n,\hat{\gamma}) = \int_0^{\infty} a_n \exp\left(-\frac{b_n\gamma}{M_n}\right) f_{\gamma,\hat{\gamma}}(\gamma,\hat{\gamma})\, d\gamma \quad \text{(C.8)}$$

$$\mathcal{J}2(n,\hat{\gamma}) = \int_0^{\gamma^l_n} \left(a_n \exp\left(-\frac{b_n\gamma}{M_n}\right) - \frac{1}{2}\right) f_{\gamma,\hat{\gamma}}(\gamma,\hat{\gamma})\, d\gamma. \quad \text{(C.9)}$$

The $\mathcal{J}2$ integral can be split up even further,

$$\mathcal{J}21(n,\hat{\gamma}) = \int_0^{\gamma^l_n} a_n \exp\left(-\frac{b_n\gamma}{M_n}\right) f_{\gamma,\hat{\gamma}}(\gamma,\hat{\gamma})\, d\gamma \quad \text{(C.10)}$$

$$\mathcal{J}22(n,\hat{\gamma}) = \frac{1}{2} \int_0^{\gamma^l_n} f_{\gamma,\hat{\gamma}}(\gamma,\hat{\gamma})\, d\gamma. \quad \text{(C.11)}$$

Thus, the integral $\overline{\mathrm{BER}}_n$ splits into three parts

$$\begin{aligned}\overline{\mathrm{BER}}_n &= \int_{\gamma_m}^{\gamma_{n+1}} \mathcal{J}1(n,\hat{\gamma}) - \mathcal{J}2(n,\hat{\gamma})\, d\hat{\gamma} \\ &= \int_{\gamma_m}^{\gamma_{n+1}} \mathcal{J}1(n,\hat{\gamma}) - (\mathcal{J}21(n,\hat{\gamma}) - \mathcal{J}22(n,\hat{\gamma}))\, d\hat{\gamma} \\ &= \mathcal{I}1(n) - (\mathcal{I}21(n) - \mathcal{I}22(n)) \end{aligned} \tag{C.12}$$

where $\mathcal{I}1(n)$, $\mathcal{I}21(n)$, and $\mathcal{I}22(n)$ are the integrals of $\mathcal{J}1(n,\hat{\gamma})$, $\mathcal{J}21(n,\hat{\gamma})$, and $\mathcal{J}22(n,\hat{\gamma})$, respectively.

Both $\mathcal{J}1(n,\hat{\gamma})$ and $\mathcal{J}22(n,\hat{\gamma})$ can be viewed as special cases of $\mathcal{J}21(n,\hat{\gamma})$. We therefore proceed to solve the integral in Eq. (C.10).

C.2.1 Calculation of $\mathcal{J}21(n,\hat{\gamma})$

By inserting the definition of $f_{\gamma,\hat{\gamma}}(\gamma,\hat{\gamma})$,

$$\begin{aligned}\mathcal{J}21(n,\hat{\gamma}) = a_n &\frac{\hat{\gamma}^{\frac{H-1}{2}}}{\Gamma(H)\bar{\gamma}_h^{H+1} r^{\frac{H+1}{2}} (1-\rho)\rho^{\frac{H-1}{2}}} e^{-\frac{\hat{\gamma}}{(1-\rho)r\bar{\gamma}_h}} \\ &\times \int_0^{\gamma_n^l} \gamma^{\frac{H-1}{2}} e^{-\gamma\left(\frac{b_n}{M_n} + \frac{1}{(1-\rho)\bar{\gamma}_h}\right)} I_{H-1}\left(\sqrt{\gamma}\frac{2}{(1-\rho)\bar{\gamma}_h}\sqrt{\frac{\rho\hat{\gamma}}{r}}\right) d\gamma,\end{aligned} \tag{C.13}$$

were the parameter $r = \bar{\hat{\gamma}}_h/\bar{\gamma}_h$, the ratio between the mean of the estimated and the mean of the the actual CSNR, has been employed.

Using the correspondences $\alpha = \frac{b_n}{M_n} + \frac{1}{(1-\rho)\bar{\gamma}_h}$ and $\beta = \frac{1}{(1-\rho)\bar{\gamma}_h}\sqrt{\frac{\rho\hat{\gamma}}{r}}$ in Eq. (C.4) and collecting terms, we get

$$\begin{aligned}\mathcal{J}21(n,\hat{\gamma}) = &\frac{a_n}{\Gamma(H)}\left(\frac{1}{\bar{\gamma}_h r}\cdot\frac{1}{(1-\rho)\frac{b_n\bar{\gamma}_h}{M_n}+1}\right)^H \hat{\gamma}^{H-1} \\ &\times \exp\left(-\hat{\gamma}\cdot\frac{1}{\bar{\gamma}_h r}\cdot\frac{\frac{b_n\bar{\gamma}_h}{M_n}+1}{(1-\rho)\frac{b_n\bar{\gamma}_h}{M_n}+1}\right) \\ &\times\left[1 - Q_H\left(\hat{\gamma}\cdot\frac{\rho}{(1-\rho)}\cdot\frac{1}{\bar{\gamma}_h r}\cdot\frac{1}{(1-\rho)\frac{b_n\bar{\gamma}_h}{M_n}+1}, \gamma_n^l\left(\frac{b_n}{M_n}+\frac{1}{(1-\rho)\bar{\gamma}_h}\right)\right)\right]\end{aligned} \tag{C.14}$$

Since $\mathcal{J}21(n,\hat{\gamma})$ will be used in an integration kernel, it is advantageous to express the formula using as simple functions as possible. Therefore, we

utilize the series representation of the Nuttall function from Eq. (C.5) and collect terms to obtain the final expression:

$$\begin{aligned}\mathcal{J}21(n,\hat{\gamma}) = \frac{a_n}{\Gamma(H)}\hat{\gamma}^{H-1}e^{-\frac{\hat{\gamma}}{(1-\rho)\bar{\gamma}_h r}} \\ \times \sum_{k=0}^{\infty}\frac{\hat{\gamma}^k}{k!}\left(\frac{\rho}{1-\rho}\right)^k\left(\frac{1}{\bar{\gamma}_h r}\cdot\frac{1}{(1-\rho)\frac{b_n\bar{\gamma}_h}{M_n}+1}\right)^{k+H} \\ \times\left[1-Q\left(k+H,\gamma_n^l\left(\frac{b_n}{M_n}+\frac{1}{(1-\rho)\bar{\gamma}_h}\right)\right)\right]\end{aligned} \tag{C.15}$$

C.2.2 Calculation of $\mathcal{I}21(n)$

We now calculate the integral $\mathcal{I}21(n)$. In turn, $\mathcal{I}22(n)$ can be found as a special case. By inserting the expression for $\mathcal{J}21(n,\hat{\gamma})$ from Eq. (C.15), changing the order of integration and summation and then collecting terms, we get:

$$\mathcal{I}21(n) = \int_{\gamma_n}^{\gamma_{n+1}} \mathcal{J}21(n,\hat{\gamma})\,d\hat{\gamma}$$

Change order of integration and summation

$$\begin{aligned}= \frac{a_n}{\Gamma(H)}\sum_{k=0}^{\infty}\frac{1}{k!}\left(\frac{\rho}{1-\rho}\right)^k\left(\frac{1}{\bar{\gamma}_h r}\cdot\frac{1}{(1-\rho)\frac{b_n\bar{\gamma}_h}{M_n}+1}\right)^{k+H} \\ \times\left[1-Q\left(k+H,\gamma_n^l\left(\frac{b_n}{M_n}+\frac{1}{(1-\rho)\bar{\gamma}_h}\right)\right)\right] \\ \times\int_{\gamma_n}^{\gamma_{n+1}}\hat{\gamma}^{k+H-1}e^{-\frac{\hat{\gamma}}{(1-\rho)\bar{\gamma}_h r}}\,d\hat{\gamma}\end{aligned}$$

Use Eq. (C.1) and collect terms

$$\begin{aligned}\mathcal{I}21(n) = a_n\sum_{k=0}^{\infty}\frac{\Gamma(k+H)}{\Gamma(k+1)\Gamma(H)}\left(\frac{\rho}{1-\rho}\right)^k\left(\frac{1}{\frac{b_n\bar{\gamma}_h}{M_n}+\frac{1}{1-\rho}}\right)^{k+H} \\ \times\left[1-Q\left(k+H,\gamma_n^l\left(\frac{b_n}{M_n}+\frac{1}{(1-\rho)\bar{\gamma}_h}\right)\right)\right] \\ \times\left[Q\left(k+H,\frac{\gamma_n}{(1-\rho)\bar{\gamma}_h r}\right)-Q\left(k+H,\frac{\gamma_{n+1}}{(1-\rho)\bar{\gamma}_h r}\right)\right]\end{aligned} \tag{C.16}$$

C.2.3 Calculation of $\mathcal{I}22(n)$

$\mathcal{I}22(n)$ follows as a special case of $\mathcal{I}21(n)$, namely, $\mathcal{I}22(n) = \mathcal{I}21(n)|_{a_n=\frac{1}{2},b_n=0}$. Thus,

$$\begin{aligned}\mathcal{I}22(n) = \frac{1}{2}\sum_{k=0}^{\infty}\frac{\Gamma(k+H)}{\Gamma(k+1)\Gamma(H)}\rho^k(1-\rho)^H \\ \times\left[1-Q\left(k+H,\frac{\gamma_n^l}{(1-\rho)\bar{\gamma}_h}\right)\right] \\ \times\left[Q\left(k+H,\frac{\gamma_n}{(1-\rho)\bar{\gamma}_h r}\right)-Q\left(k+H,\frac{\gamma_{n+1}}{(1-\rho)\bar{\gamma}_h r}\right)\right]\end{aligned} \tag{C.17}$$

C.2.4 Calculation of $\mathcal{J}1(n,\hat{\gamma})$

$\mathcal{I}1(n)$ could have been found directly from Eq. (C.16) by letting $\gamma_n^l \to \infty$ and noting that $Q_H(x,y)|_{y\to\infty} = 0$. However, it is substantially easier to first find $\mathcal{J}1(n,\hat{\gamma})$ from Eq. (C.14). Since $\gamma_n^l \to \infty$, the parenthesis containing the Nuttall function (making Eq. (C.14) unsuitable for integration) will disappear.

$$\begin{aligned}\mathcal{J}1(n,\hat{\gamma}) = \frac{a_n}{\Gamma(H)}\left(\frac{1}{\bar{\gamma}_h r}\cdot\frac{1}{(1-\rho)\frac{b_n\bar{\gamma}_h}{M_n}+1}\right)^H \\ \times\hat{\gamma}^{H-1}\exp\left(-\frac{\hat{\gamma}}{\bar{\gamma}_h r}\cdot\frac{\frac{b_n\bar{\gamma}_h}{M_n}+1}{(1-\rho)\frac{b_n\bar{\gamma}_h}{M_n}+1}\right)\end{aligned} \tag{C.18}$$

C.2.5 Calculation of $\mathcal{I}1(n)$

Now $\mathcal{I}1(n)$ is found by once more employing Eq. (C.1) to integrate $\mathcal{J}1(n, \hat{\gamma})$:

$$\begin{aligned}\mathcal{I}1(n) &= \frac{a_n}{\Gamma(H)}\left(\frac{1}{\bar{\gamma}_h r}\cdot\frac{1}{(1-\rho)\frac{b_n\bar{\gamma}_h}{M_n}+1}\right)^H \\ &\quad\times\int_{\gamma_n}^{\gamma_{n+1}}\hat{\gamma}^{H-1}\exp\left(-\frac{\hat{\gamma}}{\bar{\gamma}_h r}\cdot\frac{\frac{b_n\bar{\gamma}_h}{M_n}+1}{(1-\rho)\frac{b_n\bar{\gamma}_h}{M_n}+1}\right)d\hat{\gamma} \\ &= a_n\left(\frac{1}{\frac{b_n\bar{\gamma}_h}{M_n}+1}\right)^H \\ &\quad\times\left[Q\left(H,\frac{\gamma_n}{\bar{\gamma}_h r}\cdot\frac{\frac{b_n\bar{\gamma}_h}{M_n}+1}{(1-\rho)\frac{b_n\bar{\gamma}_h}{M_n}+1}\right)-Q\left(H,\frac{\gamma_{n+1}}{\bar{\gamma}_h r}\cdot\frac{\frac{b_n\bar{\gamma}_h}{M_n}+1}{(1-\rho)\frac{b_n\bar{\gamma}_h}{M_n}+1}\right)\right]\end{aligned} \tag{C.19}$$

Now, Eqs. (C.19), (C.16), and (C.17) can be combined in Eq. (C.12) to provide $\overline{\text{BER}}_n$.

Appendix D

Proofs of the Theorems in Ch. 4

D.1 Moments of McKay's Type I Distribution

In this appendix a proof of Theorem 1 is given. Let Σ be distributed according to the PDF stated in Definition 2. The moments of Σ are given by:

$$\begin{aligned} E[\Sigma^n] &= \int_{-\infty}^{\infty} \sigma^n f_\Sigma(\sigma)\, d\sigma \\ &= E_0 \pi \cdot \int_0^{\infty} \sigma^{a+n} e^{-\sigma \frac{c}{b}} I_a\left(\frac{\sigma}{b}\right)\, d\sigma, \end{aligned} \tag{D.1}$$

assigning $E_0 = \frac{|1-c^2|^{a+1/2}}{\sqrt{\pi} 2^a b^{a+1} \Gamma(a+1/2)}$. We employ the identity

$$\begin{aligned} &\int_0^{\infty} x^{\mu-1} e^{-\eta x} J_\nu(\psi x)\, dx \\ &\qquad = \frac{\left(\frac{\psi}{2\eta}\right)^\nu \Gamma(\nu+\mu)}{\eta^\mu\, \Gamma(\nu+1)}\, {}_2F_1\left(\frac{\nu+\mu}{2}, \frac{\nu+\mu+1}{2}; \nu+1; -\frac{\psi^2}{\eta^2}\right) \end{aligned} \tag{D.2}$$

(Gradshteyn and Ryzhik, 2000, Eq. 6.621-1) and utilize

$$I_\nu(z) = (-j)^\nu J_\nu(jz) \tag{D.3}$$

where $J_\nu(\cdot)$ is the Bessel function of the first kind and order ν (Abramowitz and Stegun, 1972, Eq. 9.6.3). Letting $z = -j\psi x = \beta x$ in Eq. (D.3), the following formula can be deduced:

$$\begin{aligned} &\int_0^{\infty} x^{\mu-1} e^{-\eta x} I_\nu(\beta x)\, dx \\ &\qquad = \frac{\beta^\nu}{2^\nu \eta^{\mu+\nu}} \frac{\Gamma(\mu+\nu)}{\Gamma(\nu+1)}\, {}_2F_1\left(\frac{\mu+\nu}{2}, \frac{\mu+\nu+1}{2}; \nu+1; \frac{\beta^2}{\eta^2}\right) \end{aligned} \tag{D.4}$$

valid for $\beta > 0$, $\eta > 0$, and $\beta < \eta$. Let

$$\begin{aligned} \mu &= n + a + 1, \\ \nu &= a, \\ \beta &= 1/b, \\ \eta &= c/b, \end{aligned} \tag{D.5}$$

(noting that $c > 1$ so that the requirements for Eq. (D.4) are fulfilled,) and utilize the "doubling formula" (Gradshteyn and Ryzhik, 2000, Eq. 8.335-1: $\sqrt{\pi}\Gamma(2x) = 2^{2x-1}\Gamma(x)\Gamma(x+\frac{1}{2})$) to arrive at the following expression:

$$\begin{aligned} E[\Sigma^n] = \frac{(c^2-1)^{a+\frac{1}{2}} b^n}{c^{2a+n+1}} \frac{\Gamma(2a+n+1)}{\Gamma(2a+1)} \\ \times {}_2F_1\Big(\frac{2a+n+1}{2}, \frac{2a+n+2}{2}; a+1; \frac{1}{c^2}\Big), \end{aligned} \tag{D.6}$$

where ${}_2F_1(\cdot,\cdot;\cdot;\cdot)$ is Gauss' hypergeometric function (quoted for instance by Gradshteyn and Ryzhik, 2000, Section 9.1). This concludes the proof of Theorem 1.

D.2 Moments of McKay's Type II Distribution

In this appendix we give a proof of Theorem 2. Let Δ be distributed according to the PDF stated in Definition 3. We find the moments of Δ as given by:

$$\begin{aligned} E[\Delta^n] &= \int_{-\infty}^{\infty} \delta^n f_\Delta(\delta)\, d\delta \\ &= E_0 \cdot \int_{-\infty}^{\infty} \delta^n |\delta|^a e^{-\delta\frac{c}{b}} K_a\Big(\frac{|\delta|}{b}\Big)\, d\delta \\ &= E_0 \cdot \int_0^{\infty} \delta^{n+a} \big((-1)^n e^{\delta\frac{c}{b}} + e^{-\delta\frac{c}{b}}\big) K_a\Big(\frac{\delta}{b}\Big)\, d\delta, \end{aligned} \tag{D.7}$$

where E_0 is as defined in Appendix D.1. The integral can be solved in terms of Gauss' Hypergeometric function ${}_2F_1(\cdot,\cdot;\cdot;\cdot)$ with the aid of (Gradshteyn and Ryzhik, 2000, Eq. 6.621-3), cited here for convenience:

$$\begin{aligned} &\int_0^{\infty} x^{\mu-1} e^{-\eta x} K_\nu(\beta x)\, dx \\ &= \frac{\sqrt{\pi}(2\beta)^\nu}{(\eta+\beta)^{\mu+\nu}} \frac{\Gamma(\mu+\nu)\Gamma(\mu-\nu)}{\Gamma(\mu+1/2)} {}_2F_1\Big(\mu+\nu, \nu+\tfrac{1}{2}; \mu+\tfrac{1}{2}; \frac{\eta-\beta}{\eta+\beta}\Big), \end{aligned} \tag{D.8}$$

where it is required that $\mu > |\nu|$ and $\eta + \beta > 0$. Employ the same parameters μ, ν, β as in Eq. (D.5), and $\eta = \pm\frac{c}{b}$, noting that $|c| < 1$ so the requirements are fulfilled. After some algebraic manipulations, we arrive at the desired expression:

$$\begin{aligned} E[\Delta^n] = {} & \frac{b^n}{(1-c^2)^{a+n+\frac{1}{2}}} \frac{\Gamma(2a+n+1)\Gamma(n+1)}{\Gamma(a+n+\frac{3}{2})\Gamma(a+\frac{1}{2})} \\ & \times \Bigg[(-1)^n (1+c)^{2a+n+1} {}_2F_1\Big(2a+n+1, a+\tfrac{1}{2}; a+n+\tfrac{3}{2}; -\frac{1+c}{1-c}\Big) \\ & + (1-c)^{2a+n+1} {}_2F_1\Big(2a+n+1, a+\tfrac{1}{2}; a+n+\tfrac{3}{2}; -\frac{1-c}{1+c}\Big) \Bigg], \end{aligned} \tag{D.9}$$

which ends the proof of Theorem 2.

D.3 Moments of the McKay Distributions (Special Case)

In the special case that arises when a is restricted to $a = 1/2$, the formula for the moments becomes particularly simple. In the following, this will be shown with the aid of two lemmas.

First, the expression for the moments of a type I McKay distribution is investigated:

Lemma 4 (Moments, Type I, $a = 1/2$)
In Eq. (4.4), let $a = 1/2$. By using the formula ${}_2F_1\big(\frac{n+2}{2}, \frac{n+2}{2} + \frac{1}{2}; \frac{3}{2}; \frac{1}{c^2}\big) = \frac{c^{n+2}}{2(n+1)}\big((\frac{1}{c-1})^{n+1} - (\frac{1}{c+1})^{n+1}\big)$, (deduced from Abramowitz and Stegun, 1972, Eq. 15.1.10), we get the following expression:

$$\begin{aligned} E[\Sigma^n] &= \frac{(c^2-1)b^n}{c^{n+2}} \frac{\Gamma(n+2)}{\Gamma(2)} {}_2F_1\Big(\frac{n+2}{2}, \frac{n+3}{2}; \frac{3}{2}; \frac{1}{c^2}\Big) \\ &= \frac{b^n(c^2-1)\Gamma(n+2)}{2(n+1)} \Big(\frac{1}{(c-1)^{n+1}} - \frac{1}{(c+1)^{n+1}}\Big) \\ &= \frac{n!}{2} b^n (c^2-1) \Big(\frac{1}{(c-1)^{n+1}} - \frac{1}{(c+1)^{n+1}}\Big) \\ &= \frac{n! b^n}{2(c^2-1)^n} \big((c+1)^{n+1} - (c-1)^{n+1}\big) \end{aligned} \tag{D.10}$$

Note that $n \in \mathbb{Z}^+$ so that the Γ function can be replaced by the factorial.

Next, we turn to the expression for the type II McKay distribution:

Lemma 5 (Moments, Type II, $a = 1/2$)
In Eq. (4.5), let $a = 1/2$. Next, employ that ${}_2F_1(a,b;c;z) = {}_2F_1(b,a;c;z)$ by the series representation of the ${}_2F_1$ function (Gradshteyn and Ryzhik, 2000, Eq. 9.100) and that ${}_2F_1(b,a;a;-z) = (1+z)^{-b}$ (which follows from Gradshteyn and Ryzhik, 2000, Eq. 9.121-1). Then the expression for the moments reduces to the following formula:

$$\begin{aligned}
E[\Delta^n] &= \frac{b^n}{(1-c^2)^{n+1}} \frac{\Gamma(n+2)\Gamma(n+1)}{\Gamma(n+2)\Gamma(1)} \\
&\quad \times \left[(-1)^n (1+c)^{n+2} {}_2F_1\Big(n+2,1;n+2;-\frac{1+c}{1-c}\Big) \right. \\
&\quad \left. + (1-c)^{n+2} {}_2F_1\Big(n+2,1;n+2;-\frac{1-c}{1+c}\Big) \right] \\
&= \frac{b^n \Gamma(n+1)}{(1-c^2)^{n+1}} \left[(-1)^n \frac{(1+c)^{n+2}}{1+\frac{1+c}{1-c}} + \frac{(1-c)^{n+2}}{1+\frac{1-c}{1+c}} \right] \\
&= \frac{n! b^n}{2(1-c^2)^n} \left[(-1)^n (1+c)^{n+1} + (1-c)^{n+1} \right] \\
&= \frac{n! b^n}{2(c^2-1)^n} \left[(c+1)^{n+1} - (c-1)^{n+1} \right] \qquad \text{(D.11)}
\end{aligned}$$

This shows that the expressions for the moments of the two McKay distributions are in fact identical, for the special case of $a = \frac{1}{2}$.

D.4 Sum of Two Correlated Gamma RVs

Let $X_1, X_2 \sim \mathcal{G}(\alpha, \beta_1, \beta_2, \rho)$. Nakagami and Nishio (1955, Eq. 43) and (Nakagami, 1960, Eq. 142) provide the PDF of the square root R of the sum of the squares of two correlated Nakagami-distributed RVs. This is equivalent to the square root of the sum of two gamma-distributed RVs, i.e., $R = \sqrt{X_1 + X_2}$. The expression is as follows:

$$f_R(r) = \frac{2r\sqrt{\pi}}{(\beta_1\beta_2(1-\rho))^\alpha \Gamma(\alpha)} e^{-\frac{(\beta_1+\beta_2)r^2}{2\beta_1\beta_2(1-\rho)}} \left(\frac{r^2}{2\tilde{\beta}}\right)^{\alpha-1/2} I_{\alpha-1/2}(\tilde{\beta} r^2) \qquad \text{(D.12)}$$

where

$$\tilde{\beta}^2 = \frac{(\beta_1-\beta_2)^2 + 4\beta_1\beta_2\rho}{4\beta_1\beta_2(1-\rho)^2}. \qquad \text{(D.13)}$$

By using a standard transformation of variables, it can be shown that $\Sigma = R^2$ follows the distribution described by

$$f_\Sigma(\sigma) = \frac{\sqrt{\pi}}{(\beta_1\beta_2(1-\rho))^\alpha \Gamma(\alpha)} e^{-\frac{(\beta_1+\beta_2)\sigma}{2\beta_1\beta_2(1-\rho)}} \left(\frac{\sigma}{2\tilde{\beta}}\right)^{\alpha-1/2} I_{\alpha-1/2}(\tilde{\beta}\sigma) H(\sigma) \qquad \text{(D.14)}$$

By inserting a, b, and c from Eq. (4.15) into Eq. (4.1) and comparing the result with Eq. (D.14), we see that Nakagami's result is indeed on the form of McKay's distribution.

D.5 Difference Between Two Correlated Gamma RVs

In this appendix, we give a direct proof of Theorem 6 [1]. Let $X_1, X_2 \sim \mathcal{G}(\alpha, \beta_1, \beta_2, \rho)$ and let their difference $\Delta = X_1 - X_2$.

Since Δ can be viewed as a function of X_1, $\Delta = g(X_1) = X_1 - X_2$, we can use transformation of variables and find

$$f_{X_1\Delta}(x_1, \delta) = \frac{f_{X_1X_2}(x_1, x_2)}{|dg/dx_2|}\Big|_{x_2=g^{-1}(\delta)} = f_{X_1X_2}(x_1, x_1 - \delta). \tag{D.15}$$

The PDF of Δ can be found by integrating Eq. (D.15) over the support of X_1. Since X_1, X_2 are gamma RVs, x_1, x_2 are always positive and therefore $\delta \leq x_1$. Consequently, when $\delta > 0$, $x_1 \geq \delta$ whereas when $\delta \leq 0$, $x_1 \geq 0$. The lower limit of integration is thus $x_0 = \max(0, \delta)$ and hence

$$\begin{aligned} f_\Delta(\delta) &= \int_{x_0}^{\infty} f_{X_1X_2}(x_1, x_1 - \delta)\, dx_1 \\ &= \frac{e^{\frac{\delta}{(1-\rho)\beta_2}}}{\Gamma(\alpha)(\beta_1\beta_2)^{(\alpha+1)/2}(1-\rho)\rho^{(\alpha-1)/2}} \\ &\quad \times \int_{x_0}^{\infty} e^{\frac{x_1}{1-\rho}\left(\frac{1}{\beta_1}-\frac{1}{\beta_2}\right)} \left(x_1(x_1-\delta)\right)^{(\alpha-1)/2} I_{\alpha-1}\left(\frac{2\sqrt{\rho}\sqrt{x_1(x_1-\delta)}}{(1-\rho)\sqrt{\beta_1\beta_2}}\right) dx_1. \end{aligned} \tag{D.16}$$

Eq. (D.16) must be treated separately for the cases $\delta = 0$ and for $\delta \neq 0$. For $\delta = 0$, we have

$$\begin{aligned} f_\Delta(0) &= \frac{1}{\Gamma(\alpha)(\beta_1\beta_2)^{(\alpha+1)/2}(1-\rho)\rho^{(\alpha-1)/2}} \\ &\quad \times \int_{0}^{\infty} e^{\frac{x_1}{1-\rho}\left(\frac{1}{\beta_1}-\frac{1}{\beta_2}\right)} x_1^{\alpha-1} I_{\alpha-1}\left(\frac{2\sqrt{\rho}\cdot x_1}{(1-\rho)\sqrt{\beta_1\beta_2}}\right) dx_1, \end{aligned} \tag{D.17}$$

[1] By direct proof, we mean that we are providing in this Appendix a proof that start from the bivariate gamma distribution. Alternatively, this theorem can be proved by first using a linear transformation of random variables to convert two correlated gamma RVs into independent ones and then by using the result of Theorem 4.

which can be viewed as a Laplace transform, and to which a closed-form solution can be found (Gradshteyn and Ryzhik, 2000, Eq. 17.13-110) as

$$f_\Delta(0) = \frac{1}{\Gamma(\alpha)(\beta_1\beta_2)^{(\alpha+1)/2}(1-\rho)\rho^{(\alpha-1)/2}} \times 2^{\alpha-1}\pi^{-\frac{1}{2}}\Gamma(\alpha-\tfrac{1}{2})\Big(\frac{2\sqrt{\rho}}{(1-\rho)\sqrt{\beta_1\beta_2}}\Big)^{\alpha-1} \times \left(\Big(\frac{1}{1-\rho}\big(\frac{1}{\beta_1}+\frac{1}{\beta_2}\big)\Big)^2 - \Big(\frac{2\sqrt{\rho}}{(1-\rho)\sqrt{\beta_1\beta_2}}\Big)^2\right)^{-(\alpha-\frac{1}{2})},$$

which can be further simplified by combining terms to

$$f_\Delta(0) = \frac{\Gamma(\alpha-\frac{1}{2})}{\sqrt{\pi}\Gamma(\alpha)} \frac{\big(4\beta_1\beta_2(1-\rho)\big)^{\alpha-1}}{\big((\beta_1+\beta_2)^2-4\beta_1\beta_2\rho\big)^{\alpha-\frac{1}{2}}}. \tag{D.18}$$

The previous expression is valid for $\alpha > 1/2$.

For $\delta \neq 0$, we rely on the series expansion for the Bessel function $I_\nu(z) = \sum_{k=0}^{\infty} \frac{1}{k!\Gamma(\nu+k+1)}(\frac{z}{2})^{\nu+2k}$ (Gradshteyn and Ryzhik, 2000, Eq. 8.445) to solve the integral in Eq. (D.16). In particular, using the series expansion, changing the order of integration and summation, and then combining terms, Eq. (D.16) can be rewritten as

$$f_\Delta(\delta) = \frac{e^{\frac{\delta}{(1-\rho)\beta_2}}}{\Gamma(\alpha)(\beta_1\beta_2)^{(\alpha+1)/2}(1-\rho)\rho^{(\alpha-1)/2}} \times \sum_{k=0}^{\infty}\left\{\frac{1}{k!\Gamma(\alpha+k)}\Big(\frac{\sqrt{\rho}}{(1-\rho)\sqrt{\beta_1\beta_2}}\Big)^{2k+\alpha-1} \times \int_{x_0}^{\infty}\big(x_1(x_1-\delta)\big)^{k+\alpha-1}e^{-\frac{1}{1-\rho}\left(\frac{1}{\beta_1}+\frac{1}{\beta_2}\right)x_1}dx_1\right\}. \tag{D.19}$$

To solve the integral in Eq. (D.19), we use the following lemma:

Lemma 6 (A Useful Integral)
We combine two results from Gradshteyn and Ryzhik (2000, Eqs. (3.383-3) and (3.383-8), respectively),

$$\int_\beta^\infty x^{\nu-1}(x-\beta)^{\nu-1}e^{-\mu x}dx = \frac{1}{\sqrt{\pi}}\Big(\frac{\beta}{\mu}\Big)^{\nu-1/2}e^{-\frac{\beta\mu}{2}}\Gamma(\nu)K_{\nu-1/2}\Big(\frac{\beta\mu}{2}\Big), \quad [\mathrm{Re}\,\mu\beta > 0, \mathrm{Re}\,\nu > 0], \tag{D.20}$$

$$\int_0^\infty x^{\nu-1}(x+\beta)^{\nu-1}e^{-\mu x}dx = \frac{1}{\sqrt{\pi}}\Big(\frac{\beta}{\mu}\Big)^{\nu-1/2}e^{\frac{\beta\mu}{2}}\Gamma(\nu)K_{\nu-1/2}\Big(\frac{\beta\mu}{2}\Big),$$
$$[|\arg\beta| < \pi, \operatorname{Re}\mu > 0, \operatorname{Re}\nu > 0]. \quad \text{(D.21)}$$

Eq. (D.20) can apply to the case of positive δ, and thus we set $\beta = \delta$—which means that $\beta > 0$. Likewise, Eq. (D.21) can apply to the case where δ is negative, if we set $\beta = -\delta$. This still means that $\beta > 0$ so that the requirements for the identities are fulfilled. Together, they give the identity

$$\int_{\max(0,\delta)}^\infty \big(x(x-\delta)\big)^{\nu-1}e^{-\mu x}dx = \frac{1}{\sqrt{\pi}}\Big(\frac{|\delta|}{\mu}\Big)^{\nu-1/2}e^{\frac{\delta\mu}{2}}\Gamma(\nu)K_{\nu-1/2}\Big(|\delta|\frac{\mu}{2}\Big),$$
$$[\operatorname{Re}\delta \neq 0, \operatorname{Re}\mu > 0, \operatorname{Re}\nu > 0]. \quad \text{(D.22)}$$

Since the integral in Eq. (D.19) is in the form of Eq. (D.22) and $\mu = \frac{1}{1-\rho}\big(\frac{1}{\beta_1} + \frac{1}{\beta_2}\big) > 0$, $\nu = k+\alpha > 0$, and remembering that $x_0 = \max(0,\delta)$, the conditions of Eq. (D.22) are met. In particular, inserting Eq. (D.22) in Eq. (D.19) and collecting similar terms leads to

$$\begin{aligned} f_\Delta(\delta) = {} & \frac{|\delta|^{\alpha-1/2}}{\sqrt{\pi}\Gamma(\alpha)}\frac{1}{(\beta_1+\beta_2)^{\alpha-1/2}\sqrt{(1-\rho)\beta_1\beta_2}} \\ & \times \exp\left(\frac{1}{1-\rho}\left(\frac{\rho}{\beta_2} - \frac{\delta}{2\beta_1} - \frac{\delta}{2\beta_2}\right)\right) \\ & \times \sum_{k=0}^\infty \frac{1}{k!}\left(|\delta|\frac{\rho}{(1-\rho)(\beta_1+\beta_2)}\right)^k \\ & \times K_{k+\alpha-1/2}\left(\frac{|\delta|}{2}\frac{\beta_1+\beta_2}{(1-\rho)\beta_1\beta_2}\right). \end{aligned} \quad \text{(D.23)}$$

The sum can be solved by the aid of the multiplication theorem for Bessel functions:

Lemma 7 (Multiplication Theorem for Bessel Functions)
The Multiplication Theorem for modified Bessel functions states (quoted by Abramowitz and Stegun, 1972, Eq. 9.6.51):

$$\mathcal{Z}_\nu(\lambda z) = \lambda^\nu \sum_{k=0}^\infty \frac{(\lambda^2-1)^k(\frac{1}{2}z)^k}{k!}\mathcal{Z}_{\nu+k}(z), \qquad [|\lambda^2-1|<1],$$

where for the modified Bessel function of the second kind, $\mathcal{Z}_\nu$ represents $e^{\nu\pi i}K_\nu$. Thus $\mathcal{Z}_{\nu+k} = (-1)^k e^{\nu\pi i}K_{\nu+k}$, and we have the following formula:

$$\lambda^{-\nu}K_\nu(\lambda z) = \sum_{k=0}^\infty \frac{1}{k!}\Big((1-\lambda^2)\frac{z}{2}\Big)^k K_{k+\nu}(z), \qquad [|\lambda^2-1|<1]. \quad \text{(D.24)}$$

Since the sum in Eq. (D.23) is on the form of Eq. (D.24) with $\nu = \alpha - 1/2$, $z = \frac{|\delta|}{2}\frac{\beta_1+\beta_2}{(1-\rho)\beta_1\beta_2}$, and $\lambda = \sqrt{1 - \frac{4\rho\beta_1\beta_2}{(\beta_1+\beta_2)^2}}$, we are able to solve the sum in Eq. (D.23) in closed-form.[2]

After using Eq. (D.24) in Eq. (D.23) and collecting terms, we arrive at the final desired result given by

$$\begin{aligned} f_\Delta(\delta) = &\frac{|\delta|^{\alpha-1/2}}{\Gamma(\alpha)\sqrt{\pi}\sqrt{\beta_1\beta_2(1-\rho)}} \\ &\times \left(\frac{1}{(\beta_1+\beta_2)^2 - 4\rho\beta_1\beta_2}\right)^{\frac{2\alpha-1}{4}} \\ &\times \exp\left(\frac{\delta/2}{1-\rho}\left(\frac{1}{\beta_2} - \frac{1}{\beta_1}\right)\right) \\ &\times K_{\alpha-1/2}\left(|\delta|\frac{\sqrt{(\beta_1+\beta_2)^2 - 4\rho\beta_1\beta_2}}{2(1-\rho)\beta_1\beta_2}\right), \end{aligned} \tag{D.25}$$

which proves Theorem 6. Note that the Eq. (D.18), the special case for the limit when $\delta \to 0$, can also be found by using the formula devised in Proposition 1.

[2]It can be shown that $\frac{4\rho\beta_1\beta_2}{(\beta_1+\beta_2)^2} < 1$ except when $\rho = 1$ and $\beta_1 = \beta_2$. The latter case is the trivial one when $X_1 = X_2 \Rightarrow \Delta = 0$ and is thus not particularly interesting. The condition in Eq. (D.24), $|\lambda^2 - 1| < 1$, is therefore met so that Lemma (7) can safely be used to simplify Eq. (D.23).

References

Aalo, V. A. (1995, August).
Performance of maximal-ratio diversity systems in a correlated Nakagami-fading environment.
IEEE Trans. Commun. COM-43, 2360–2369.

Abbas, S. A. and A. U. Sheikh (1997, May).
On understanding the nature of slow fading in LOS microcellular channels.
In *Proc 47th IEEE Veh. Technol. Conf. (VTC'97)*, Volume 2, Phoenix, Arizona, pp. 662–666.

Abramowitz, M. and I. E. Stegun (Eds.) (1972).
Handbook of Mathematical Functions (Tenth Printing ed.).
United States Department of Commerce.

Abu-Dayya, A. A. and N. C. Beaulieu (1991, November).
Outage probabilities of cellular mobile radio systems with multiple Nakagami interferers.
IEEE Trans. Veh. Technol. 40(4), 757–768.

Aghamohammadi, A., H. Meyr, and G. Ascheid (1989, November).
Adaptive synchronization and channel parameter estimation using an extended Kalman filter.
IEEE Trans. Commun. 37(11), 1212–1219.

Alouini, M.-S. and A. Goldsmith (1997, May).
Capacity of Nakagami multipath fading channels.
In *Proc 47th IEEE Veh. Technol. Conf. (VTC'97)*, Phoenix, Arizona, pp. 358–362.

Alouini, M.-S. and A. Goldsmith (2000).
Adaptive modulation over Nakagami fading channels.
Wireless Personal Communications 13, 119–143.

Alouini, M.-S. and M. K. Simon (1998, September).
Multichannel reception of digital signals over correlated Nakagami fading channels.
In *Proc. of the 36th Allerton Conference on Communication, Control, and Computing (Allerton'98)*, Allerton Park, IL, pp. 146–155.

Barnett, S. and T. M. Cronin (1986).
Mathematical Formulae (Fourth ed.).
England: Longman Scientific & Technical.

Bhattacharyya, B. C. (1942).
The use of McKay's Bessel function curves for graduating frequency distributions.
Sankhyā 6, 175–182.

Biglieri, E., D. Divsalar, P. J. McLane, and M. K. Simon (1991).
Introduction to Trellis-Coded Modulation with Applications.
New York: MacMillan Publishing Company.

Cavers, J. K. (1991, November).
An analysis of pilot symbol assisted modulation for Rayleigh fading channels.
IEEE Trans. Veh. Technol. 40(4), 686–693.

Eng, T. and L. B. Milstein (1995, February/March/April).
Coherent DS-CDMA performance in Nakagami multipath fading.
IEEE Trans. Commun. 43(2/3/4), 1134–1143.

ETSI (1999).
Digital Video Broadcasting (DVB); Framing structure, channel coding and modulation for digital terrestrial television.
Standard ETSI EN 300 744 v1.2.1 (1999-07), European Brodcasting Union; European Telecommunications Standards Institute (ETSI), F-06921 Sophia Antipolis Cedex, France.

Forney, Jr., G. D., R. G. Gallager, G. R. Lang, F. M. Longstaff, and S. U. Qureshi (1984, Sept.).
Efficient modulation for band-limited channels.
IEEE J. Select. Areas Commun. 2(5), 632–647.

Goldsmith, A. J. and S.-G. Chua (1997, October).
Variable-rate variable-power MQAM for fading channels.
IEEE Trans. Commun. 45(10), 1218–1230.

Goldsmith, A. J. and S.-G. Chua (1998, May).
Adaptive coded modulation for fading channels.
IEEE Trans. Commun. 46(5), 595–602.

Goldsmith, A. J. and P. P. Varaiya (1997, November).
Capacity of fading channels with channel side information.
IEEE Trans. Inform. Theory 43(6), 1986–1992.

Gradshteyn, I. S. and I. M. Ryzhik (2000).
Table of Integrals, Series, and Products (Sixth ed.).
San Diego: Academic Press.

Hanzo, L., W. T. Webb, and T. Keller (2000).
Single- and Multi-carrier Quadrature Amplitude Modulation.
Chichester, England: John Wiley & Sons.

Hashem, B. and E. Sousa (1997, October).
On the capacity of a cellular DS/CDMA system under slow multipath fading and fixed step power control.
In *6th International Conference on Universal Personal Communications Record*, Volume 2, San Diego, CA, pp. 352–355. IEEE.

Hole, K. J., H. Holm, and G. E. Øien (2000, July).
Analysis techniques for adaptive coded modulation on flat fading channels.
IEEE J. Select. Areas Commun. 18(7), 1153–1158.

Hole, K. J., H. Holm, and G. E. Øien (2001, September).
Analysis of adaptive coded modulation with antenna diversity and feedback delay.
In *Proc. Mobile Communications Summit (IST-2001)*, Barcelona, Spain, pp. 865–870.

Hole, K. J., H. Holm, and G. E. Øien (2002).
Performance analysis of adaptive coded modulation with antenna diversity and feedback delay.
To appear in *Telektronikk*, Special Issue – "Information theory and its applications".

Hole, K. J. and G. E. Øien (2001, January).
Spectral efficiency of adaptive coded modulation in urban microcellular networks.
IEEE Trans. Veh. Technol. 50(1), 205–222.

Holm, H. (2001, October).
Probability distributions of SNR estimation error in Rayleigh fading channels.
In *Proc. Norwegian Signal Processing Symposium (NORSIG-2001)*, Trondheim, Norway, pp. 83–88.

Holm, H. and M.-S. Alouini.
Sum and difference of two squared correlated Nakagami variates in connection with the McKay distribution.
Submitted to *IEEE Trans. Commun. Theory*.

Holm, H. and M.-S. Alouini (2001, March).
On the difference of squares of two correlated Nakagami variates with application to outage probability evaluation.
In *Proc. 35th Annual Conference on Information Sciences and Systems (CISS-2001)*, Baltimore, MD, pp. 94–98. The Johns Hopkins University.

Holm, H., K. J. Hole, and G. E. Øien (1999, September).
Spectral efficiency of variable-rate coded QAM for flat fading channels.
In *Proc. Norwegian Signal Processing Symposium, (NORSIG-99)*, Asker, Norway, pp. 130–135.

Jakes, W. C., Y. S. Yeh, M. J. Gans, and D. O. Reudnik (1994).
Microwave Mobile Communications (Second ed.)., Chapter 5, pp. 309–329.
Piscataway, NJ: IEEE Press.

Jamali, S. H. and T. Le-Ngoc (1994).
Coded-Modulation Techniques for Fading Channels, Chapter 1.
Norwell, Massachusetts: Kluwer Academic Publishers.

Johnson, N. L., S. Kotz, and N. Balakrishnan (1994).
Continuous Univariate Distributions (Second ed.), Volume 1.
New York: Wiley Series in Probability and Mathematical Statistics.

Kendall, M. G. (1947).
The Advanced Theory of Statistics (Third ed.), Volume 1, Chapter 3, pp. 49–86.
London: C. Griffin.

Ko, Y.-C. and M.-S. Alouini.
Estimation of Nakagami-*m* fading channel parameters with application to optimized transmitter diversity systems.
Journal version in revision for IEEE Trans. on Wireless Commun.

Laha, R. G. (1954).
On some properties of the Bessel function distributions.
Bulletin of the Calcutta Mathematical Society 46, 59–72.

Ligeti, A. (2000, January).
Outage probability in the presence of correlated lognormal useful and interfering components.
IEEE Commun. Lett. 4(1), 15–17.

Lombardo, P., G. Fedele, and M. M. Rao (1999, January).
MRC performance for binary signals in Nakagami fading with general branch correlatio.
IEEE Trans. Commun. COM-47, 44–52.

McKay, A. T. (1932, May).
A Bessel function distribution.
Biometrika XXIV(1/2), 39–44.

Meyr, H., M. Moeneclaey, and S. A. Fechtel (1998).
Digital Communication Receivers: Synchronization, Channel Estimation, and Signal Processing.
Wiley Series in Telecommunications and Signal Processing. New York, NY: Wiley.

Murakami, S. and M. Nakagami (1971).
Adaptive feedback communication system in a fading environment.
Memoirs of the Faculty of Engineering, Kobe University 17, 127–147.

Nagao, M. and M. Kadoya (1971, March).
Two-variate exponential distribution and its numerical table for engineering applications.
Bull. Disas. Prev. Res. Inst., Kyoto Univ. 20(178), 183–210.

Nakagami, M. (1960, June).
The *m*-distribution—a general formula of intensity distribution of rapid fading.
In W. C. Hoffman (Ed.), *Statistical Methods in Radio Wave Propagation*, pp. 3–36. Pergamon Press (London, Oxford, New York, Paris).
Proceedings of a Symposium held at the University of California, Los Angeles, June 18–20, 1958.

Nakagami, M. and M. Nishio (1955).
The distribution of the sum of squares of two correlated *m*-variables.
J. Inst. Elec. Commun. Engrs. Japan 38(10), 782–787.

(In Japanese).

Nakagami, M. and M. Ōta (1957).
The distribution of the product of two correlated m-variables.
Rep. Radio Wave Prop. Res. Commit. Japan.

Nuttall, A. H. (1974, May).
Some integrals involvong the Q_M-function.
Technical Report 4755, Naval Underwater Systems Center, New London Laboratory, New London, CT.

Ōta, M. (1956).
The distribution of the ratio of the squares of two correlated m-variables.
Rep. Information Theory Res. Commit. Japan.

Papoulis, A. (1991).
Probability, Random Variables, and Stochastic Processes (Third ed.).
New York: McGraw-Hill International Editions.

Pearson, K. (1932).
Table of Incomplete Beta Functions.
London: Cambridge University Press.

Pearson, K., S. A. Stouffer, and F. N. David (1932, November).
Further applications in statistics of the $T_m(x)$ Bessel function.
Biometrika XXIV(3/4), 293–350.

Prasad, R. (1998).
Universal Wireless Personal Communications.
Boston–London: Artech House Publishers.

Sheikh, A. U. H., M. Handforth, and M. Abdi (1993, May).
Indoor mobile radio channel at 946 MHz: Measurements and modeling.
In *Proc. 43rd IEEE Veh. Technol. Conf. (VTC'93)*, Secaucus, NJ, pp. 73–76.

Springer, M. D. (1979).
The Algebra of Random Variables.
New York: John Wiley & Sons.

Steele, R. and W. T. Webb (1991, June).
Variable rate QAM for data transmission over mobile radio channels.
In *Proceedings of WIRELESS '91*, Calgary, Alberta, Canada, pp. 1–14.

Sterian, C.-E. D. (1997, Nov.–Dec.).

Exact formulas for computing the energy of "square" and "cross" two-dimensional rectangular signal constellations. *European Trans. on Telecommunications 8*(6), 547–549.

Stüber, G. L. (2001). *Principles of Mobile Communication* (Second ed.). Norwell, MA: Kluwer Academic Publishers.

Tang, X., M.-S. Alouini, and A. Goldsmith (1999, December). Effect of channel estimation error on M-QAM BER performance in Rayleigh fading. *IEEE Trans. Commun. 47*(12), 1856–1864.

Tellambura, C. and A. D. S. Jayalath (2000, May). Generation of bivariate Rayleigh and Nakagami-*m* fading envelopes. *IEEE Commun. Lett. 4*(5), 170–172.

Temme, N. M. (1996). *Special Functions: An Introduction to the Classical Functions of Mathematical Physics*. New York: John Wiley & Sons, Inc.

Therrien, C. W. (1992). *Discrete Random Signals and Statistical Signal Processing*. Signal Processing Series. Englewood Cliffs, NJ: Prentice Hall.

Torrance, J. M. and L. Hanzo (1995, September). Comparative study of pilot symbol assisted modem schemes. In *Sixth International Conference on Radio Receivers and Associated Systems*, Bath, UK, pp. 36–41. IEE.

Ungerboeck, G. (1982, Jan.). Channel coding with multilevel/phase signals. *IEEE Trans. Inform. Theory 28*(1), 55–67.

Webb, W. T., L. Hanzo, and R. Steele (1991, June). Bandwidth efficient QAM schemes for Rayleigh fading channels. *IEE Proceedings I: Communications, Speech, and Vision 138*(3), 169–175.

Webb, W. T. and R. Steele (1995, July). Variable rate QAM for mobile radio. *IEEE Trans. Commun. 43*(7), 2223–2230.

Wicker, S. B. (1995).
Error Control Systems for Digital Communication and Storage.
Upper Saddle River, NJ: Prentice-Hall.

Win, M. Z. and J. H. Winters (1999, December).
Exact error probability expressions for MRC in correlated Nakagami channels with unequal fading parameters and branch powers.
In *Proc. IEEE Global Commun. Conf. (GLOBECOM'99)*, Volume 5, Rio de Janeiro, Brazil, pp. 2331–2335.

Wong, D. and D. C. Cox (1999, May).
Estimating local mean signal power level in a Rayleigh fading environment.
IEEE Trans. Veh. Technol. 48(3), 956–959.

Yacoub, M. D., J. E. V. Bautista, and L. G. de Rezende Guedes (1999, May).
On higher order statistics of the Nakagami-*m* distribution.
IEEE Trans. Veh. Technol. 48(3), 790–794.

Yao, Y.-D. and A. U. H. Sheikh (1992, May).
Investigations into cochannel interference in microcellular mobile radio systems.
IEEE Trans. Veh. Technol. 41(2), 114–123.

Zhang, Y., M. P. Fritz, and S. B. Gelfand (1997).
Soft output demodulation on frequency-selective rayleigh fading channels using AR channel models.
In *IEEE Global Telecommunications Conference (GLOBECOM '97)*, Volume 1, pp. 327–331.

Øien, G. E. and K. J. Hole (2001, February).
Maximum average spectral efficiency for slowly varying rayleigh fading channels with pilot-symbol-assisted channel estimation.
In *Proc. European Personal Mobile Communications Conference*, Vienna, Austria.

Øien, G. E., H. Holm, and K. J. Hole (2002).
Channel prediction for adaptive coded modulation on Rayleigh fading channels.
submitted to *European Signal Processing Conference (EUSIPCO) 2002*; Toulouse, France, Sept. 2002.